Practical Recommendations for Evaluation and Mitigation of Soil Liquefaction in Arkansas

Principal Investigator and Graduate Student:

Dr. Brady R. Cox

Shawn C. Griffiths

Project Number: MBTC 3017

Date: February 2010

ACKNOWLEDGEMENT
This material is based upon work supported by the U.S. Department of Transportation under Grant Award Number DTRT07-G-0021. The work was conducted through the Mack-Blackwell Rural Transportation Center at the University of Arkansas.

Table of Contents

List of Tables

List of Figures

Chapter 1

Introduction

1.1 Motivation for Research

Northeastern Arkansas has some of the largest design earthquake ground motions in the continental U.S. due to its location within the New Madrid Seismic Zone (NMSZ). These large earthquake ground motions are particularly problematic when coupled with the unknown seismic response of the deep, soft soils of the Mississippi Embayment. Based on empirical standard penetration test (SPT) liquefaction triggering analyses, many soils in this area exhibit apparent liquefaction susceptibility at depths up to 30-plus m (100-plus ft). However, there is very little guidance in the literature on what to do in these situations, because soils soft enough to liquefy at great depths (i.e. greater than approximately 20 m [65 ft]) have not been documented in the case history databases from previous earthquakes.

Currently, the Arkansas State Highway and Transportation Department (AHTD), and others in involved with bridge construction in the NMSZ, are forced to drive piles for bridge foundations to significant depths in order to mitigate against the loss of strength in these potentially liquefiable soils during an earthquake. This is both costly and time consuming. The current research is aimed primarily at helping AHTD and other interested entities determine the best possible liquefaction triggering procedures for soils at depths between approximately 15-30 m (50-100 ft). While it is understood that the extrapolation of the simplified liquefaction triggering procedures to depths greater than approximately 20 m (65 ft) is of uncertain validity (Youd et al. 2001, Idriss and

Boulanger 2008), designers must do something to determine the liquefaction susceptibly of these soils. This work systematically evaluates similarities and differences between the available SPT-based simplified methods at significant depths so that a rational decision regarding the liquefaction susceptibility of deep soils in the Mississippi Embayment can be made.

1.2 PROBLEM STATEMENT

The primary task of the research discussed herein is to help AHTD and other interested entities review and update procedures used to evaluate earthquake-induced soil liquefaction triggering, particularly for deep soil deposits. Specific subtasks of this research project include providing recommendations and insights concerning: (1) appropriate use of SPT-based liquefaction triggering procedures, (2) residual shear strength of liquefied soils, and (3) potential liquefaction mitigation measures (i.e. possible ground improvement techniques). To help evaluate potential liquefaction susceptibility of deep soil deposits in the Mississippi Embayment, the three most commonly used SPT-based liquefaction triggering procedures have been examined, systematically compared, and programmed into user-friendly Excel workbooks. These three procedures are documented by Youd et al. (2001), Cetin et al. (2004), and Idriss and Boulanger (2008). Evaluating the differences between these three procedures, especially in regards to evaluating liquefaction susceptibility at significant depths, is a main focus of this research. This is not a trivial topic, as the most appropriate method to use for liquefaction triggering is currently debated at the highest levels of the geotechnical earthquake engineering community (Seed 2010, Finn et al. 2010).

1.3 Analysis of Site Specific Data

AHTD has provided a total of 19 boring logs from eight different bridge sites in eastern Arkansas to use in trial liquefaction triggering analyses. The locations of these bridge sites are shown relative to one another in Figure 1.1 and are grouped by AHTD Job No. These borings have been analyzed for soil liquefaction potential using all three of the newly-developed liquefaction triggering workbooks documented herein. Four of the eight bridge sites are part of AHTD Job No. 001992 and contain a total of eight boring logs. This job is located along U.S. highway 63 between Marked Tree and Gilmore, Arkansas. Design peak ground accelerations (PGA) for these bridges are very high, ranging from 0.82-1.03g. Nine of the boring logs come from three other bridge sites classified as Job No.'s 110514, 110527, and 110524. These bridges are all near Edmondson Arkansas, and have design PGA values of approximately 0.48g. The remaining two boring logs are from Job No. 020417 near Lagrue, Arkansas. This bridge has a design PGA value of 0.24g, the lowest of all sites considered. It will be noted that only one example boring from each of these three groups is discussed in detail herein (refer to Chapter 4). These example boring logs are discussed in great depth and were chosen to illustrate similarities and differences between liquefaction triggering procedures for typical conditions in eastern Arkansas. Although each of the subsurface profiles differ slightly from one another, the soil is generally clay (CL, CH) from the surface to a depth of 6-10 m (20-30 ft), underlain by sand (SW, SM) to depths between 30-36 m (100-120 ft).

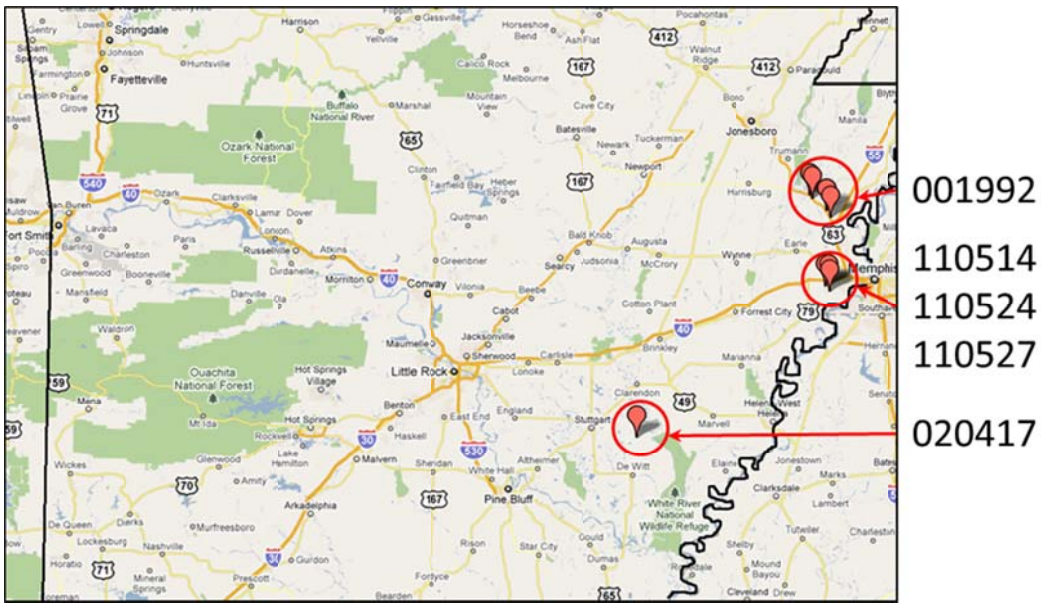

Figure 1.1. Map of the locations of the soil borings provided from AHTD (map generated with Google maps).

1.4 THESIS OVERVIEW

This thesis is composed of 7 chapters. Chapter 1 includes some general information and an introduction to this project. Chapter 2 encompasses a review of relevant literature, which includes pertinent information regarding soil liquefaction triggering procedures. Chapter 3 is a user's guide which should serve to clarify any questions that may arise while implementing the liquefaction triggering workbooks. Chapter 4 summarizes the liquefaction triggering results from three different bridge sites in eastern Arkansas. The results obtained from each of the three SPT-based procedures are compared in-depth to determine what factors most influence the differences between procedures. Chapter 5 includes a review of current literature concerning residual shear strength of liquefied soil, and recommendations for estimating residual shear strength. Chapter 6 presents potential liquefaction mitigation techniques, and Chapter 7 presents the overall conclusions and recommendations from this work.

Chapter 2

Review of Relevant Literature

2.1 New Madrid Seismic Zone (NMSZ)

Fuller (1912) coupled personal journals and geologic evidence to describe the events of the earthquakes that occurred within the NMSZ in the year 1811-1812. A brief account of these events is provided below.

On the night of December 16 in the year 1811 around 2:00 A.M. an earthquake shook the small town of New Madrid, Missouri on the banks of the Mississippi River. This initial shock was followed by two others before morning. Although the main shocks subsided for a time, tremors frequented the area until January 23, 1812 when another shock equal to the first was felt. This second shock was followed by two weeks of quiet, then, on February 7, 1812 the largest and final shock hit the area. This event was so powerful that it caused minor structural damage as far away as St. Louis, Missouri and Cincinnati, Ohio (Tuttle et al. 2002) people nearly 1000 miles away reported ground shaking (Fuller 1912).

This nearly three month period of tremors and earthquakes was not recorded by any instrumentation. As such, journal accounts and recent mapping of the geologic features left by the earthquake events have been used to infer earthquake magnitude, recurrence interval, and ultimately seismic ground motion hazard maps like those found in the International Building Code (IBC 2009) and the American Association of State Highway and Transportation Officials Seismic Bridge Design Guidelines (AASHTO 2009). Recent geodetic measurements estimate the three earthquake moment magnitudes

(M_w) of the 1811-1812 events to be around M_w 7-8 (Tuttle et al. 2002). Furthermore, geologic evidence indicates that the NMSZ has produced at least three large earthquake events in the past 1000 years, suggesting a return period of around 500 yrs +/- 300 yrs (Tuttle et al. 2002). These earthquake events have produced large sand blows up to 10 m (30 ft) wide and hundreds of meters long that range from 0.15 to 1.5 m (0.5 to 5 ft) thick. Because prior liquefaction is a good indication of a soils susceptibility to liquefaction during subsequent earthquakes (Idriss and Boulanger 2008), it is expected that the sandy soils in the Mississippi Embayment are still susceptible to liquefaction. However, the maximum depth to which the liquefaction occurred in the 1811-1812 earthquakes is unknown, and current research on deep liquefaction is still evolving.

2.2 Simplified Procedure for Evaluating Liquefaction Triggering

The 'simplified procedure' for evaluating soil liquefaction triggering was so named because of a simplified approach to computing the stress induced on the soil from earthquake forces (Seed and Idriss 1971). This dynamic stress imparted by the earthquake is termed the cyclic stress ratio (CSR). Conversely, the dynamic stress the soil can withstand before liquefying is often termed the cyclic resistance ratio (CRR). The CRR of the in-situ soil is primarily based on empirical correlations to the Standard Penetration Test (SPT), Cone Penetration Test (CPT) or shear wave velocity (Vs) measurements (Youd et al. 2001). These empirical correlations have been developed from case history data-bases of liquefied and non-liquefied soils documented in previous earthquakes. For example, Figure 2.1 presents the SPT liquefaction triggering curves for magnitude 7.5 earthquakes detailed in Youd et al. (2001). In this figure, arrows indicate

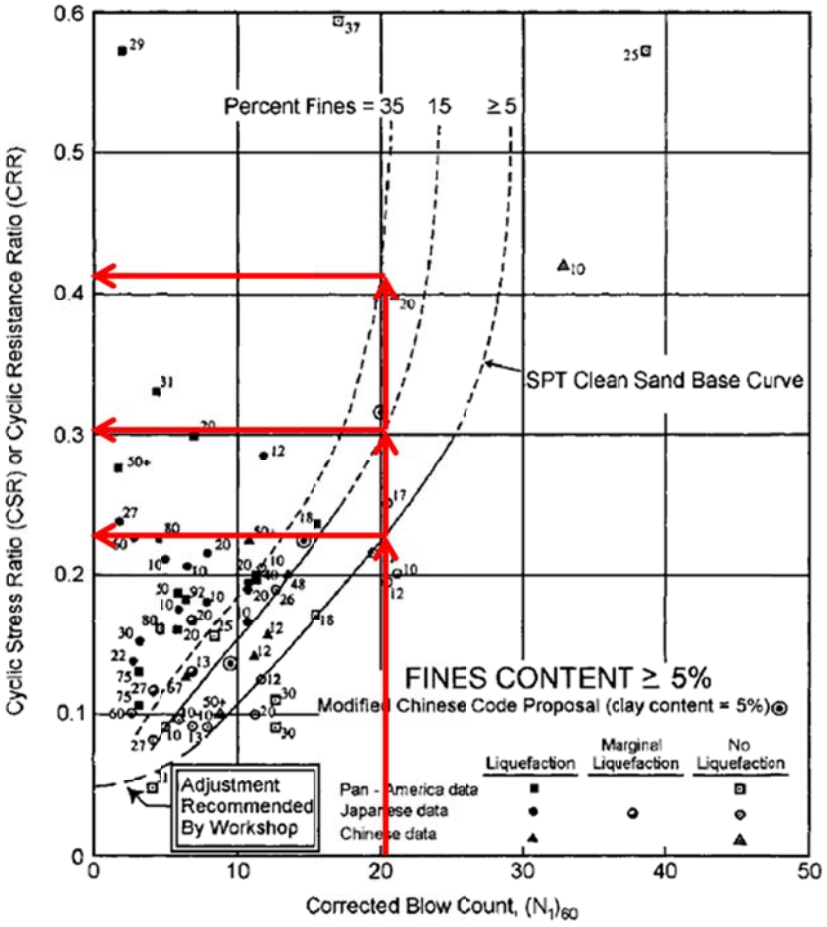

Figure 2.1. SPT CRR curves for magnitude 7.5 earthquake (modified from Seed et al 1985, obtained from Youd et al. 2001).

how the chart would be used to determine the CRR of the soil from a corrected blow count [$(N_1)_{60}$] of approximately 20. Sands with higher fines contents have been shown to be more resistant to liquefaction triggering than clean sands (Seed et al. 1985), accordingly the CRR curves for fines contents greater than 5% shift up and to the left as fines content increases, with the maximum permissible shift occurring for a fines content of 35%. The CRR values for $(N_1)_{60} = 20$ are approximately 0.22, 0.30, and 0.41 for fines contents of 5%, 15%, and 35%, respectively. Once the CRR of the soil has been determined, the CSR induced by the earthquake can be computed as outlined in Section

2.3, both of these factors are necessary to determine if the soil is potentially susceptible to liquefaction.

To compute the factor of safety (F.S.) against liquefaction triggering, the stress the soil can withstand without liquefying (i.e. the CRR) is divided by the stress induced by the earthquake (i.e. the CSR), according to Equation 2.1.

$$F.S. = \frac{CRR}{CSR} \qquad \text{Equation 2.1}$$

Hypothetically, a F.S. less than 1.0 suggests that the soil is susceptible to initiation of liquefaction, whereas a F.S. greater than 1.0 suggests that the soil is not susceptible to liquefaction. However, in reality, it is well understood that this boundary is not a distinct line and that engineering judgment needs to be applied to evaluate the liquefaction susceptibility of soils with a F.S. near unity. Furthermore, there are several possible procedures that may be employed for each in-situ test method (i.e. SPT, CPT, Vs) and the F.S. obtained from each of the procedures are not equivalent for the same input data. Therefore, caution must be exercised when establishing a F.S. and it is advisable to check the results from more than one procedure.

The following sections examine the primary reasons for variations in the F.S. predicted by different liquefaction triggering procedures. The discussion is focused on SPT-based procedures, as these are the oldest and most commonly used, and the only procedures currently employed by the Arkansas State Highway and Transportation Department (AHTD), whom this research is aimed at helping. Specifically, the three most commonly used SPT-based procedures of Youd et al. (2001), Cetin et al. (2004), and Idriss and Boulanger (2008) are discussed in detail.

2.3 THE CYCLIC STRESS RATIO (CSR)

The simplified procedure was developed by Seed and Idriss (1971) as an easy approach to estimate earthquake-induced stresses without the need for a site response analysis, and has been the primary method used to determine the CSR for the past 40 years. The simplified CSR is calculated as follows:

$$\mathrm{CSR} = \frac{\tau_{av}}{\sigma'_v} = 0.65\left(\frac{a_{max}}{g}\right)\left(\frac{\sigma_v}{\sigma'_v}\right) r_d \qquad \text{Equation 2.2}$$

where a_{max} is the peak horizontal ground surface acceleration modified for site specific soil conditions, g is the acceleration due to gravity, σ_v is the total overburden stress, σ'_v is the initial effective overburden stress, and r_d is a stress reduction coefficient which takes into account the flexibility of the soil column. All simplified liquefaction evaluation procedures use this common equation to determine the CSR. However, the various procedures often use different relationships to determine the coefficient r_d. As such, differences in the CSR calculations between various simplified methods are primarily a direct result of the uncertainty in determining r_d.

2.3.1 Stress Reduction Coefficient, r_d

The basis of the simplified CSR equation is Newton's second law of motion (i.e. force is equal to mass times acceleration), which assumes rigid body motion. In reality, the soil column is not a rigid body and behaves in a very non-linear fashion, therefore Seed and Idriss (1971) introduced r_d to account for the fact that the soil column is a deformable body. This relationship was only presented graphically in 1971 (refer to

Figure 2.2) and was plotted as a range of possible values that increased with depth (i.e. notice the hatched area suggesting the variability and uncertainty of r_d with depth).

Subsequently, many researchers have attempted to quantify r_d in various manners (i.e. Ishihara 1977, Iwasaki et al. 1978, Imai et al. 1981, Golesorkhi, 1989, Idriss 1999 and Seed et al. 2001). They have found that r_d is a complex parameter that depends on a combination of factors including site stiffness, input motion frequency content, absolute depth, relative layer thicknesses, earthquake magnitude and other criteria. Because of this complexity, consensus on the best approach to quantify r_d in a simplified manner has not been reached. Therefore, each procedure recommends a different r_d correlation. Regardless of which r_d correlation is "most correct", r_d curves cannot be "mixed and matched"; each correlation should only be used within its recommended procedure (Idriss and Boulanger 2008, Seed 2010).

Youd et al. (2001) adopted the recommendation by Seed and Idriss (1971) for use in determining r_d (refer to Figure 2.3). The mean value of the graphical representation may be approximated with Equation 2.3:

$$r_d = \frac{(1.000+0.4113z^{0.5}+0.04052z+0.001753z^{1.5})}{(1.000-0.4177z^{0.5}+0.05729z-0.006205z^{1.5}+0.00121z^{2})} \qquad \text{Equation 2.3}$$

where z is the depth below the ground surface in meters. The use of Equation 2.3 below a depth of approximately 15 m (50 feet) is not recommended by Youd et al. (2001) because as stated therein "evaluation of liquefaction at these greater depths is beyond the depths where the simplified procedure is verified and where routine applications should be applied." However, no alternative is provided for deeper evaluations.

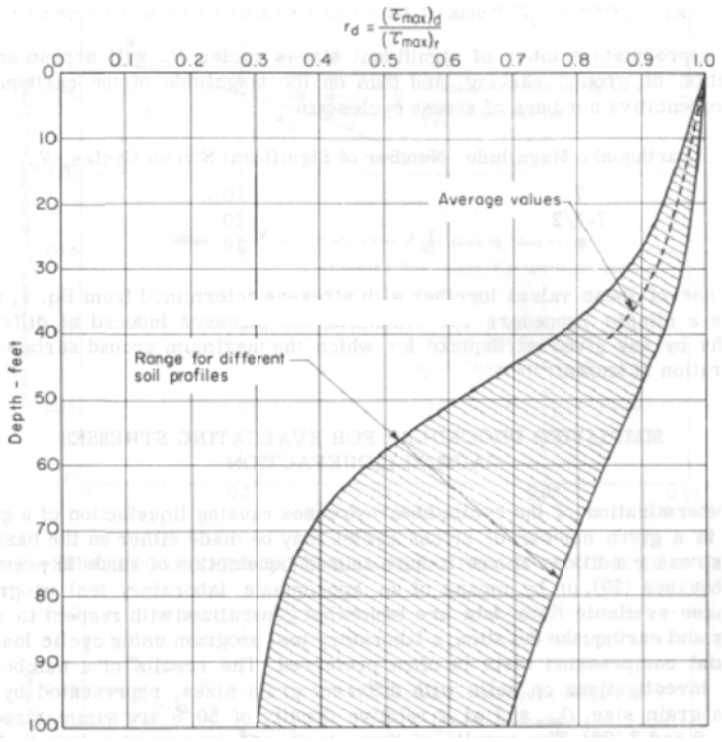

Figure 2.2. Stress reduction coefficient (r_d) as proposed by Seed and Idriss (1971).

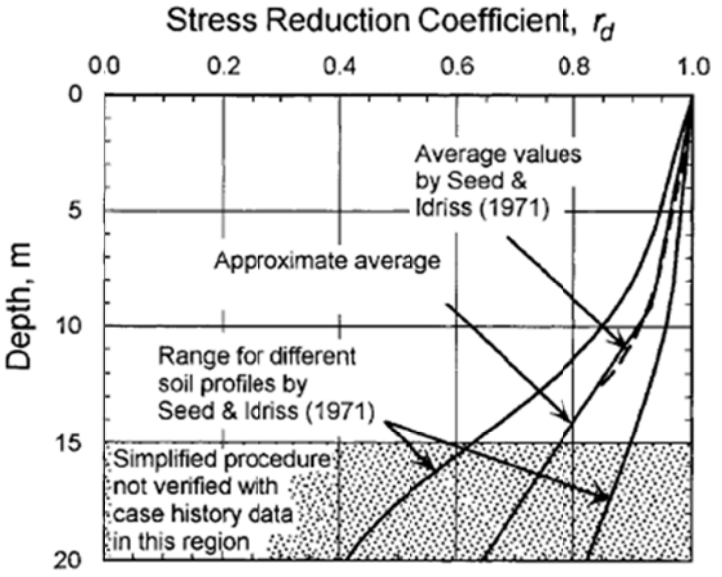

Figure 2.3. The r_d relationship adopted by Youd et al. (2001) with approximate average values from Equation 2.3.

Cetin et al. (2004) investigated r_d using a total of 2,153 site response analyses performed with the program SHAKE91. These response analyses were separated into bins according to the input parameters of moment magnitude (M_w), a_{max}, and average site stiffness over the top 12 m (40 feet) of soil, evaluated via shear wave velocity ($Vs_{,12}$). Mean estimates of r_d with standard deviations were fit using a Bayesian regression approach. The r_d expression fit by Cetin et al. (2004) is provided in Equation 2.4 (the standard deviation term has not been included here for brevity). It is a function of four variables (z, M_w, a_{max}, and $Vs_{,12}$) and must be used with appropriate units (i.e. z in meters and $Vs_{,12}$ in meters per second). This equation is only applicable to depths of less than 20 m (65 feet). A slightly modified equation found in Cetin et al. (2004) can be used for depths greater than 20 m (65 feet). Rather than recommending a depth where this equation is no longer valid the standard deviation term (not shown here) quantifies the uncertainty, which increases with depth to around 12 m (40 feet) and then remains nearly constant for all depths.

$$r_d\left(z, M_w, a_{max}, \mathrm{V}_{s,12}\right) = \frac{\left[1+\frac{-23.013-2.949*a_{max}+0.999*M_W+0.0525*V_{S,12}}{16.258+0.201*e^{0.341\left(-z+0.0785*V_{S,12}+7.586\right)}}\right]}{\left[1+\frac{-23.013-2.494*a_{max}+0.999*M_W-0.0525*V_{S,12}}{16.258+0.201*e^{0.341\left(0.0785*V_{S,12}+7.586\right)}}\right]} \quad \text{Equation 2.4}$$

Idriss (1999) introduced a relationship for r_d based on work by Golesorkhi (1989). This relationship expresses r_d as a function of depth and earthquake magnitude and is included as Equations 2.5 - 2.7. These are the same r_d equations published by Idriss and Boulanger (2008). To use these equations properly, z should be input in meters and the arguments within the sine terms should be input in radians. Idriss and Boulanger (2008) have recommended using Equations 2.5 - 2.7 to a maximum depth of 20 m (65 feet)

because of increasing uncertainty with depth, and suggest using a site specific response analyses for deeper and/or critical r_d evaluations.

$$r_d = e^{(\alpha(z)+\beta(z)M_w)} \qquad \text{Equation 2.5}$$

$$\alpha(z) = -1.012 - 1.126sin\left(\frac{z}{11.73} + 5.133\right) \qquad \text{Equation 2.6}$$

$$\beta(z) = 0.106 + 0.118sin\left(\frac{z}{11.28} + 5.142\right) \qquad \text{Equation 2.7}$$

The variation of r_d versus depth for the three most common simplified SPT procedures is plotted in Figure 2.4. This figure includes dual vertical axes that represent the depth and approximate vertical effective stress. In order to make effective stress calculations, a uniform soil with a unit weight of 18.8 kN per cubic meter (120 pcf) and a water table at the ground surface have been assumed. These same assumptions have been made for all other figures in this report that include dual vertical axes for depth and stress unless stated otherwise. While it is understood that this is an oversimplification of the uniformity of the soil profile and ground water level, the dual axes serve the purpose of giving the reader an idea of the depth and approximate vertical effective stress on the same plot.

The Youd et al. (2001) and Idriss and Boulanger (2008) relationships presented in Figure 2.4 are nearly identical at depths less than 12 m (40 feet) (assuming a M_w=7.5 earthquake), but deviate significantly with increasing depth. For a wide range of a_{max} (0.1 to 0.6g) and a reasonable $Vs_{,12}$ value for potentially liquefiable soils (180 m/s or 600 ft/s), the Cetin et al. (2004) expression generally yields lower r_d estimates than the others. At

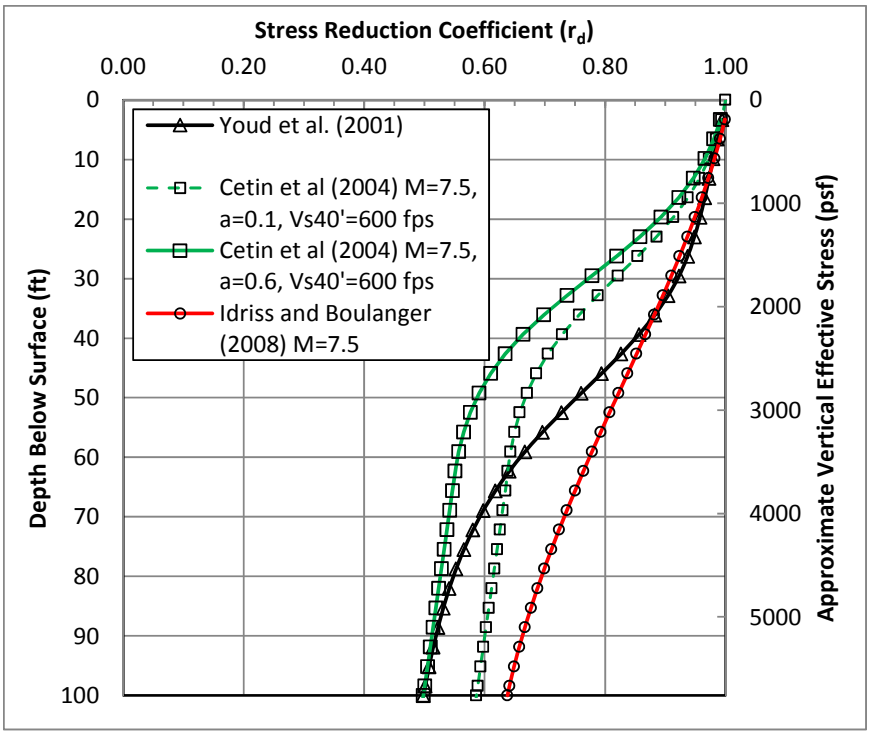

Figure 2.4. Comparison of three stress reduction coefficient (r_d) relationships as a function of depth and approximate vertical effective stress.

depths greater than 15 m (50 feet), all of the procedures vary significantly from one another, reflecting the increased uncertainty in r_d estimates at depth. The r_d values near 15 m (50 feet) vary by approximately 39%, at 24 m (80 feet) they vary by approximately 32%, and at 30 m (100 feet) they vary by approximately 28%. These variations in r_d lead to equal variations in CSR, all other things being equal. According to Equation 2.1, lower CSR estimates should yield higher F.S. values against liquefaction (i.e. based on CSR alone, one would expect the F.S. of Youd et al. [2001] and Cetin et al. [2004] to be greater than the F.S. of Idriss and Boulanger [2008]). However, this cannot be assumed because the CRR also varies significantly between procedures.

2.4 THE CYCLIC RESISTANCE RATIO (CRR)

The CRR is the dynamic stress the soil can withstand before liquefying. SPT-based liquefaction triggering procedures use blow count (N) as the basis of computing CRR (refer to Figure 2.1). The SPT-based CRR relationships for Youd et al. (2001), Cetin et al. (2004) and Idriss and Boulanger (2008) are presented below. In order to compare these relationships in a meaningful manner, the CRR equations for each procedure will be presented below as $CRR_{7.5,\ 1\ atm}$ (i.e. the cyclic resistance ratio of the soil adjusted to 1 atmosphere of effective overburden pressure for a M_w=7.5 earthquake). This is necessary because the various relationships use different factors to account for earthquake magnitude and overburden stresses. It is common for CRR relationships to be normalized for this base case, and then site specific adjustments are made via magnitude scaling factors (MSF) and overburden correction factors (Kσ) to account for the earthquake magnitude under consideration and the overburden stresses at the depth of interest. The site adjusted CRR is obtained from $CRR_{7.5,\ 1\ atm}$ according to equation 2.8:

$$CRR_{M,K\sigma} = CRR_{M=7.5,1\ atm} \times MSF \times K\sigma \qquad \text{Equation 2.8}$$

where all variables are defined above. The MSF and Kσ relationships recommended in each procedure will be compared after a discussion of the $CRR_{7.5,\ 1\ atm}$ equations.

Youd et al. (2001) slightly modified the CRR curve of Seed et al. (1985). This modification simply bounds the CRR clean sand curve at N-values less than 5 and is included as a dashed line in Figure 2.1. The equation used to approximate the modified curve is the presented as Equation 2.9:

$$CRR_{7.5,1\ atm} = \frac{1}{34-(N_1)_{60cs}} + \frac{(N_1)_{60cs}}{135} + \frac{50}{[10*(N_1)_{60cs}+45]^2} - \frac{1}{200}$$ Equation 2.9

where again $CRR_{7.5,1\ atm}$ is the cyclic resistance ratio of the soil adjusted to 1.0 atmosphere of effective overburden pressure for a M_w=7.5 earthquake, and $(N_1)_{60cs}$ is the overburden and energy corrected blow count adjusted to a clean sand (cs) equivalent. This equation should not be applied at corrected blow counts greater than 30 because as Youd et al. (2001) states, "For $(N_1)_{60cs} \geq 30$, clean granular soils are too dense to liquefy and are classed non-liquefiable."

Cetin et al. (2004) developed a probabilistic approach to evaluate soil liquefaction triggering. Their probabilistic CRR relationship is presented in Equation 2.10:

$$CRR_{7.5,1\ atm} = exp\left[\frac{\left((N_1)_{60}*(1+0.004*F.C.)-29.53*ln(\boldsymbol{M_w})-3.7*ln\left(\frac{\sigma'_v}{P_a}\right)+0.05*F.C.+16.85+2.7*\phi^{-1}(P_L)\right)}{13.32}\right]$$

Equation 2.10

where once again $CRR_{7.5,1\ atm}$ is the cyclic resistance ratio of the soil adjusted to 1.0 atmosphere of effective overburden pressure for a M_w=7.5 earthquake, $(N_1)_{60}$ is the overburden and energy corrected blow count, F.C. is the fines content of the soil, M_w is the earthquake magnitude under consideration (M_w = 7.5 for $CRR_{7.5,1\ atm}$), σ'_v is the initial effective overburden stress (σ'_v = 1 atm for $CRR_{7.5,1\ atm}$), P_a is atmospheric pressure, ϕ^{-1} is the inverse of the cumulative normal distribution, and P_L is the probability of liquefaction. In order to use this relationship deterministically rather than probabilistically, Cetin et al. (2004) recommends using M_w = 7.5, σ'_v = 1 atm (2116 psf),

and P_L = 15%, as indicated within Figure 2.5. When Cetin et al. (2004) developed the probabilistic curves they were compared with the CRR curve developed by Seed et al. (1985). An effort was made to determine a P_L that would yield the two curves congruent, unfortunately the methods differed so greatly that a range of possible probabilities from 10 - 40% was found acceptable. Cetin et al. (2004) chose a P_L = 15% based on the range above and: "Seed's intent that the recommended (1985) boundary should represent approximately a 10 - 15% probability of liquefaction" (Seed 2010).

Equation 2.10 is only valid for CRR's less than 0.4. At higher CRR's, the dashed line portion of Figure 2.5 was sketched by hand and reflects what Cetin et al. (2004) believe to be the best possible deterministic boundary given limited data. As no equation exists to determine the CRR for values greater than 0.4, the deterministic procedure presented in Cetin et al. (2004) is difficult to automate. Therefore, the author has taken the liberty of fitting an equation to the dashed line portion of the curves shown in Figure 2.5. Equations 2.11 – 2.13 are shown below and are applicable to CRR values between 0.4-0.6. These equations are dependent on $(N_1)_{60}$ and fines content (F.C.), which are the same dependent variables within Equation 2.10 once the proper constants (i.e. M_w = 7.5, σ'_v = 1 atm, and P_L = 15%) are employed. At CRR values less than 0.4 Equation 2.10 should be used, while at CRR values greater than or equal to 0.4 Equations 2.11 – 2.13 should be employed. Note that the original deterministic CRR curves of Cetin et al. (2004) only extend to a value of 0.6 (refer to Figure 2.5). While Equations 2.11 – 2.13 may be employed to extend these curves to CRR values greater than 0.6, these extrapolations are of uncertain validity and are not recommended.

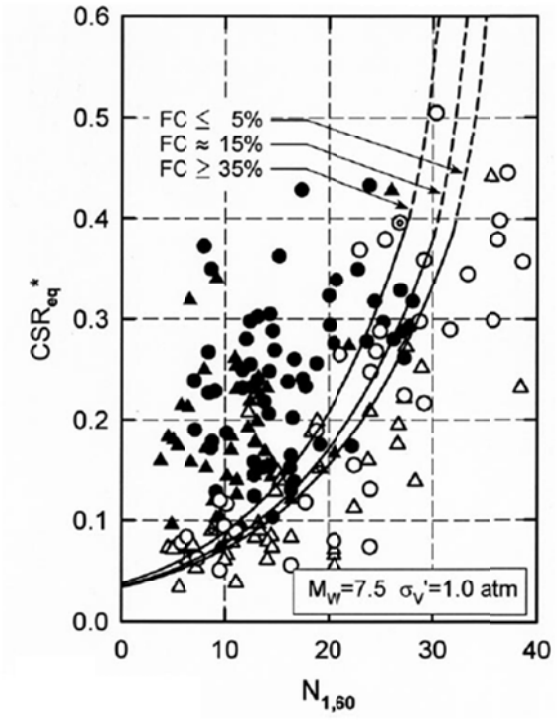

Figure 2.5. The deterministic CRR curves from Cetin et al. (2004) with a P_L=15%.

$$CRR_{7.5,1\,atm} = Ae^{(B(N_1)_{60})} \qquad \text{Equation 2.11}$$

$$A = 0.0052 + \left(0.001 * (F.C. - 5)\right) \qquad \text{Equation 2.12}$$

$$B = 0.135 * 1.005 + \left(0.00015 * (F.C. - 5)\right) \qquad \text{Equation 2.13}$$

Cetin et al. (2004) do not recommend a specific limiting upper value for $(N_1)_{60cs}$ as proposed by Youd et al. (2001). However, if the F.C. is fixed at 5% in Equations 2.10-2.13, and $(N_1)_{60cs}$ is used instead of $(N_1)_{60}$, a limiting upper value of $(N_1)_{60cs}$ = 35 can be inferred because it yields a CRR of approximately 0.6, which is the maximum CRR specified in Figure 2.5. When the Cetin et al. (2004) procedure is used deterministically, it is easiest to program in a spreadsheet by fixing the F.C. at 5%, using $(N_1)_{60cs}$ instead of $(N_1)_{60}$, and using a limiting upper value of $(N_1)_{60cs}$ = 35. In this work, $(N_1)_{60cs}$ = 35 has

been interpreted as the upper-bound cutoff between liquefiable and non-liquefiable soils for the Cetin et al. (2004) procedure.

The Idriss and Boulanger (2008) CRR relationship is presented in Equation 2.14:

$$CRR_{7.5,1\,atm} = exp\left[\frac{(N_1)_{60cs}}{14.1} + \left(\frac{(N_1)_{60cs}}{126}\right)^2 - \left(\frac{(N_1)_{60cs}}{23.6}\right)^3 + \left(\frac{(N_1)_{60cs}}{25.4}\right)^4 - 2.8\right]$$

Equation 2.14

where all variables have been defined previously. This relationship is presented graphically in Figure 2.6, which was initially proposed in Idriss and Boulanger (2004).

Although no upper-bound $(N_1)_{60cs}$ value is explicitly recommended with the equation, in Appendix A of Idriss and Boulanger (2008), $(N_1)_{60cs}$ values greater than 37.5 are assigned a CRR of 2.0. Therefore, in this work $(N_1)_{60cs} = 37.5$ has been interpreted as the upper-bound cutoff between liquefiable and non-liquefiable soils.

Figure 2.7 compares the CRR relationships presented in Equations 2.9-2.14. The Youd et al. (2001) and Idriss and Boulanger (2008) curves are very similar for most blow counts. The Cetin et al. (2004) curve, plots lower than the others primarily because the r_d relationship used to back calculate the CSR in the development of the case-history data set is lower than the others, especially for shallow (<15 m, 50 feet) sites which make up the majority of the case-history data set (Seed 2010).

While interesting to look at, the various liquefaction triggering procedures cannot be compared solely on CRR plots like Figure 2.7. For example, even though the CRR for Cetin et al. (2004) is lower for any given corrected blow count, it will also be noted that

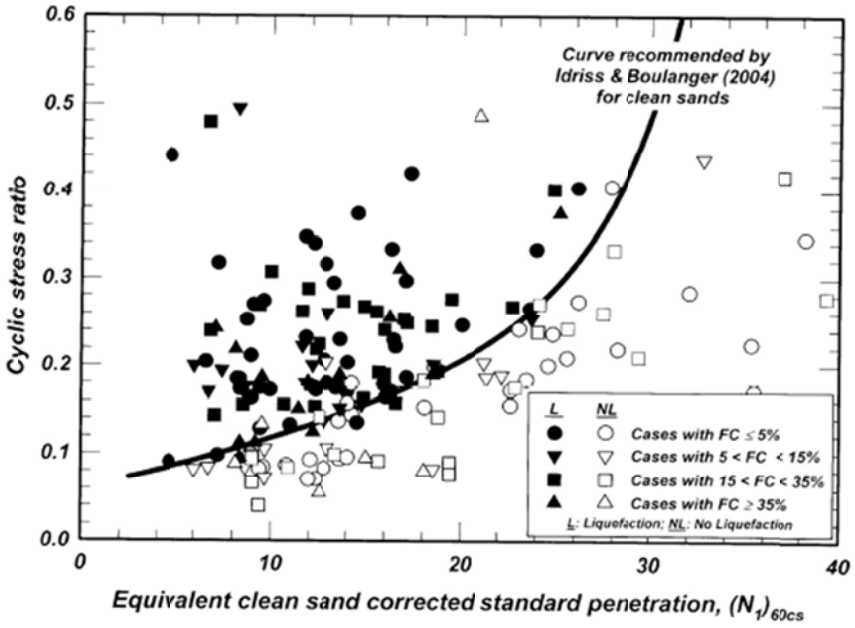

Figure 2.6. The CRR relationship proposed by Idriss and Boulanger (2008).

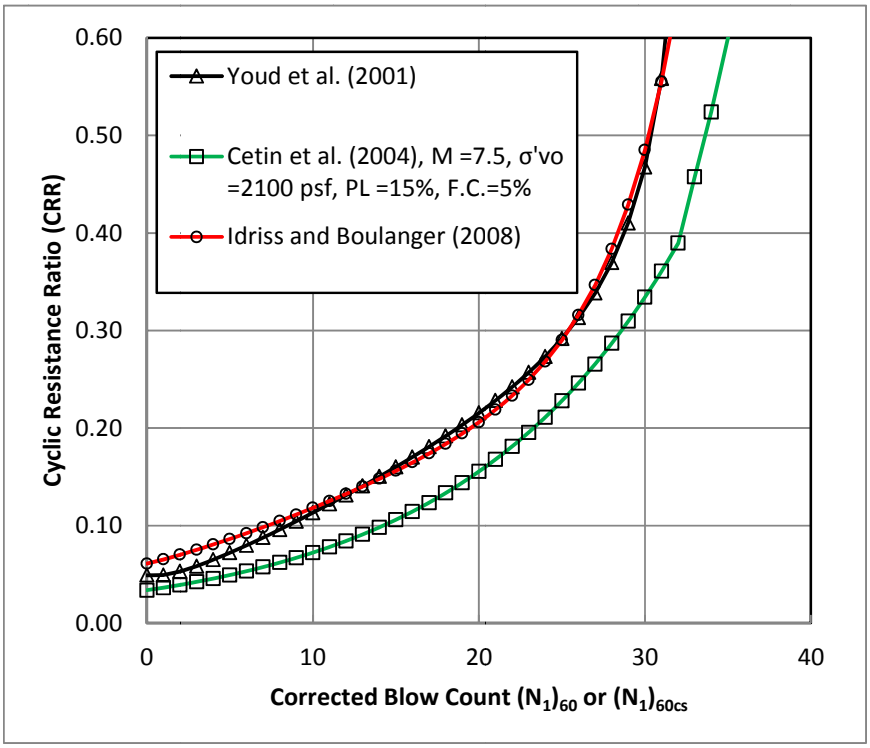

Figure 2.7. Comparison of the three $CRR_{7.5,1\ atm}$ curves for clean sand.

their procedure generally yields a lower CSR (refer to Section 2.3, Figure 2.4). Furthermore, while the Youd et al. (2001) and Idriss and Boulanger (2008) CRR relationships appear to be very similar, one would not necessarily obtain the same CRR value for a given raw blow count (N value) because the factors used to correct N to $(N_1)_{60cs}$ can vary significantly between relationships. Specifically, the overburden blow count correction factor (C_N) used in each relationship appears to be most variable.

2.4.1 Standardized Overburden Blow Count Correction Factor (C_N)

Before computation of the CRR, the raw N values are generally corrected/adjusted using five corrections. These five corrections include: (1) overburden blow count correction (C_N), (2) energy correction (C_E), (3) drill rod length correction (C_R), (4) borehole diameter correction (C_B), and (5) sampler liner correction (C_S). These corrections are applied as shown in Equation 2.15:

$$(N_1)_{60} = N * C_N * C_E * C_R * C_B * C_S \qquad \text{Equation 2.15}$$

where $(N_1)_{60}$ is the energy and overburden/stress corrected blow count. In liquefaction analyses, it is also common to adjust the corrected blow count further using the F.C. of the soil to obtain the clean sand (cs) equivalent corrected blow count, $(N_1)_{60cs}$. Among all these corrections, only C_N contributes significantly to major variations in corrected blow count as a function of depth. As such, the remainder of this section is focused on the various C_N relationships.

The need to normalize the results of the standard penetration resistance for overburden effects was well documented by Gibbs and Holtz (1957). In their study, a

large barrel type container was made and sand was compacted inside at a constant relative density (D_R) with varying overburden pressures being applied to the top of the container. A standard split spoon sampler was driven into the sand layer, with the test repeated for a range of D_R and overburden pressures. This resulted in a correlation between overburden pressure and blow count for a given D_R. Many C_N correlations have been presented since that time (Teng 1962, Peck et. al 1974, Seed 1979, Liao and Whitman 1985, Kayen et. al 1992). Most of the correlations are similar to one another for relatively low overburden pressures. Differences in peak values and slope are noted by Liao and Whitman (1986).

Youd et al. (2001) recommend using either the C_N correlation proposed by Liao and Whitman (1986) or Kayen et al. (1992). The Youd et al. (2001) worksheet accompanying this report utilizes the correlation proposed by Kayen et al. (1992) over Liao and Whitman (1986) because, as stated by Youd et al. (2001) "in these writers' opinion, [Kayen et al. (1992)] provides a better fit to the original curve specified by Seed and Idriss (1982)". This correlation is presented below as Equation 2.16:

$$C_N = \frac{2.2}{1.2+\frac{\sigma'_v}{P_a}} \qquad \text{Equation 2.16}$$

where all variables have been defined previously. This equation limits the maximum C_N value to 1.7.

Cetin et al. (2004) adopted Liao and Whitman's (1986) correlation with the caveat that C_N should not exceed a maximum value of 1.6. This correlation is presented below as Equation 2.17:

$$C_N = \left[\frac{P_a}{\sigma'_v}\right]^{0.5} \qquad \text{Equation 2.17}$$

Gibbs and Holtz (1957) noted the difficulty in separating the effects of confining pressure and D_R. They found that C_N is not solely a function of overburden pressure, but relies also on D_R and soil type. Marcuson and Bieganousky (1977a,b) conducted research similar to Gibbs and Holtz (1957) and also noted the influence D_R had on C_N. Seed (1979) plotted C_N as two different curves depending on the D_R of the sand. His correlations were the first to directly combine D_R and effective overburden stress. Boulanger (2003) used data from Marcuson and Bieganousky (1977a,b) along with a weighted least squares nonlinear regression that modeled both density and overburden stress. His correlation takes a form similar to Liao and Whitman (1986), with the advent of the exponent being a function of relative density. Boulanger and Idriss (2004) have modified the equation one step further by substituting a correlation that relates $(N_1)_{60}$ to D_R. The C_N equation recommended by Idriss and Boulanger (2008) is presented as Equation 2.18:

$$C_N = \left(\frac{P_a}{\sigma'_v}\right)^{0.748-0.0768\sqrt{(N_1)_{60}}} \qquad \text{Equation 2.18}$$

The authors recommend maximum values of $C_N = 1.7$ and $(N_1)_{60} = 46$ in this equation. The Idriss and Boulanger (2008) workbook accompanying this report requires that iterative calculations option be allowed. This is because the calculation of $(N_1)_{60}$ is dependent on C_N which is again dependent on $(N_1)_{60}$.

All three of the C_N correlations (Equations 2.16-2.18) are compared in Figure 2.8. In order to show the effect different $(N_1)_{60}$ values can have on the correlation of Idriss

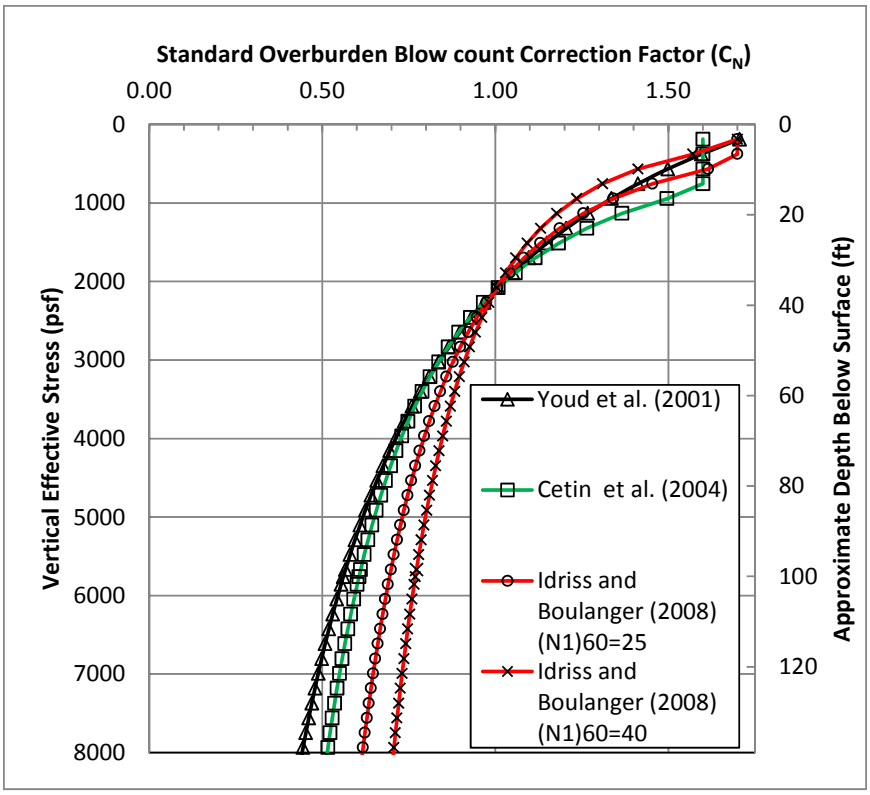

Figure 2.8. Comparison of three C_N correlations as a function of vertical effective stress and approximate depth.

and Boulanger (2008), two different curves with $(N_1)_{60} = 25$ and $(N_1)_{60} = 40$ have been included, as indicated on the graph. In general, for effective overburden stresses greater than 1 atm, the Youd et al. (2001) procedure yields the lowest C_N values, while the Idriss and Boulanger (2008) procedure yields the highest C_N values. Meaning, all other things being equal, the Idriss and Boulanger (2008) procedure will yield the highest $(N_1)_{60}$ values for soils at depth. The maximum C_N differences between the procedures, assuming a $(N_1)_{60} = 25$ for Idriss and Boulanger (2008), are 12%, 20%, and 40% at 0.47 atm (1000 psf), 2.36 atm (5000 psf) and 3.78 atm (8000 psf), respectively.

2.4.2 Overburden Correction Factor (Kσ)

The overburden correction factor (Kσ) is currently the factor used to extrapolate liquefaction triggering relationships to high overburden pressures. Because this research is aimed primarily at determining liquefaction susceptibility at depth, Kσ has received a rigorous review herein. The influence of overburden or effective stress on resistance of saturated sands to liquefaction initiation has been noted by many (Maslov 1957, Florin and Ivanov 1961, Seed and Lee 1966). The Kσ factor was first introduced by Seed (1983) as a variable used to account for the decrease in the CSR required to cause a pore pressure ratio of 100% as overburden stresses increase. The Seed (1983) correlation was developed from cyclic simple shear and cyclic triaxial tests at different overburden stresses. This first attempt to quantify Kσ was published graphically and consisted of a range of possibilities. Vaid et al. (1985) subjected sands to very high confining pressures, up to 24 atm (50,000 psf), and found that the density of the sand was interrelated to the overburden pressure, which made it difficult to separate the two variables. Vaid et al. (1985) also found that the cyclic resistance ratio of the sand decreased with increasing overburden pressure, which is consistent with other studies.

Seed and Harder (1990) proposed a new Kσ relationship based on Harder's (1988) Ph.D. thesis. Although both studies used the same data set, Seed and Harder's (1990) relationship lies slightly below Harder's (1988) relationship, as detailed in Figure 2.9. Pillai and Byrne (1994) researched Kσ as part of the seismic assessment of Duncan Dam in British Columbia. Their study combined frozen sampling techniques and cyclic laboratory tests with field SPT tests to determine Kσ. Their results lie above Seed and

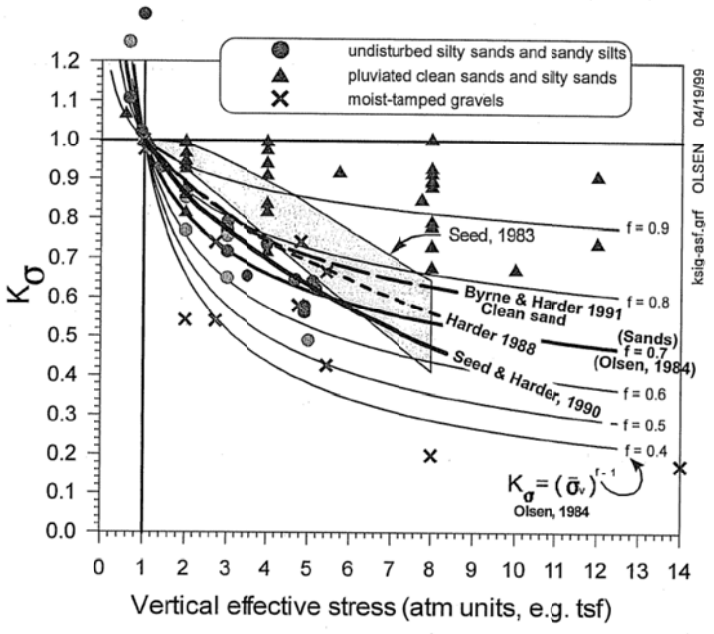

Figure 2.9. Comparison of Kσ values from different researchers, with expanded data set (reproduced from Hynes and Olsen 1999).

Harder's (1990) values and are not included within figure 2.9. Hynes and Olsen (1999) published a Kσ relationship that was a function of D_R after using a stress focus method to determine the exponential factor (f). Their relationship is included as Equation 2.19.

$$K_\sigma = \left(\frac{\sigma'_v}{P_a}\right)^{f-1} \qquad \text{Equation 2.19}$$

The expanded data set used by Hynes and Olsen (1999) to determine Kσ curves, as well as various prior Kσ relationships, are presented in Figure 2.9. For medium dense sands, an f value of 0.7 is recommended. However, f values can range from 0.6 to 0.95 depending on; D_R, stress history, method of deposition, and age of the deposit (Hynes and Olsen 1999). Equation 2.19 is the equation adopted by both Youd et al. (2001) and Cetin et al. (2004).

Because the f value within Equation 2.19 is dependent on the D_R of the soil, Youd et al. (2001) recommend an f value between 0.6 - 0.8 for D_R between 80-40%. Cetin et al (2004) recommend an f value between 0.6 - 0.8 as a function of $(N_1)_{60cs}$ varying from 5 to 40 blows per foot, this is probably a misprint because all other trends show that the f value increases with decreasing D_R (i.e. it should have been written that f varies from 0.6 – 0.8 as $(N_1)_{60cs}$ varies from 40 to 5 blows per foot). In the Youd et al. (2001) workbook, the determination of f is a two-step process; the D_R is correlated to $(N_1)_{60}$ and then f is correlated to D_R. While in the Cetin et al. (2004) workbook, the f value is linearly interpolated between 0.6 – 0.8 from 40 to 5 blows per foot respectively.

Work to determine the effects of overburden stress on liquefaction susceptibility continued at the U.S. Army Engineering Research and Development Center (ERDC) located in Vicksburg, Mississippi. Steedman et al. (2000) completed centrifuge tests with fine Nevada sand in homogeneous and dense-over-loose configurations. Their tests revealed that at high confining pressures, above 3 atm (6000 psf), a rise in pore pressure may soften and degrade the soil under earthquake conditions, but may not generate 100% excess pore water pressure necessary for "true liquefaction". The study concluded that liquefaction of deep soils may not be the hazard it is assumed to be (Steedman et al. 2000). However, Sharp and Steedman (2000) continued research with the centrifuge and found that 100% excess pore water pressure, or liquefaction, can occur at high confining stresses in the range of 3-12 atm (6,300-25,000 psf), contradicting the findings published earlier in the year by Steedman et al. (2000).

Gonzalez et al. (2002) conducted centrifuge tests at Rensselaer Polytechnic Institute (RPI) modeling homogenous and dense-over-loose configurations of deep soil

deposits. One model simulated a 38 m (125 feet) deposit of a saturated, uniform, loose (D_r = 55%) sand. This model subjected the soil to a maximum initial effective overburden stress of about 3.8 atm (8,000 psf) at the bottom of the soil deposit. Liquefaction was observed throughout its entire depth, including 100% excess pore water pressure. The input motion was 0.2 g with a frequency of 1.5 Hz. The entire column of soil was liquefied in less than 20 seconds (around 24 cycles of shaking). This study also collected and reported shear stress along with shear strain, which helped confirm the acceleration and pore pressure data as well as the propagation of the liquefaction front and its association with shear strength degradation. This study is confirmation that 100% excess pore pressures can develop within deep sandy deposits.

Boulanger (2003) used a relative state parameter index derived from the relative dilatancy index to correlate Kσ to the D_R of sand. Boulanger and Idriss (2004) presented a substitution for relative density based on blow count, similar to the C_N correction presented earlier. This relationship relies on the correlation of relative density to blow count, which as Marcuson and Bieganousky (1977a,b) state is dependent on many factors and can vary by as much as +/- 15%. These new Kσ relationships are included as Equations 2.20 and 2.21:

$$K_\sigma = 1 - C_\sigma ln\left(\frac{\sigma'_v}{P_a}\right) \qquad \text{Equation 2.20}$$

$$C_\sigma = \frac{1}{18.9 - 2.55\sqrt{(N_1)_{60}}} \qquad \text{Equation 2.21}$$

Even with uncertainty in the correlation, these equations may be an improvement to the current Kσ relationships based on the interrelation of relative density and overburden pressure. Equation 2.20 should be restricted to a maximum value of 1.1, and Equation

2.21 should be restricted to a maximum value of 0.3 (or conversely $(N_1)_{60}$ can be restricted to a maximum value of 37).

Both Youd et al. (2001) and Cetin et al. (2004) adopted Hynes and Olsen's (1999) relationship (Equation 2.19) for use when computing Kσ. Youd et al. (2001) recommends a maximum value of 1.0 for Kσ, while Cetin et al. (2004) recommends a maximum of 1.5. The Kσ relationship adopted in Idriss and Boulanger (2008) is the same one presented in Boulanger and Idriss (2004) (Equations 2.20 and 2.21). The limiting values for Kσ in each relationship can make a substantial difference in the predicted CRR values of shallow soils (i.e. less than 1 atm [2000 psf]), but do not influence liquefaction susceptibility at depth.

Kσ values for each of the three procedures are plotted in Figure 2.10 as a function of vertical effective stress and approximate depth. Cetin et al. (2004) and Youd et al. (2001) use the same equation to calculate Kσ, with slightly different f values and different maximums at low confining pressures. Idriss and Boulanger (2008) use a maximum value of 1.1. Two curves are provided for the Idriss and Boulanger (2008) procedure because Kσ varies with $(N_1)_{60}$. The $(N_1)_{60}$ =10 and $(N_1)_{60}$ =25 curves both plot above the other relationships for effective overburden stresses greater than 1 atm (2000 psf), which increases the CRR at depth according to Equation 2.8. For example, at an effective overburden stress of 3 atm (6000 psf) and an $(N_1)_{60}$ value of 25, Idriss and Boulanger (2008) report a Kσ value 13% greater than both Youd et al. (2001) and Cetin et al. (2004), which relates to an equal increase in CRR, all other things remaining equal.

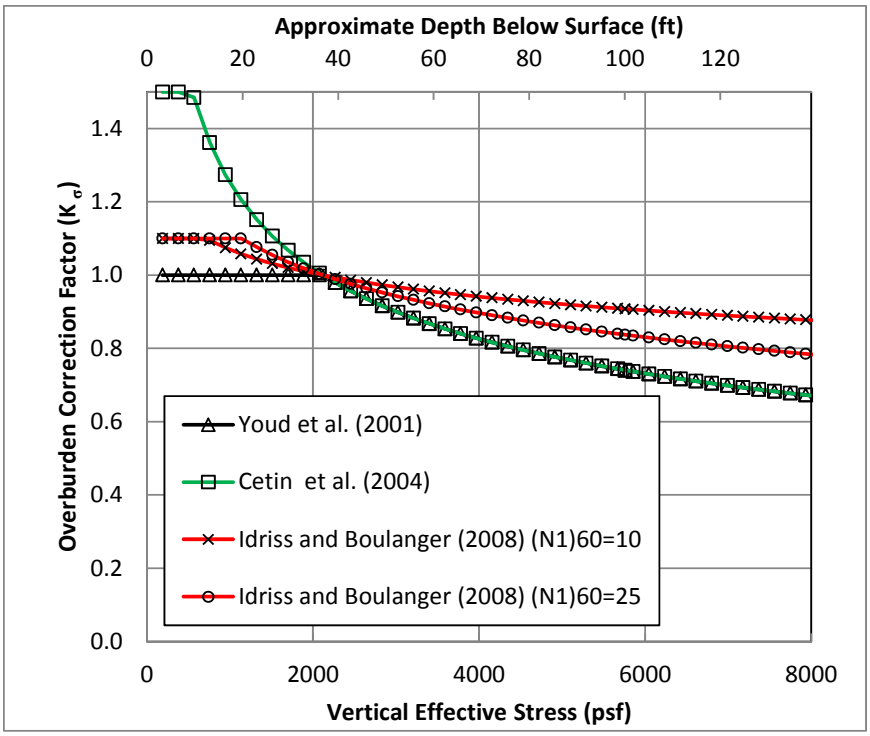

Figure 2.10. Comparison of all three Kσ correction factors as a function of vertical effective stress and approximate depth.

2.4.3 Magnitude Scaling Factor (MSF)

The magnitude scaling factor (MSF) is used to adjust the $CRR_{7.5,\ 1\ atm}$ to a site specific earthquake magnitude via Equation 2.8. This adjustment is necessary because of the strong correlation between CRR and the number of loading cycles the earthquake imparts to the soil (Seed et al. 1975). Although the MSF's can result in differences between the three most common liquefaction triggering procedures (refer to Figure 2.11), the MSF's are not a function of depth, and hence do not directly account for differences at high confining pressures. Furthermore, the MSF for all three procedures are virtually identical for $M_w > 7.0$.

Youd et al. (2001) published a range of acceptable values for the MSF, but the lower bound of that range was recommended for routine engineering practice. It is

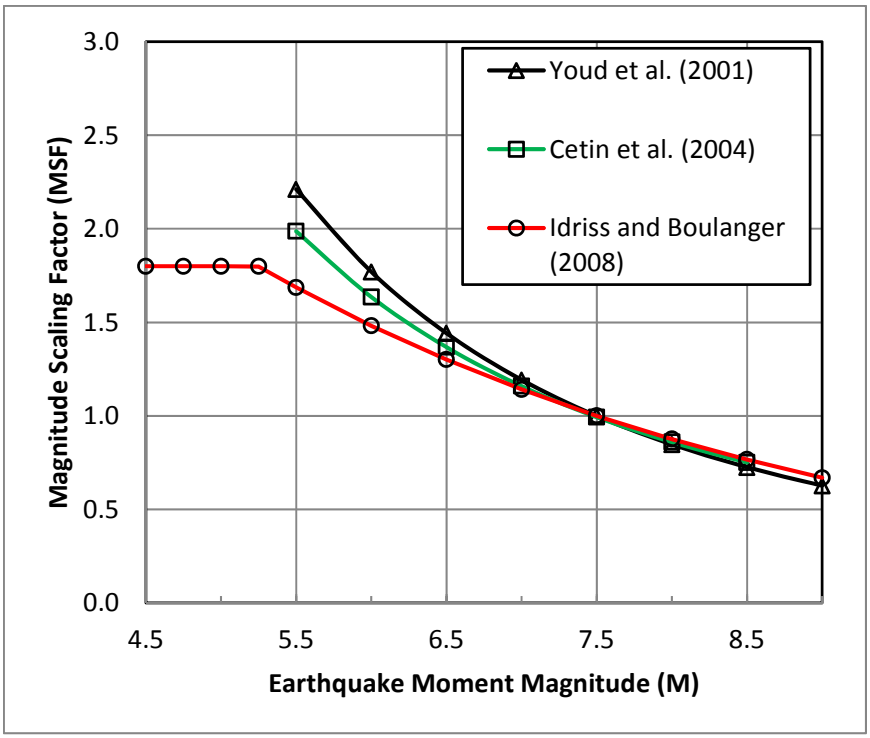

Figure 2.11. Magnitude scaling factors (MSF) of the three most commonly used procedures.

included as Equation 2.22. Cetin et al. (2004) presented the MSF graphically. In order to more easily use this relationship, their curve was digitized and a regression analysis was used to fit the data with an exponential equation, which is included as Equation 2.23. Idriss and Boulanger (2008) recommend an equation proposed by Idriss (1999), which is provided below as Equation 2.24. Equations 2.22-2.24 are plotted in Figure 2.11.

$$MSF = \frac{10^{2.24}}{M_w{}^{2.56}} \qquad \text{Equation 2.22}$$

$$MSF = 89.861 M_w{}^{-2.236} \qquad \text{Equation 2.23}$$

$$MSF = 6.9e^{\left(\frac{-M_w}{4}\right)} - 0.058 \qquad \text{Equation 2.24}$$

The lower-bound MSF proposed by Youd et al. (2001) plots above the MSF relationships of both Cetin et al. (2004) and Idriss and Boulanger (2008). At an earthquake M_w of 6.0, differences between the largest and smallest MSF's are almost 20%. In order to distinguish between depth dependent variables (i.e. r_d, C_N, $K\sigma$), a M_w of 7.5 can be utilized to eliminate any differences the MSF would induce. The mean earthquake magnitude used in code-based design for most sites in NE Arkansas (obtained from deaggregation) is so close to $M_w = 7.5$ that the impact of various MSF's is irrelevant.

2.5 FINE-GRAIN SCREENING CRITERIA

The evaluation of liquefaction triggering susceptibility of fine-grained soils is inseparably connected to both the percentage, and plasticity of the fines within the soil. Empirical procedures for screening fine-grained soils for liquefaction susceptibility were first developed following the Chinese earthquakes of Haicheng and Tangshan, in 1975 and 1976, respectively. Chinese researchers observed the liquefaction of silty sands and slightly silty sands in these earthquakes. Seed and Idriss (1982) documented these findings and the fine-grained screening criteria became known as the Chinese criteria (Andrews and Martin 2000, Cox 2001). These criteria applied three screens to evaluate fine-grained soils susceptibility to liquefaction triggering. If a soil had: (1) a clay content (% finer than 0.005 mm) less than 15%, (2) a liquid limit (LL) less than 35, or (3) an in-situ water content (w_c) greater than 90% of the LL, it was considered susceptible to liquefaction. Andrews and Martin (2000) used the case histories from earlier studies along with some newer histories to transpose the Chinese criteria to U.S. conventions (Seed et al. 2003).

Following the 1999 Adapazari earthquake, the Chinese criteria were found to be inadequate, and were strongly advised to be abandoned in practice (Seed et al. 2003, Bray and Sancio 2006). The main problem being, that the percentage of clay size particles was much less important than the plasticity of the fines within the soil (Bray et al. 2001). Seed et al. (2003) recommended an interim assessment of liquefaction susceptibility of fine-grained soils based on research in progress. These criteria were based on the plasticity index (PI), LL and in-situ w_c. They categorized fine-grained soils susceptibility into three zones; (1) a zone susceptible to classic cyclic liquefaction, (2) a transition zone, and (3) a zone where the fine-grained soils are not susceptible to classic liquefaction, but may still be vulnerable to cyclic degradation.

Bray and Sancio (2006) relied on the w_c, the LL, and PI to determine fine-grained soil liquefaction susceptibility. In this approach, the soil can be classified as: (1) susceptible, (2) moderately susceptible, or (3) not susceptible. To more easily represent the criteria presented by Bray and Sancio (2006), Table 2.1 is included along with Figure 2.12. The table and figure break the soil into groups depending on PI and w_c/LL ratio. If the PI if less than 12 and the w_c/LL is greater than 0.85, the soil is susceptible to classic cyclic liquefaction. If the PI is between 12 and 18 and the w_c/LL is greater than 0.8, the soil is moderately susceptible, and if the either the PI is greater than 18 or the w_c/LL is less than 0.8, the soil is not susceptible to classic cyclic liquefaction, but may still be susceptible to strain softening and degradation of strength during earthquake loading.

Idriss and Boulanger (2008) didn't classify the fine-grained soils as susceptible or not, but instead developed equations that can be used to determine the F.S. for fine-grained soils. First, the soil is classified as behaving more sand-like or clay-like

Table 2.1. Susceptibility of fine-grained soil to liquefaction triggering after Bray and Sancio (2006)

Susceptible	PI < 12	w_c/ LL > 0.85
Moderatly Susceptible	12 < PI < 18	w_c/ LL > 0.80
Not Susceptible	PI > 18	w_c/ LL <0.80

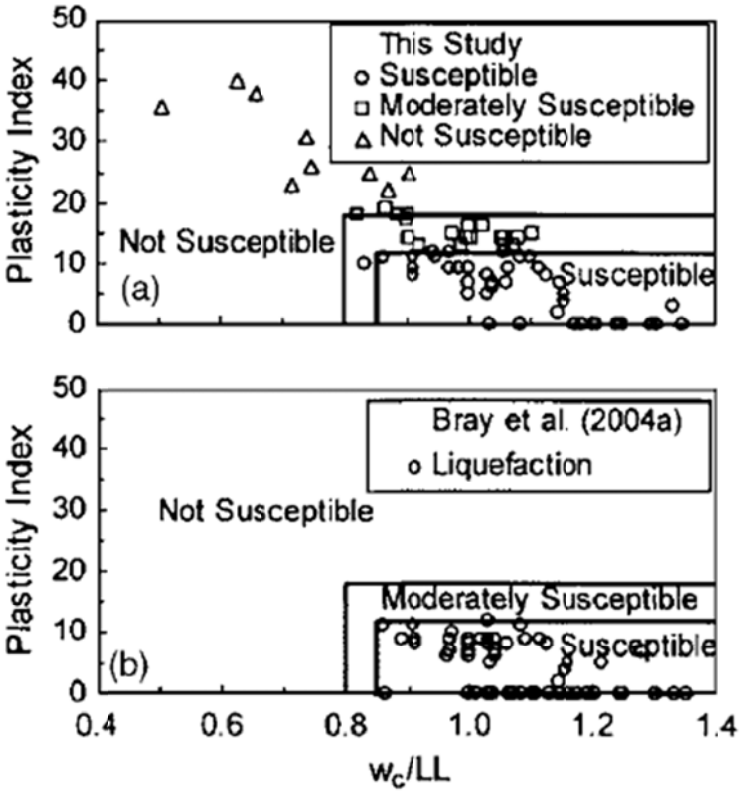

Figure 2.12. Graphical representation of fine-grained liquefaction susceptibility criteria (reproduced from Bray and Sancio 2006)

depending on the PI; if the PI ≥ 7 "clay-like" behavior is expected, if the PI < 7 "sand-like" behavior is expected. Sand-like behavior is analyzed in the traditional manner according to blow count, and is synonymous with classic defined "cyclic liquefaction". Clay-like behavior is analyzed according to the undrained shear strength of the soil and has been designated as "cyclic softening". Although previous researchers have noticed

the potential for clayey soil to degrade during earthquake loading (Seed et al. 2003, Bray and Sancio 2006), this F.S. computation for cyclic softening is the first attempt to quantify a clayey soils "liquefaction" susceptibility using simplified procedures.

The fine-grained screening criteria of Bray and Sancio (2006) has been incorporated into the workbooks of Youd et al. (2001) and Cetin et al. (2004). While, the "clay-like or "sand-like" procedures are incorporated in the Idriss and Boulanger (2008) workbook.

2.6 SUMMARY

Regarding evaluation of liquefaction triggering at depth (> 15 m [50 ft] or approximately 1.5 atm) via simplified procedures, the three variables most responsible for differences between the Youd et al. (2001), Cetin et al. (2004), and Idriss and Boulanger (2008) procedures are r_d, C_N, and K_σ. In terms of earthquake loading, the various r_d relationships tend to produce CSR's which are lowest for Cetin et al. (2004) and highest for Idriss and Boulanger (2008). It is common for these r_d relationships to vary by 30% or more at depths greater than 15 m (50 ft), yielding equal variations in the CSR estimates. In terms of soil resistance at depth, the various C_N relationships tend to yield $(N_1)_{60}$ values that are lowest for Youd et al. (2001) and highest for Idriss and Boulanger (2008). It is common for these C_N relationships to vary by 20% or more at depths greater than about 20 m (65 ft), yielding equal variations in the $(N_1)_{60}$ values obtained from the same raw blow count. General trends concerning Kσ are dependent on stress levels; at vertical effective stresses larger than 1 atm (2116 psf) the Youd et al. (2001) and Cetin et al. (2004) procedures are identical and yield the lowest CRR values.

The Idriss and Boulanger (2008) procedure produces Kσ values that are a least 10% greater than the others at effective confining stresses greater than 2 atm (4232 psf). Therefore, while the Idriss and Boulanger (2008) procedure will yield the highest CSR at depth, it will also tend to yield the highest CRR at depth.

Although these comparisons are important and help discern key differences in current liquefaction triggering procedures, it is important to realize the limitations of comparisons made in this broad manner. The figures depicting direct comparison between r_d, C_N, and Kσ, pose two main problems when used to infer overall differences between the F.S. predicted by each of the procedures: (1) relative differences on these plots may not transfer directly into the final F.S. because of how the various components within each procedure work together, and (2) the assumption of constant parameters with depth (such as $(N_1)_{60}$, F.C., etc..) used to make these plots are not consistent with site specific information. In order to overcome these obstacles, actual site specific liquefaction evaluations should be completed using each of the procedures and then comparisons between site specific r_d, C_N, Kσ, $(N_1)_{60}$, and other variables can be used to directly infer differences between the F.S. predicted by the three procedures. Site specific liquefaction triggering evaluations have been completed as part of this project and are included in Chapter 4.

Chapter 3

Liquefaction Triggering Workbook User's Guide

3.1 INTRODUCTION

Each of the three most commonly used SPT-based liquefaction triggering procedures (Youd et al. 2001, Cetin et al. 2004, and Idriss and Boulanger 2008) have been programmed into Microsoft Excel workbooks. The purpose of this chapter is to provide guidance for using these workbooks to perform a liquefaction susceptibility evaluation. The internal formulas within each workbook will not be discussed in detail, but some concepts regarding certain calculations warrant special attention and will be discussed herein. This user's guide is not all encompassing, and should be used to supplement the comments in the worksheet cells. The information will be most clear if read while viewing the worksheet under consideration.

Each of the workbooks are designed to work in English units. If Metric units are provided on the boring log, the user will have to convert them to English units before they are entered into the workbook. Likewise, if the user desires an output in Metric units the English units within the worksheet will have to be converted to Metric units. Some of the data within the workbooks are programmed in Metric units. This is done, only to remain consistent with the formulations in a particular procedure, and not as an invitation to enter Metric units into the workbooks.

3.2 WORKBOOK OVERVIEW

The workbooks are available in the 1997-2003 Microsoft Excel file format (i.e. [*.xls]), but where built using Microsoft Excel 2010 (i.e. [*.xlsx]), so directions expressed herein may not be exactly the same for versions other than 2010. The basic formats of the three workbooks are as similar as possible to facilitate data entry and information exchange from one workbook to another. After a brief section outlining some of the workbook similarities, a detailed section concerning the Youd et al. (2001) workbook will be discussed. Following the Youd et al. (2001) discussion, the Cetin et al. (2004) and Idriss and Boulanger (2008) workbooks will be discussed in detail. Some of the calculations in each workbook are identical, as such, the discussions for the Cetin et al. (2004) and Idriss and Boulanger (2008) workbooks will only focus on the portions that differ from the Youd et al. (2001) workbook. Before beginning the individual workbook sections, it is prudent to discuss the general appearance and common characteristics of the workbooks.

Each SPT-based liquefaction triggering workbook (i.e. individual Excel file) includes tabs near the bottom of the screen which allow the user to see different worksheets within the workbooks. A screenshot of the tabs is included as Figure 3.1. The tabs are labeled: Input Data, Calculations, Calculation Tables, Output Boring El., Output Grade El., Output Graphs, and References. The Idriss and Boulanger (2008) workbook contains one additional tab which is discussed in Section 3.5.

The Input Data tab is the only worksheet that requires input information from the user. The Calculation and Calculation Tables tabs are for the worksheets which are used to perform all the necessary calculations. The Output Boring El., Output Grade El., and

Figure 3.1. Individual worksheet tabs within the liquefaction triggering workbooks.

Output Graphs tabs are the worksheets used to display information from the Calculations worksheet in a more compact or graphical manner. The Reference tab houses all the references used in the development of the workbook.

The cells in all worksheets, except for the Input Data worksheet, are locked to prevent accidental data entry and modifications to the existing formulas. If the user desires to view the formula in a cell, simply select the cell and look in the formula bar. The worksheet does not need to be unlocked to view the formulas. The user should only unlock cells for a compelling reason (i.e. if a mistake in one of the formulas is identified and needs to be corrected). To unlock the worksheet cells, the user must access the Review menu on the Excel Ribbon bar, near the top of the screen, and select the Unprotect Sheet icon in the Changes panel. Then, enter the password, which is "UofA" (case sensitive) in the prompted menu.

In order for the Cetin et al. (2004) and Idriss and Boulanger (2008) worksheets to function properly, iterative calculations must be allowed. This is done in Microsoft Excel 2010 by accessing the File menu on the Ribbon bar and selecting Options. This should open the Excel Options menu, presented in Figure 3.2. Clicking on the Formulas option on the left of the menu will provide the user with the option to check the "Enable iterative calculation" box, which will allow the workbook to perform iterative calculations. If this box has not been checked, a circular reference warning will appear. If for some reason the circular reference warning doesn't appear despite the iterative calculation box not

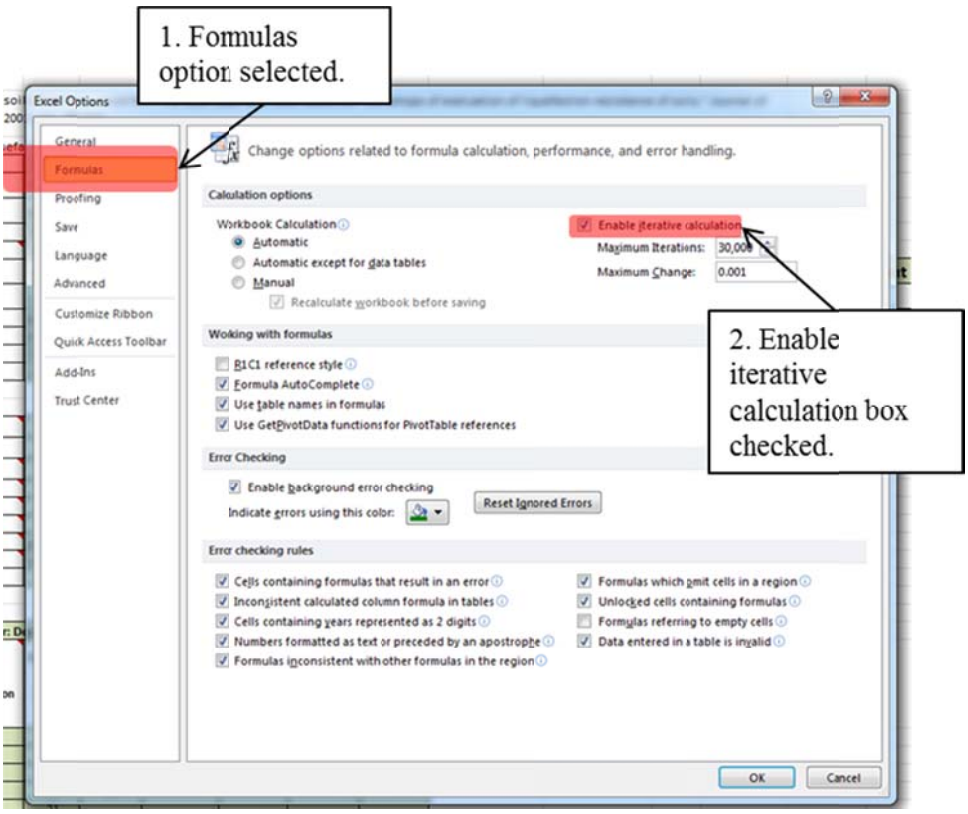

Figure 3.2. Excel Options menu with guidance for enabling iterative calculations.

being checked, the output tabs will have little or no information in them. This will serve as an additional reminder to activate iterative calculations.

3.3 YOUD ET AL. (2001) WORKBOOK

The Youd et al. (2001) SPT-based procedure is the result of a soil liquefaction workshop funded by the National Center for Earthquake Engineering Research (NCEER). The workshop was convened to establish the state of practice for soil liquefaction triggering and to update the simplified procedures. The symposium gathered experts in the field of liquefaction and attempted to reach a consensus about procedures used to predict liquefaction susceptibility. These recommendations, along with

engineering practicality and a proven track record, have made the Youd et al. (2001) procedure well accepted within the engineering community.

Many of the individual cells in the worksheets contain comments, as indicated by a red triangle in the upper right-hand corner of the cell. These comments explain, clarify, or expound on the function and use of the worksheet cells. This user's guide will not specifically address each comment, but will present what information should be entered into each of the cells, starting with the Input Data worksheet. This guide has been written to accompany the worksheets and it may be beneficial to have a copy of the worksheets readily accessible while reading.

3.3.1 Input Data

Most of the Input Data necessary for the soil liquefaction triggering evaluation should be available from the boring logs obtained during the site investigation and subsequent laboratory testing. Note that **only the cells highlighted in a light green color should be input**. All other cells should not be altered. The first group of input cells, rows 5-15, at the top of the Input Data worksheet (refer to Figure 3.3), primarily contain job identification information such as: job number, job name, job location (latitude and longitude), date of boring, drilling equipment, type of drilling, hammer energy, etc. Most of these cells are for documentation purposes only. However, the hammer energy correction factor is critical, as it is used to correct the measured SPT blow count (N) to the standardized N_{60} value (refer to Section 2.4.1). The hammer energy correction factor (C_E) is equal to the measured hammer energy ratio (in percent) divided by the standard energy ratio of 60%. If hammer energy has not been measured

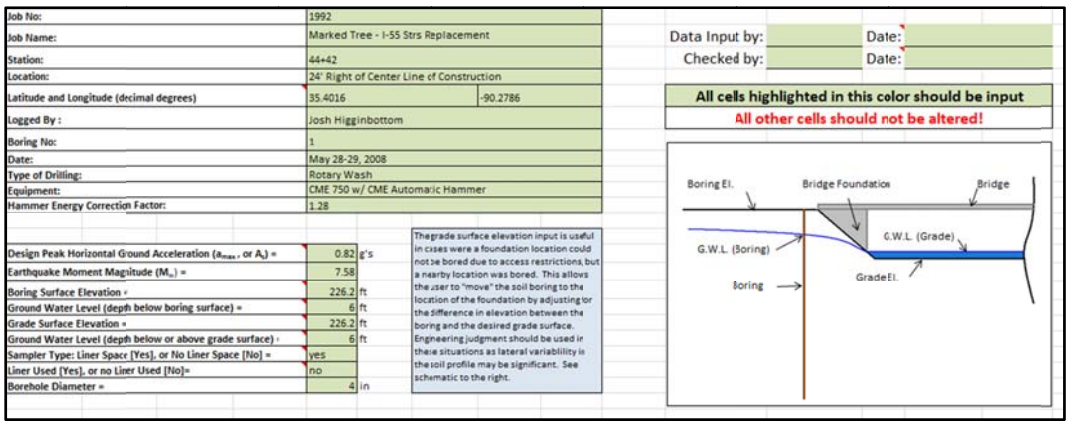

Figure 3.3. Input Data worksheet with job identification information and site specific input options.

directly, the user should assume a hammer energy correction factor of 1.0 (i.e. 60% energy ratio).

The Data Input by and Checked by boxes can be used in one of two ways. The initials of the user can be typed into the boxes and they will be copied to the Output worksheets, or after the input and output pages have been printed the user can initial them by hand. If the date is typed it must be entered in the correct format so that it can be properly copied throughout the workbook. The chosen format is month/day/year separated by a backslash in numerical format (i.e. October 11, 1984 should be entered 10/11/84).

The remaining input cells, rows 18-26, shown in the bottom left-hand corner of Figure 3.3, are critical for the liquefaction calculations and have been grouped together. Cells in this group include the design peak horizontal ground acceleration (a_{max} or As), earthquake moment magnitude (M_w), boring surface elevation, ground water level below boring surface, grade surface elevation, ground water level below grade surface, etc. Each of these items is discussed in more depth below.

3.3.1.1 Design Peak Ground Acceleration and Moment Magnitude

All of the workbooks require the design peak horizontal ground acceleration and the earthquake moment magnitude to be entered in the Input Data worksheet. These values must be obtained using external sources such as building codes and the U.S. Geological Survey website (www.usgs.gov).

The selection of design peak horizontal ground acceleration is generally controlled by procedures recommended by the appropriate governing body/building code. Regardless of the code used, the procedures should contain provisions for obtaining ground motions on "rock" for a given return period or annual rate of exceedance (e.g. the 2500 year ground motions, or equivalently the ground motions with a 2% probability of exceedance [PE] in 50 years). After obtaining the "rock" ground motions, the code should provide guidance for adjustment to site-specific soil conditions. While the selected rate of exceedance varies between codes (e.g. 2% PE in 50 years for IBC and ASCE-7, versus 7% PE in 75 years for AASHTO), the simplified procedures used to account for local site conditions are generally the same for all U.S. codes.

As this guide is meant primarily for those involved in bridge design, only the procedures recommended by AASHTO will be discussed herein. The peak horizontal ground acceleration adjusted for site classification (As, or a_{max}) is obtained using the software provided with AASHTO (2009). In order to use this software properly, the user must know: (1) the latitude and longitude of the bridge location, and (2) the seismic site classification based on Table 3.4.2.1-1 in the AASHTO (2009) guide specifications (reproduced below as Table 3.1).

Table 3.1. Site Class definitions reproduced from AASHTO 2009

Site Class	Soil Type and Profile
A	Hard rock with measured shear wave velocity, Vs > 1500 m/s [5000 fps]
B	Rock with 760 m/s [2500 fps] < Vs < 1500 m/s [5000 fps]
C	Very dense soil and soil rock with 360 m/s [1200 fps] < Vs < 760 m/s [2500 fps], or with either N > 50 blows/ft or Su > 100 kN/m^2 [2.0 ksf]
D	Stiff soil with 180 m/s [600 fps] < Vs < 360 m/s [1200 fps], or with either 15 blows/ft < N < 50 blows/ft or 50 kN/m^2 [1.0 ksf] < Su < 100 kN/m^2 [2.0 ksf]
E	Soil profile Vs < 180 m/s [600 fps], or with either N < 15 blows/ft or Su < 50 kN/m^2 [1.0 ksf], or any profile with more than 3 m [10 ft] of soft clay defined as soil with PI > 20, w_c > 40%, and Su < 25 kN/m^2 [0.5 ksf]
F	Soils requiring site-specific ground motion response evaluations, such as: Peats of highly organic slays (H > 3 m [10 ft] of peat or highly organis clay, where H = thickness of soil) Very high plasticity clays (H > 7 m [25 ft] with PI > 75) Very thick soft/medium stiff clays (H > 35 m [120 ft])

The worksheets have the ability to automatically determine the seismic site classification for Site Classes C, D and E using the raw SPT blow count (N) values from the boring log. However, the user must explicitly check to see if the site classifies as Site Class E or F using the criteria specified in Table 3.1. After the boring log information has been entered into the Input Data worksheet, the seismic site classification will be calculated and displayed in the Calculations, Output Boring El., and Output Grade El. worksheets. The classification is in a large yellow box near the top of each worksheet. In order for the workbook to determine the site classification, the boring must be complete to at least 95 feet below the boring surface elevation. If the boring is terminated at depths less than 95 feet, no classification can be determined automatically within the worksheet and the user will have to classify the site by other means.

Once the seismic site classification has been determined, As/a_{max} can be obtained from the USGS probabilistic ground motion hazard maps. AASHTO requires that ground motions with a 7% PE in 75 years be used. These ground motions have been

programmed into the CD titled "Seismic Design Parameters Version 2.10" by the USGS (2008), which is provided with AASHTO (2009). This CD allows the user to specify the latitude and longitude coordinates, calculate PGA for a rock site (Site Class B). Then adjust the rock PGA to an equivalent site-adjusted design value (As or a_{max}) using site amplification factors based on the site classification. The user may perform these steps by either clicking on the "Calculate As, SDs, and SD1" button, or the "Design Spectrum" button (refer to Figure 3.4). However, the author recommends using the "Design Spectrum" button because a bug exists in the "Calculate As, SDs, and SD1" calculations, wherein incorrect values of As can be obtained. The bug appears to be caused by using the site amplification factor for short-period spectral acceleration (Fa) instead of the site amplification factor for PGA (Fpga). However, this bug does not exist when using the "Design Spectrum" button directly to obtain As. When using the "Design Spectrum" option, the design peak ground acceleration (As, or a_{max}) is the spectral acceleration (Sa) at a period of 0.0 sec (refer to Figure 3.4). As a check, the user should always ensure that this value has been properly adjusted for local soil conditions (i.e. site classification) using the proper site amplification factors.

The proper design earthquake magnitude (M_w) can be found using the 2008 Interactive Deaggregation software available on the web from the USGS. The site can be accessed directly using <http://eqint.cr.usgs.gov/deaggint/2008/index.php>, or by logging onto <www.usgs.gov> and entering "deaggregation" into the search bar. Regardless, the link titled 2008 Interactive Deaggregation (Beta) needs to be used. The website offers instructions about how to use the deaggregation software. The deaggregation calculation box is presented in Figure 3.5. The return period that should be used, for deaggregation

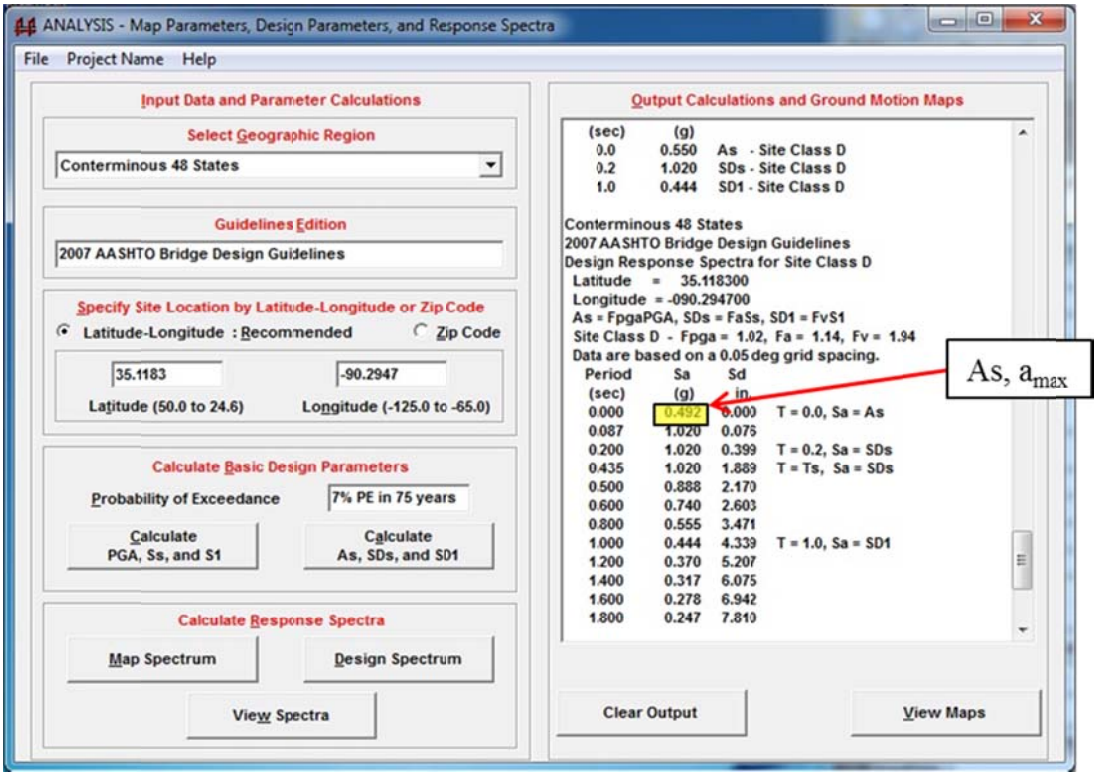

Figure 3.4. Seismic Design Parameters Version 2.10 from the USGS, included with AASHTO (2009).

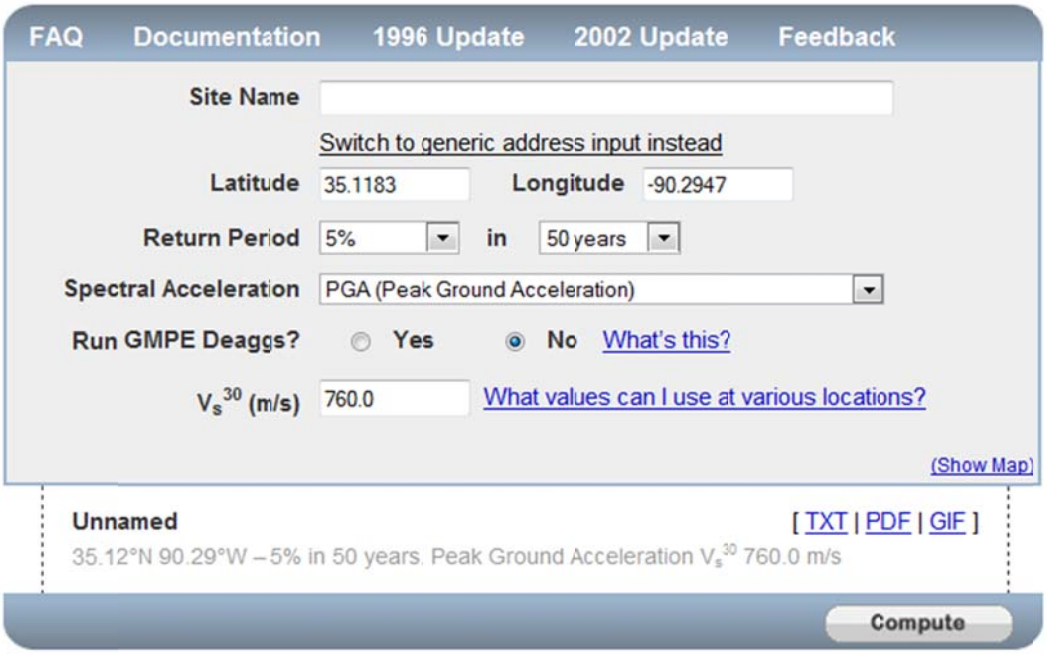

Figure 3.5. 2008 Interactive Deaggregation (Beta) website, available from the USGS.

according to AASHTO (2009), is 5% in 50 years. Peak Ground Acceleration (PGA) should be selected from the spectral acceleration dropdown box. The average shear wave velocity over the top 30 m (100 ft) (Vs^{30}) may be left as the default value of 760 m/s (i.e. a rock site classification) if site specific data is not available. The "Compute" icon will calculate the magnitude deaggregation. Both the mean and modal magnitudes are calculated in this analysis, and in many cases for the NMSZ the two magnitudes are nearly the same. In the author's opinion, the mean magnitude is the closest match to the deaggregation magnitude selection techniques discussed in Finn and Wightman (2010) and should be used within the workbooks provided. The user can read the mean magnitude from one of the three output file options (TXT, PDF, GIF).

3.3.1.2 Boring Elevation versus Grade Elevation

This worksheet includes the option for entering two reference elevations. One reference elevation is for the actual boring performed (i.e. the Boring Surface Elevation). The other reference elevation (i.e. the Grade Surface Elevation) is included so that liquefaction potential can be evaluated at a nearby location that couldn't feasibly be drilled. Both of these reference elevations require a separate Ground Water Level to be entered into the corresponding labeled cells. The worksheet will allow the user to enter water levels above or below the reference elevations. Note that the *elevations* of the water table are not input, but rather a depth/distance below or above the respective reference surface is input. Water levels above the grade and boring elevations should be input as a negative number (i.e. if the boring was completed through 5 feet of water enter the value -5). Figure 3.3 includes a schematic found in the worksheet to help the user

remember which elevation to assign each cell. The schematic depicts a situation where the boring was completed behind the abutment of the bridge (Boring Surface Elevation) instead of the river bottom (Grade Surface Elevation) near the future location of the bridge foundation.

Boring surface elevations should be included within the boring logs, while the grade surface elevations may require information from topographic maps, bathymetry, or other sources. When calculating the liquefaction potential at the grade elevation, the boring log data is simply ignored from the boring surface elevation down to the grade surface elevation. Furthermore, the stresses are re-calculated based on the new grade surface elevation and water table locations. Engineering judgment should be employed when using the Grade Surface Elevation due to lateral variability within the soil profile. Meaning, care should be taken when assuming the soil profile behind an abutment is representative of the soil profile at an intermediate pier.

3.3.1.3 Sampler Type and Borehole Diameter Correction Factors

To incorporate sampler correction factors, yes or no answers must be entered into two cells: (1) the Sampler Type cell identifies if the sampler has room for liners or not [enter Yes or No], and (2) the Liner Used cell indicates if the sampler was used with or without liners [enter Yes or No]. It is common for AHTD to use samplers which have liner space and not use the liners. Therefore, as shown in Figure 3.3, Yes should be entered into the Sampler Type input cell, while No should be entered into the Liner Used input cell. The Borehole Diameter input cell is used to account for the borehole correction factor, which only applies to boreholes larger than 115 mm (4.5 in). The diameter of the borehole should be specified on the boring logs.

3.3.1.4 Depth-dependent Input Data

The remaining input information is all depth dependent. The headings for columns A through J are shown in Figure 3.6. The first two columns, Sample Number and Elevation at Sample Location, are composed of values that have been calculated directly in the worksheet. No values should be directly input by the user into these columns, they simply contain information that should aid the user in tracking individual sample locations (depths) throughout the workbook. To better explain the remaining data input columns, each of the individual column headings are discussed below in separate paragraphs.

Depth to Sample Location (ft) – This is the depth at which each SPT sample was obtained relative to the boring surface elevation. Typically, the interval between SPT sample locations is a constant number such as 1 m or 1.5 m (3 ft or 5 ft). This information is available on the boring log.

USCS Classification – The user **must input the Unified Soil Classification System (USCS) designation for each depth**. This information should be provided on the boring log if sufficient laboratory tests (i.e. grain size analysis and Atterberg Limits) have been performed on the split-spoon samples. For dual classifications, the user should enter both symbols separated with a dash and no spaces (i.e. SW-SP). If the USCS designation is not provided, the user will have to assign a USCS designation for each sample using the general soil descriptions included on the boring log. As stated within the cell comment in the worksheet, the user can assume CL for clays, ML for silts, SP for sands and GP for gravels if no additional information is provided. A USCS designation

		Must Enter: Depth, USCS Classification (estimate if unknown) and N value							
Sample Number	Elevation at Sample Location (ft)	Depth to Sample Location (ft)	USCS Classification	Raw SPT Blow Count, N	Fines Content (%)	Measured Unit Weight of Soil (pcf)	Plastic Limit, PL	Liquid Limit, LL	In-Situ Water Content, w_c

Figure 3.6. Headings for columns A-J in the Input Data worksheet.

is necessary to correlate unit weight and to determine if the soil is "cohesive" or "cohesionless". No output data will be available if a USCS designation is not input.

Raw SPT Blow Count (N) – The raw blow count is available from the boring log. If the recorded value is "0" (i.e. weight of the rod) a value of "1" should be entered so that further correction factors can be applied.

Fines Content (%) – If possible, the fines content (F.C.) should be measured from split-spoon samples recovered during testing because liquefaction susceptibility has been shown to be dependent on F.C. (refer to Section 2.2). If the F.C. has not been measured, leave the cell blank and a conservative value (i.e. a F.C. $\leq$ 5%) will be assigned.

Measured Unit Weight of the Soil – If this value has not been measured in the laboratory (which it rarely is), leave the cell blank and a typical value will be assigned based on the USCS designation and blow count information. The unit weight correlation is based on a relationship presented in Teng (1962). It is provided in the Calculation Tables worksheet and discussed below in Section 3.3.2.1.

Plastic Limit, Liquid Limit, and In-situ Water Content – This information helps determine the fine-grained liquefaction susceptibility of the soil, as detailed within Section 2.5. If this information has not been determined, or if the soil is non-plastic, leave these cells blank.

3.3.2 Calculations and Calculation Tables Worksheets

The Calculation and Calculation Tables worksheets are the backbone of the entire workbook. Data is transferred into these worksheets from the Input Data worksheet, and data is copied out of these worksheets into the various output worksheets. These worksheets should not be altered unless a mistake is found in the calculations. If the user is comfortable with the liquefaction calculations, these worksheets will not need to be viewed during routine liquefaction evaluations. In order for the user to have a sense of how these worksheets compute and use information, a review of each of the columns will be presented. Additionally, many of the column headings in the workbooks include cell comments, which provide clarification concerning the column's function.

When the Calculations worksheet is first viewed, the user will notice that most of the information entered into the Input Data worksheet has been copied over to this worksheet (refer to Figure 3.7). However, the user must not try to re-enter or change data in the Calculations worksheet. The cells have been locked to prevent this mistake. As shown in the lower left-hand corner of Figure 3.7, many of the standard blow count correction factors that are not depth-dependent (i.e. hammer energy, borehole diameter, sampler liner) are calculated directly below the Input Data in rows 26-33. The magnitude scaling factor is also calculated in this block of cells. The specific equations and tables from the Youd et al. (2001) paper that were used to obtain these factors are referenced in the cells so the user can easily follow the worksheet development.

It will be noted that row 33 was originally reserved for the sloping ground correction factor (K_α). However, this function was removed from the spreadsheet

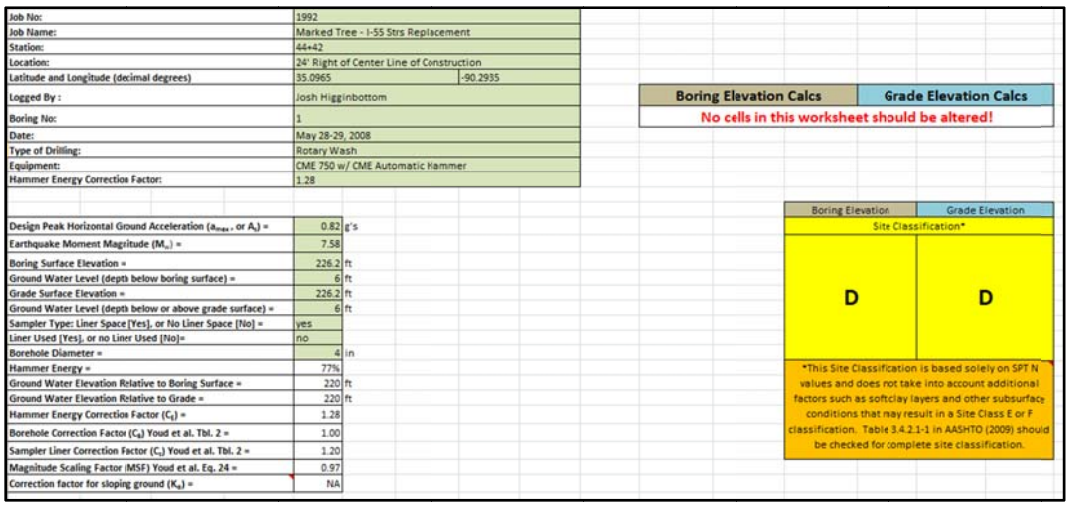

Job No:	1992	
Job Name:	Marked Tree - I-55 Strs Replacement	
Station:	44+42	
Location:	24' Right of Center Line of Construction	
Latitude and Longitude (decimal degrees)	35.0965	-90.2935
Logged By :	Josh Higginbottom	
Boring No:	1	
Date:	May 28-29, 2008	
Type of Drilling:	Rotary Wash	
Equipment:	CME 750 w/ CME Automatic Hammer	
Hammer Energy Correction Factor:	1.28	

Design Peak Horizontal Ground Acceleration (a_{max}, or A_s) =	0.82	g's
Earthquake Moment Magnitude (M_w) =	7.58	
Boring Surface Elevation =	226.2	ft
Ground Water Level (depth below boring surface) =	6	ft
Grade Surface Elevation =	226.2	ft
Ground Water Level (depth below or above grade surface) =	6	ft
Sampler Type: Liner Space [Yes], or No Liner Space [No] =	yes	
Liner Used [Yes], or no Liner Used [No]=	no	
Borehole Diameter =	4	in
Hammer Energy =	77%	
Ground Water Elevation Relative to Boring Surface =	220	ft
Ground Water Elevation Relative to Grade =	220	ft
Hammer Energy Correction Factor (C_E) =	1.28	
Borehole Correction Factor (C_B) Youd et al. Tbl. 2 =	1.00	
Sampler Liner Correction Factor (C_S) Youd et al. Tbl. 2 =	1.20	
Magnitude Scaling Factor (MSF) Youd et al. Eq. 24 =	0.97	
Correction factor for sloping ground (K_α) =	NA	

Boring Elevation Calcs	Grade Elevation Calcs
No cells in this worksheet should be altered!	

Boring Elevation	Grade Elevation
Site Classification*	
D	D

*This Site Classification is based solely on SPT N values and does not take into account additional factors such as softclay layers and other subsurface conditions that may result in a Site Class E or F classification. Table 3.4.2.1-1 in AASHTO (2009) should be checked for complete site classification.

Figure 3.7. Calculations worksheet, job identification and site classification.

because there is a lack of consensus on how to handle static driving shear stresses in soil liquefaction triggering. Therefore, the correction factor for sloping ground is not accounted for in this spreadsheet and the cell is populated with 'NA' to notify the user of this fact.

The large yellow boxes shown in Figure 3.7 contain the seismic site classification previously discussed in Section 3.3.1.1. The user will note that there is a separate site classification for both the boring surface reference elevation and the grade surface reference elevation (refer to Section 3.3.1.2). However, in order for the grade elevation site classification to be calculated automatically, the soil boring must extend at least 30m (100 ft) below grade elevation, which could require the boring to extend significantly deeper than the 30 m (100 ft) required for the boring surface elevation, depending on the height of the embankment. The calculations used to provide these site classifications are discussed in greater detail below.

3.3.2.1 Depth-dependent Calculations

The remaining calculations are all depth dependent and are associated with a given SPT sample location. When viewing the Calculations worksheet, the user will note that many more columns are populated than in the Input Data worksheet (i.e. from column K through column AL). The Calculations worksheet is also split vertically, with rows 35-65 being dedicated to calculations relative to the boring surface elevation, and rows 67-97 being dedicated to calculations relative to the grade surface elevation (refer to Section 3.3.1.2).

For clarity, each of the column headings in the Calculations worksheet will be discussed below in the same order as they are presented within the worksheet. Each column heading will be followed by information regarding the function of the column. Once again, the user is reminded that additional useful comments may be provided in the cells within the worksheet. These comments are indicated by red triangles in the upper right-hand corner of the cell. Furthermore, whenever possible, the specific equations from the Youd et al. (2001) paper that were used to program the calculations are referenced in the column headings so the user can easily follow the worksheet development. To avoid repetition, the column headings copied directly from the Input Data worksheet will not be discussed again. Also, a few of the calculation column headings have been grouped together for discussion purposes. The calculations performed in columns K-R are discussed below. For reference, these column headings are presented in Figure 3.8.

General Soil Type – This column uses a lookup function based on the USCS soil classification to determine general "cohesive" or "cohesionless" soil behavior. A table

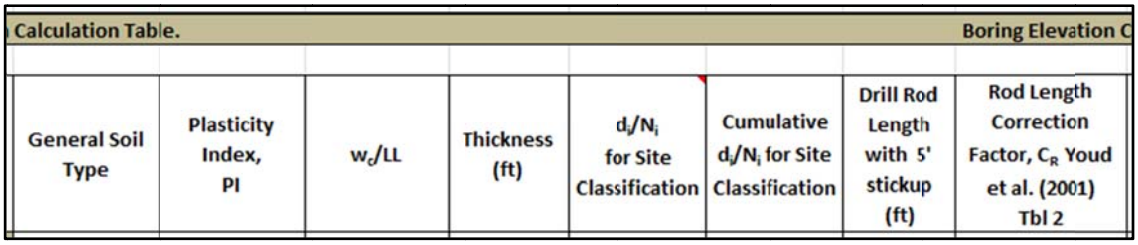

Figure 3.8. Headings for columns K-R in the Calculations worksheet.

titled General Soil Classification based on USCS has been used to make this determination and can be found in the Calculation Tables worksheet.

Plasticity Index – This column determines the Plasticity Index (PI) of the soil based on the Plastic Limit (PL) and Liquid Limit (LL) entered in the Input Data worksheet. If the necessary index tests have not been performed, the column will simply return a "cohesive" or "cohesionless" designation based on the General Soil Type.

w_c/LL – This column divides the water content (w_c) by the LL if these values were provided in the Input Data worksheet. This ratio is helpful in determining the liquefaction susceptibility of fine-grained soils, as described in Section 2.5. This column will simply return a general "cohesive" or "cohesionless" designation if the needed laboratory tests have not been performed.

Thickness – This column determines the thickness of the layer in question. The layer thicknesses are necessary in order to determine seismic site classification, and the stresses within the soil profile.

d_i /N_i and Cumulative d_i /N_i – These two columns are used to calculate the individual and cumulative values of layer thickness divided by blow count that are necessary for seismic site classification via SPT blow count. The Method B procedures

outlined on pages 3-43 thru 3-46 of Section 3.4.2 in AASHTO (2009) were used. These procedures are identical to the SPT seismic site classification procedures found in IBC (2009). The actual site classification is obtained from these calculations using a lookup command relative to a table titled Site Classification Based on SPT N Values in the Top 100 ft found in the Calculation Tables worksheet. The resulting site classification is displayed in the large yellow boxes at the top of the worksheet, as discussed above. The user is reminded of the discussion on appropriate site classification found in Section 3.3.1.1 of this chapter.

Drill Rod Length and Rod Length Correction Factor (C_R) – The Drill Rod Length column calculates the total length of the drill rod by assuming that the rod sticks up above the ground surface 1.5 m (5 feet). The Drill Rod Length Correction Factor column uses the drill rod length to look up C_R from the Drill Rod Length Correction Factor table in the Calculation Tables worksheet. The C_R values in the Grade Elevation Calculation Table are copied directly from the Boring Elevation Calculation Table, and not calculated independent of the actual data collected at the boring elevation.

The calculations performed in columns S-Z are discussed below. For reference purposes, these column headings are presented in Figure 3.9.

N_{60} Only Corrected for Energy – This column is used to determine the blow count corrected to 60% hammer efficiency. This column is only used to correlate unit weight of the soil and is not used for successive liquefaction triggering calculations.

Total Unit Weight of the Soil – A lookup formula in this column uses a table titled N Value – Unit Weight Correlation found in the Calculation Tables workbook to

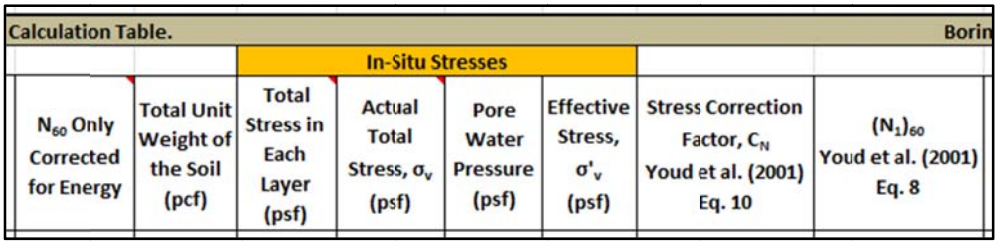

Figure 3.9. Headings for columns S-Z in the Calculations worksheet.

determine approximate soil unit weight using the relationship presented in Teng (1962). The correlation is based upon the general soil type and the blow count corrected for energy (N_{60}). This correlation was originally published using N instead of N_{60}. However, it was assumed herein that most hammers in use at that time were approximately 60% efficient. Therefore, for the purpose of estimating unit weight, N_{60} is used within the worksheet to correlate unit weight instead of N. If the unit weight has been measured and entered in the Input Data worksheet (refer to Section 3.3.1.4) it will override this correlation.

In-Situ Stresses – The in-situ stress calculations are calculated in a four-column group using the elevation data, unit weight and thickness to compute the total, pore water, and effective stresses within the soil column. The total stress computation assumes that the total unit weight of the soil layer between sample intervals is constant. This assumption is reasonable so long as small sampling intervals (≈ 1.5 m [5ft]) are maintained.

Stress Correction Factor (C_N) – Here, the standardized overburden blow count correction factor is calculated based on the effective stresses in the soil column. The

relationship proposed by Kayen et al. (1992), and detailed in Youd et al. (2001), has been used. Additional details on stress correction are provided in Section 2.4.1.

$(N_1)_{60}$ – All of the blow count correction factors (C_N, C_R, C_B, C_E, C_S) are multiplied by the raw blow count (N) to determine the corrected blow count [$(N_1)_{60}$]. The $(N_1)_{60}$ values are always rounded down to the nearest whole number.

The calculations performed in columns AA-AF are discussed below. For reference purposes, these column headings are presented in Figure 3.10.

Alpha (α) – Alpha is calculated based on the fines content information provided in the Input Data worksheet and the formulas detailed in Youd et al. (2001). If fines content has not been input, alpha is conservatively assumed equal to zero.

Beta (β) – Beta is calculated based on the fines content information provided in the Input Data worksheet and the formulas detailed in Youd et al. (2001). If fines content has not been input, beta is conservatively assumed equal to one.

$(N_1)_{60cs}$ – This column utilizes alpha and beta to calculate an equivalent clean sand blow count [$(N_1)_{60cs}$]. This clean sand equivalent blow count is used to calculate the CRR of the soil.

Stress Reduction Coefficient (r_d) – This column uses a lookup function to determine r_d. The stress reduction coefficient is actually calculated in the Calculation Tables worksheet within the Stress Reduction Coefficient table. The comment in this column heading is from the r_d figure contained in Youd et al. (2001), and reminds the user that the simplified procedure is not verified with case history data for depths greater

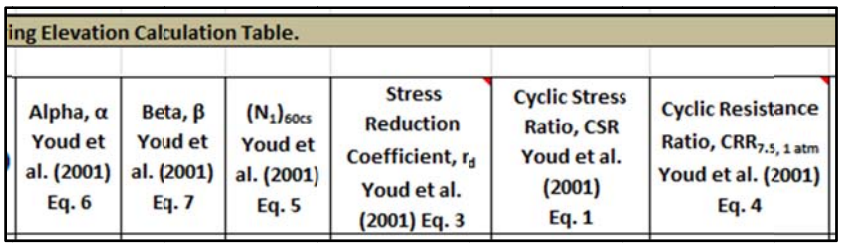

Figure 3.10. Headings for columns AA-AF in the Calculations worksheet.

than 50 feet. The user will note that significant scatter exists in various r_d relationships and that this scatter increases with depth (refer to Section 2.3.1).

Cyclic Stress Ratio (CSR) – This column calculates the cyclic stress ratio imparted by the earthquake, and the same formula is used for all of the simplified procedures (refer to Section 2.3).

Cyclic Resistance Ratio ($CRR_{7.5, 1\ atm}$) – This calculation is unique for each of the three procedures. In this workbook, it is calculated using $(N_1)_{60cs}$, as specified in Youd et al. (2001). If the $(N_1)_{60cs}$ value is larger than 30 blows/ft, a large CRR of 2.0 is assigned to account for the fact that the soil is classified as non-liquefiable according to the Youd et al. (2001) procedure (refer to Section 2.4). Once a CRR of 2.0 has been assigned, the F.S. calculation is meaningless. To account for this, both the preliminary and final factors of safety are assigned a value of 2.0.

The calculations performed in columns AG-AL are discussed below. For reference purposes, these column headings are presented in Figure 3.11.

Overburden Correction Factor (Kσ) – The calculation of Kσ is based on the exponential factor "f", a variable within the Kσ equation which depends on the density of the soil (refer to Section 2.4.2). This f exponent ranges from 0.6 - 0.8 based on relative

Boring Elevation Calculation Table.					
		Fine-grained Soil Screening			
Overburden Correction Factor, Kσ Youd et al. (2001) Eq. 31	Preliminary Factor of Safety, F.S. Youd et al. (2001) Eq. 23	Bray & Sancio (2006) PI Criteria	Bray & Sancio (2006) w_c/LL Criteria	Final F.S.	Liquefaction Occurrance Check

Figure 3.11. Headings for columns AG-AL in the Calculations worksheet.

density, as discussed in Youd et al. (2001). Therefore, the relative density has been determined from the corrected blow count, $(N_1)_{60}$, using Equation No. 37 from Idriss and Boulanger (2008). The maximum and minimum relative densities that are applicable to the Kσ evaluation, according to Youd et al. (2001), are 80 and 40%, respectively. These maximum and minimum relative densities correlate to $(N_1)_{60}$ values of about 30 and 7 blows/foot, respectively. Accordingly, blow counts above 30 are assigned a relative density of 80%, and blow counts below 7 are assigned a relative density of 40%. Blow counts between 30 and 7 are correlated to relative density using the Idriss and Boulanger (2008) equation directly. Once relative densities are correlated, f can be determined. An f value of 0.8 is assigned to relative densities less than or equal to 40% (i.e. blow counts less than or equal to 7), and an f value of 0.6 is assigned to relative densities greater than or equal to 80% (i.e. blow counts greater than or equal to 30). Intermediate values of f are linearly interpolated according to the relative density of the soil. The table containing this correlation is included in the Calculation Tables worksheet titled Exponential "f" factor for Kσ Equation.

Preliminary Factor of Safety (F.S.) – This column contains a preliminary assessment of the factor of safety against soil liquefaction triggering at each depth. The MSF and Kσ factors are both applied to the F.S. in this column. This F.S. is preliminary

because it only considers if the soil is soft enough to liquefy, based upon SPT blow count, and does not consider the type of soil. Cohesive soils must be further evaluated according to the fine-grained screening criteria of Bray and Sancio (2006) to determine the final F.S. Soil layers with a CRR of 2.0 are automatically assigned a preliminary F.S. of 2.0. Soil layers above the water table are classified as "Unsat", and can be assumed non-liquefiable.

Bray and Sancio (2006) PI and w_c/LL Criteria – These criteria can only be evaluated if the proper laboratory tests have been completed. If no laboratory testing has been performed, these columns will simply display either a "cohesive" or "cohesionless" soil designation. It will then be up to the user to decide if the cohesive soils are potentially liquefiable or not. If the proper laboratory tests have been completed, the calculations performed in each column will be used to designate the soil as susceptible (Sus), moderately susceptible (Mod Sus), or not susceptible (Not Sus) to liquefaction, according to the Bray and Sancio (2006) criteria outlined in Section 2.5. In order for the soil to classified as susceptible both the PI and w_c/LL criteria must be met (i.e if either the PI or w_c/LL criteria classify the soil as Not Sus then the soil is not susceptible.

Final F.S. – The final factor of safety uses the preliminary factor of safety and the fine-grained screening criteria to determine a final "factor of safety" against soil liquefaction triggering. Possible designations in the final F.S. column include: (1) a numerical F.S. between 0.00 - 2.00, (2) "2.00" (assigned to any soil with a preliminary F.S. $\geq$ 2.00 based on high penetration resistance), (3) "Unsat" (assigned for soils above the water table), (4) "Not Sus" (designates that the fine-grained soils were screened and determined not susceptible in previous columns), or (5) "Cohesive" (designates that the

fine-grained soils have not had the proper screening tests performed and the preliminary factor of safety is less than 1.0). Soils designated as "Cohesive" require the user to apply engineering judgment to determine liquefaction susceptibility.

Liquefaction Occurrence Check – This column provides an easy way to visualize the final factor of safety. Here, any numerical factor of safety greater than 1.0 is designated "Unlikely" (meaning liquefaction is unlikely) and any factor of safety less than 1.0 is designated "Likely" (meaning liquefaction is likely). Keep in mind that designations of "Unlikely" or "Likely" do not relive the user of the responsibility to exercise engineering judgment for factors of safety near unity. The designation of "Cohesive" is carried forward for silts and clays if the preliminary F.S. is less than 1.0 and no laboratory tests have been performed to rule out liquefaction susceptibility via the fine-grained screening criteria. For soil layers above the water table, the designation of "Unsat" is carried forward from the final F.S. The engineer must ensure that fluctuating, or worst-case, water levels are taken into account when the ground water level is specified in the Input Data worksheet.

3.3.2.2 Calculation Tables

The Calculation Tables worksheet contains seven tables that are utilized within the Calculations worksheet through lookup functions. These seven tables include: (1) N Value - Unit Weight Correlation (Teng 1962), (2) Drill Rod Length Correction Factor, (3) Borehole Diameter Correction Factor, (4) Stress Reduction Coefficient, (5) General Soil Classification based on USCS, (6) Site Classification based on SPT N Value in the top 100 ft, and (7) Exponential "f" factor for the $K\sigma$ Equation. These tables make the formulas in the Calculations worksheet easier to program and review. They also provide

the user with a visual frame of reference for how the correction factors vary as a function of depth, blow count, etc.

3.3.3 Output and References Worksheets

This section details each of the three output worksheets. Two of these worksheets, Boring El. and Grade El., appear nearly identical, but represent output information relative to two different reference elevations. The Output Graphs worksheet provides the user with graphs to aid in visualizing the analyzed data. The References worksheet is provided so the user can locate additional details on the procedures used to develop the workbooks if necessary.

The Output Boring El. worksheet contains data combined from the Input Data and Calculations worksheet. This worksheet is meant to provide the user with a more compact, printable table that contains the most important information from the liquefaction triggering analysis relative to the boring surface elevation(refer to Figure 3.12). No data is input in this worksheet and no additional calculations are performed, it is simply a re-organization of the input and calculations. The Output Grade El. worksheet is identical in appearance to the Output Boring El. Worksheet. However, it provides the user with a more compact, printable table that contains the most important information from the liquefaction triggering analysis relative to the grade surface elevation

The Output Graphs worksheet is designed to help the user visually decipher the liquefaction triggering information in a quick and efficient manner. Within this worksheet, three graphs for the boring elevation and three graphs for the grade elevation

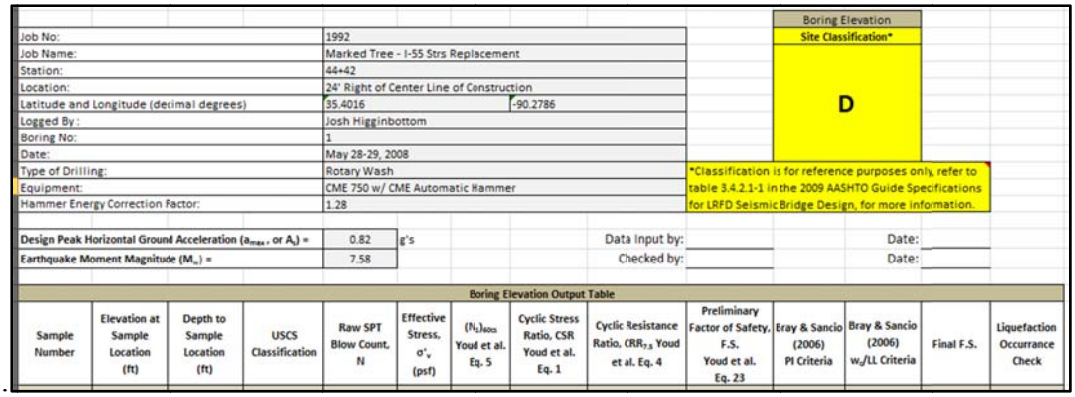

Job No:	1992		Boring Elevation
Job Name:	Marked Tree - I-55 Strs Replacement		Site Classification*
Station:	44+42		D
Location:	24' Right of Center Line of Construction		
Latitude and Longitude (decimal degrees)	35.4016	-90.2786	
Logged By :	Josh Higginbottom		
Boring No:	1		
Date:	May 28-29, 2008		
Type of Drilling:	Rotary Wash		*Classification is for reference purposes only, refer to table 3.4.2.1-1 in the 2009 AASHTO Guide Specifications for LRFD Seismic Bridge Design, for more information.
Equipment:	CME 750 w/ CME Automatic Hammer		
Hammer Energy Correction Factor:	1.28		
Design Peak Horizontal Ground Acceleration (a_{max}, or A_s) =	0.82	g's	Data Input by: Date:
Earthquake Moment Magnitude (M_w) =	7.58		Checked by: Date:

Boring Elevation Output Table

Sample Number	Elevation at Sample Location (ft)	Depth to Sample Location (ft)	USCS Classification	Raw SPT Blow Count, N	Effective Stress, σ'v (psf)	$(N_1)_{60cs}$ Youd et al. Eq. 5	Cyclic Stress Ratio, CSR Youd et al. Eq. 1	Cyclic Resistance Ratio, $CRR_{7.5}$ Youd et al. Eq. 4	Preliminary Factor of Safety, F.S. Youd et al. Eq. 23	Bray & Sancio (2006) PI Criteria	Bray & Sancio (2006) w_c/LL Criteria	Final F.S.	Liquefaction Occurrance Check

Figure 3.12. Output Boring El. liquefaction triggering summary information and column headings.

are presented. Near the top of the worksheet, in columns N-AH, plots depicting the factor of safety are followed by the adjusted clean sand base curve, and the fine grained screening criteria plots of Bray and Sancio (2006). The plots included in the Output Graphs worksheet have been included in this section as Figures 3.13-3.15.

Figure 3.13 portrays the final F.S. values, shown as red x marks, with a black line representing a F.S. = 1.0. This plot will not show any data for soils assigned as "Cohesive" or "Unsat" and will plot "Not Sus" assignments as being equal to 2.0 (refer so Section 3.3.2.1). Figure 3.14 presents the site-specific data relative to the adjusted clean sand base curve of Youd et al. (2001). Here, the curve has only been extended to a maximum $(N_1)_{60cs}$ value of 30 beyond which, soils is classified as too dense to liquefy as per Youd et. al (2001). This boundary is represented in Figure 3.14 as a dashed vertical line. This plot is populated with the CSR points calculated in the Calculations worksheet, presented as red x marks. The fine grained screening criteria of Bray and Sancio (2006), is plotted in Figure 3.15. Again, the site specific data is presented as red x marks.

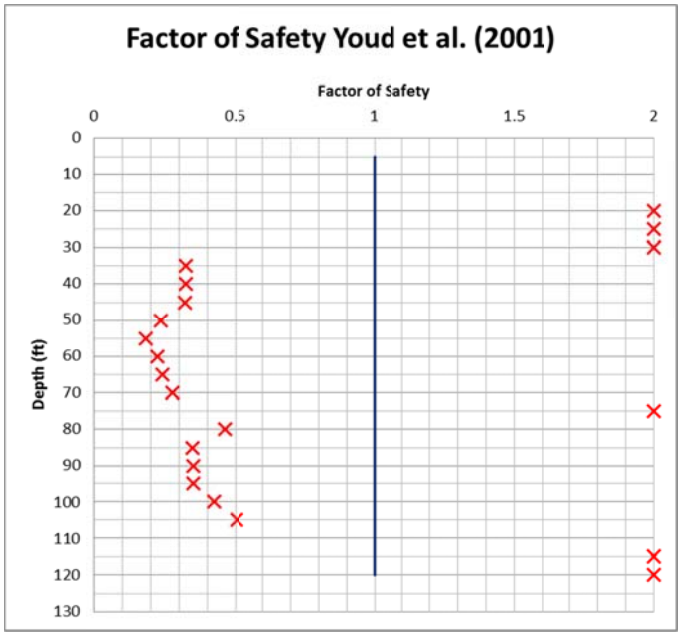

Figure 3.13. F.S. plot included within the Output Graphs workbook.

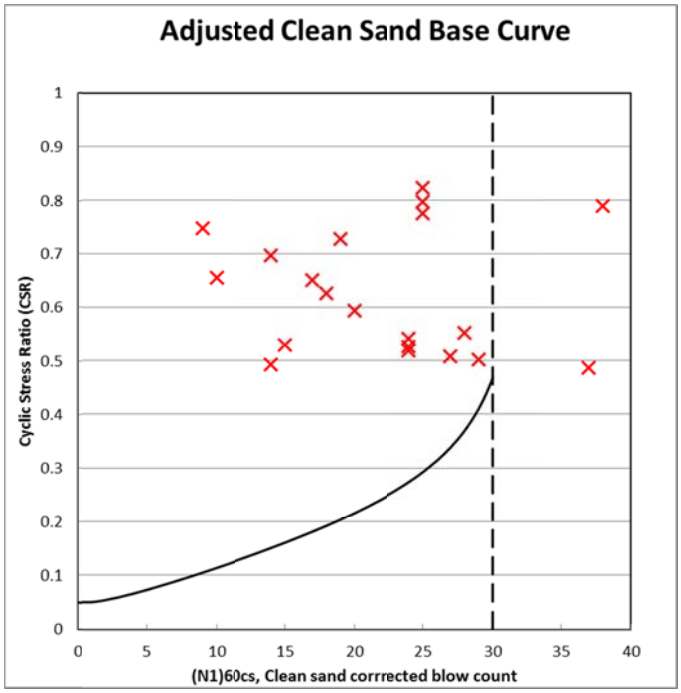

Figure 3.14. Clean sand base curve included within Output Graphs worksheet.

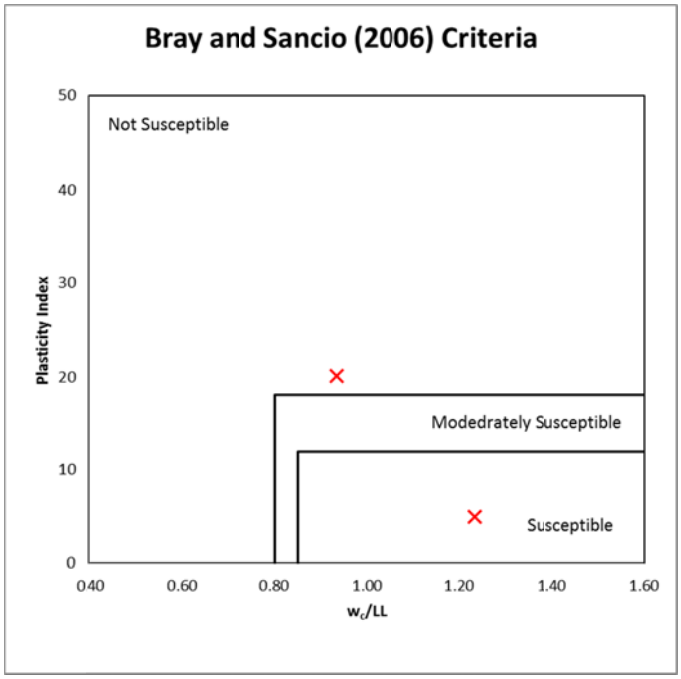

Figure 3.15. Fine grained screening criteria plot included within the Output Graphs worksheet.

3.4 CETIN ET AL. (2004) WORKBOOK

The Cetin et al. (2004) SPT-based liquefaction triggering procedure varies significantly from the one presented by Youd et al. (2001) due to its probabilistic framework, additional case history data points, and differing depth-dependent correction factors (refer to Section 2.4). This section is not meant to document the specific differences/similarities between these two procedures. Rather, it is meant to guide the user in performing deterministic liquefaction triggering analyses using the Cetin et al. (2004) workbook. The user can then compare the various methods on a site-by-site basis. This section will only present workbook information that is significantly different than the systematic, detailed descriptions already presented for the Youd et al. workbook in

Section 3.3. Once again, the user is reminded that for this workbook to function properly iterative calculations must be enabled, (refer to Section 3.2).

3.4.1 Input Data Worksheet

The Input Data worksheet is identical to the Input Data Worksheet of Youd et al. (2001). However, it will be noted that the deterministic approach, wherein a F.S. against liquefaction is calculated for a given CRR boundary curve, has been hardwired into the worksheet with a set probability of liquefaction (P_L) equal to 15%, as recommended within Cetin et al. (2004). Therefore, the user cannot input the P_L for deterministic-type evaluations at other probability levels. The full probabilistic approach is also programmed into the spreadsheet, wherein a P_L is calculated for the raw data rather than a F.S. against liquefaction. However, the probabilistic calculations are only contained in the Calculations worksheet and are not transferred to the Output worksheet.

3.4.2 Calculation and Calculation Tables

Cetin et al. (2004) uses the average shear wave velocity over the top 12 m (40 ft) [$Vs_{,12}$] to calculate r_d. These values are displayed in Cells E35 and E68 in the Calculations workbook. They are included in these cells because they are non-depth dependent parameters. The values are calculated using the Boring and Grade Elevation Calculation Tables in columns AE-AG in the Calculations workbook. This is discussed is Section 3.4.2.1.

3.4.2.1 Depth-dependent Calculations

Only the calculations that are different from those presented in Section 3.3.2.1 for the Youd et al. (2001) workbook will be discussed below.

Drill Rod Length Correction Factor (C_R) – The drill rod length correction factor is obtained using Figure 7 from Cetin et al. (2004). This graphical relationship has been digitized and is included in the Calculation Tables worksheet under the title of Drill Rod Length Correction Factor. A lookup function is used to pull the appropriate C_R from this table based on the length of the drill rod.

Sampler Liner Correction Factor (C_S) – If the sampler has been used with liners or doesn't have room for liners, as indicated on the Input Data worksheet (refer to section 3.3.1.3), then this value will be 1.0 at all depths. Conversely, if the sampler has room for liners but is used without them then this correction is depth dependent, and becomes part of the circular reference as a function of $(N_1)_{60}$.

Stress Correction Factor (C_N) – Here, the standardized overburden blow count correction factor is calculated based on the effective stresses in the soil column. The relationship proposed by Liao and Whitman (1986), with a maximum permissible C_N of 1.6 is employed as detailed in Section 2.4.1.

Columns headings AB-AG are all new within this worksheet and are presented in Figure 3.16.

Fines Content for Use in the Worksheet (%) – This column assigns a fines content between 5% and 35%. If the actual fines content is lower or higher than these values it is set equal to 5% or 35%, respectively.

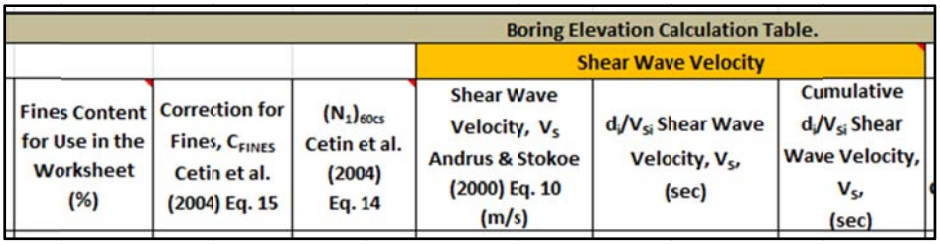

Figure 3.16. Headings for columns AB-AG in the Calculations worksheet.

Correction for Fines (C_{FINES}) – This column calculates the fines content correction based on the percentage of fines in the previous column.

$(N_1)_{60cs}$ – The corrected blow count $(N_1)_{60}$ is combined with the C_{FINES} correction to determine the clean sand corrected blow count, $(N_1)_{60cs}$. The clean sand corrected blow count is used, directly in the workbook, to compute the CRR. This is a slight variation from the procedure recommended in Cetin et al. (2004) where, $(N_1)_{60}$ is used with CRR curves modified for fines contents of 5, 15 and 35% to determine the CRR. Although the procedure is slightly different, the calculated CRR is the same. This was done to be more consistent with the other procedures and to simplify the workbook development.

Shear Wave Velocity – This group of three columns is used to determine the average shear wave velocity over the top 12 m (40 ft). The first column, Shear Wave Velocity, correlates blow count to shear wave velocity (in units of meters per second) using a relationship developed by Andrus and Stokoe (2000). The next column, d_i/V_{Si} Shear Wave Velocity each Layer, divides the sample thickness (which is converted to meters for this calculation) by the shear wave velocity. The third column, Cumulative d_i/V_{Si} Shear Wave Velocity, computes the cumulative d_i/V_{Si} as a function of depth.

Beneath these columns, Cell AG66 employs a lookup function to determine which of the cumulative d_i/V_{Si} values corresponds to a depth of 12 m (40 ft), and this value is copied into the cells E35 and E68, respectively for use in the r_d equation (refer to Section 3.4.2).

Stress Reduction Coefficient (r_d) –The computation of r_d is complex, and dependent on many variables. In order to present the algebraic expressions in a manner that is easy to understand, the expressions are divided up and color coded with assignments of A, B, C, and D, in the Calculation Tables worksheet above the Stress Reduction Coefficient tables. These tables copy information from the Calculations worksheet and then calculate r_d. A lookup function in the Calculations worksheet uses the tables and returns the proper r_d based on the depth of the sample.

Overburden Correction Factor ($K\sigma$) – The $K\sigma$ factor includes an exponent "f" which ranges from 0.6 - 0.8 based on relative density. In order to account for this, Cetin et al. (2004) recommend linear interpolation of f for $(N_1)_{60}$ values between 40 and 5 blows per foot. This is accomplished in the workbook using the table Exponential "f" factor for the $K\sigma$ Equation in the Calculation Tables worksheet. In the table, corrected blow counts greater than or equal to 40 are assigned an f = 0.6, whereas corrected blow counts less than or equal to 5 are assigned an f = 0.8. If blow counts are between 40 and 5 then the f values are linearly interpolated between 0.6 and 0.8, respectively.

Cyclic Stress Ratio adjusted for DWF_M and $K\sigma$ ($CSR_{eq\ M,\ K\sigma}$) – Cetin et al. (2004) adjust the CSR for the earthquake magnitude (DWF_M is the name chosen to represent the MSF in Cetin et al. [2004]) and overburden stress ($K\sigma$) before the initial factor of safety is calculated. Note that there is not an equivalent $CSR_{eq\ M,\ K\sigma}$ calculated in the Youd et al.

(2001) procedure because the MSF and Kσ factors are applied directly to the factor of safety.

Cyclic Resistance Ratio (CRR) – The CRR in this column is calculated using a combination of Equation 20 from Cetin et al. (2004) and Equations 2.11-2.13 in Section 2.4. However, the following variables have been fixed: (1) $M_w = 7.5$, (2) $\sigma'_v = 1$ atm, (3) F.C. = 5%, and (4) $P_L = 15\%$. Fixing these factors essentially yields the clean sand curve (i.e. FC < 5%) in Figure 14b of Cetin et al. (2004). The fines content is accounted for by using $(N_1)_{60cs}$ in the above mentioned equations instead of $(N_1)_{60}$. This was done in order to be able to set a limiting upper-bound $(N_1)_{60cs}$ in a similar manner to Youd et al. (2001) and Idriss and Boulanger (2008) (refer to Section 2.4). Therefore, if the $(N_1)_{60cs}$ value is larger than 35, a large CRR of 2.0 is assigned to account for the fact that the soil is essentially considered non-liquefiable.

Probabilistic Evaluation – The column headings for the probabilistic evaluation performed in columns AR and AS are presented in Figure 3.17. These calculations are included in the worksheet for completeness, but none of the probabilistic information is transferred to the output worksheets (refer to Section 3.4.1). The initial P_L is the probability without taking into account the soil type, whereas the final P_L uses the fine-grained screening criteria and the initial P_L in a similar manner to that described for the preliminary and final F.S. in the Youd et al. (2001) workbook.

The changes to the Calculation Tables worksheet include; an updated C_R table and chart, a DWF_M/MSF table and chart, Stress reduction coefficient tables and equations

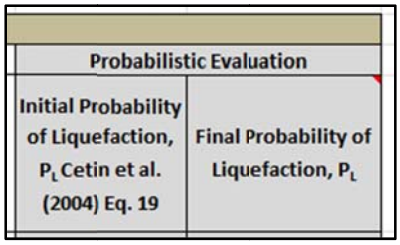

Figure 3.17. Headings in columns AR and AS in the Calculations worksheet.

plus the table titled Exponential "f" factor for Kσ Equation. All of which have been discussed previously.

3.4.3 Output and References Worksheets

Both of the Boring and Grade elevation worksheets are the same for Cetin et al. (2004) as they are for Youd et al. (2001). The Output Graph worksheet includes graphs for each sample elevation, similar to Youd et al. (2001). The CRR plot (Figure 3.18) is similar to Figure 14b in Cetin et al. (2004), but with a maximum CRR/CSR of 1.0 instead of 0.6. This is necessary because the relatively large design ground motions in the New Madrid Seismic Zone transmit to larger CSR values than would be visible if the CRR/CSR were a maximum of 0.6. Notice the break in natural slope of the CRR curve around a CSR=0.4. This represents the line Cetin et al. (2004) have drawn in by hand, and the area that has been programmed by the author according to Equations 2.11-2.14 in Section 2.4. The vertical dashed line in Figure 3.18, represents the interpreted cutoff between liquefiable and non-liquefiable material (refer to Section 2.4).

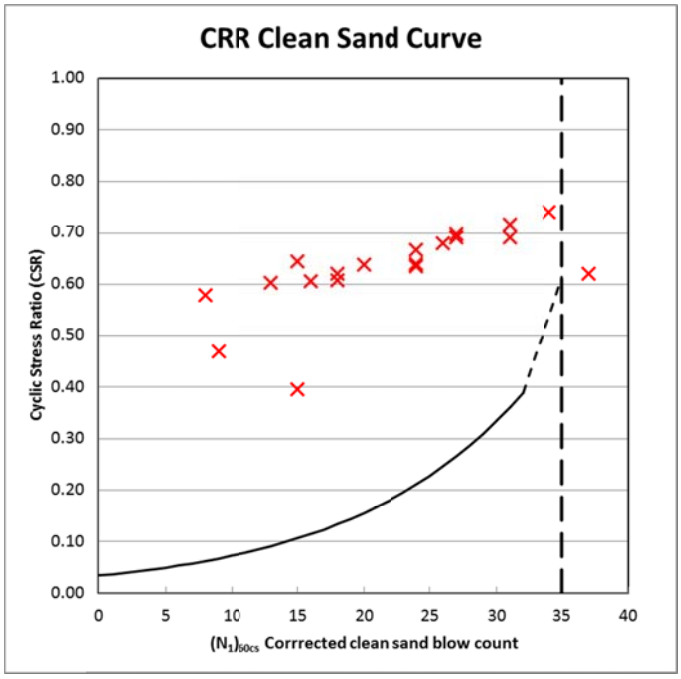

Figure 3.18. Plot of the clean sand corrected curve included in the Output Graphs worksheet.

3.5 IDRISS AND BOULANGER (2008)

Like Section 3.3, only portions of this workbook that are significantly different than the Youd et al. (2001) workbook will be discussed herein. For example, the Idriss and Boulanger (2008) workbook contains an entire extra worksheet titled SPT Su Correlations that is discussed further in Section 3.5.3. Also, this procedure includes two equations for many of the factors associated with the liquefaction triggering evaluation: one for the clay-like criteria and one for the sand-like criteria (refer to Section 2.5). This enables the engineer to quantify the liquefaction susceptibility (cyclic mobility) of plastic clays and silts separate from traditional sandy soils. Before using this workbook, ensure that the iterative calculations box is checked (refer to Section 3.2).

3.5.1 Input Data Worksheet

Column J in the Input Data worksheet has been changed from in-situ water content to undrained shear strength of the soil (Su). This change is subtle and the user must be careful not to paste the in-situ water content data into this column from previous (i.e. Youd et al. [2001], and Cetin et al. [2004]) liquefaction evaluation workbooks. The undrained shear strength (Su) is only applicable to cohesive soils, and should only be entered if the proper laboratory tests have been performed to accurately determine Su. If the proper laboratory tests have not been performed, this column should be left blank and a Su will be estimated based on a correlation with SPT blow count (refer to Section 3.5.3).

3.5.2 Calculations and Calculation Table Worksheets

The user will note that two magnitude scaling factors are calculated in the Idriss and Boulanger (2008) Calculations worksheet instead of just one, like in the Youd et al. (2001) and Cetin et al. (2004) workbooks. Two magnitude scaling factors are necessary because the relationship between the CSR and the number of loading cycles to failure is flatter for clays than sands (Idriss and Boulanger 2008). The Calculation Tables worksheet provides six tables, five of which have been previously discussed. The only table not mentioned is the Stress Reduction Coefficient, which will be discussed in Section 3.5.2.1.

3.5.2.1 Depth-dependent Calculations

The remaining calculations are all depth dependent and are associated with a given SPT sample location. Once again, the Calculations worksheet is populated with

more columns than the Input Data worksheet (i.e. from column K through column AO). Only the columns that are different from the Youd et al. (2001) workbook will be discussed further.

Clay-like or Sand-like Behavior – This column categorizes the soil as Clay-like or Sand-like depending on the USCS classification and the PI of the soil (refer to Section 2.5). The Clay-like or Sand-like designation determines if the soil will be analyzed according to liquefaction (i.e. sand-like) criteria or the newly developed cyclic softening (i.e. clay-like) criteria. If the proper index tests have not been performed to determine the soil PI, this column will simply designate any clay or silt as Cohesive. These Cohesive soils will be evaluated for liquefaction susceptibility by assuming cyclic softening behavior, but will not be given the designation of Clay-like since the PI was not directly measured.

Sampler Liner Correction Factor (C_S) –This correction factor is depth dependent and is a part of a circular reference as a function of $(N_1)_{60}$.

N_{60} – This column differs from the N_{60} Only Corrected for Energy column, which is used to correlate unit weight. It calculates the blow count corrected for all variables except C_N, and is the blow count used to correlate Su. This correlation excludes C_N because the SPT blow count – Su correlations employed herein were developed without C_N.

Estimated Undrained Shear Strength of the Soil (Su) – This column estimates the undrained shear strength for cohesive or clay-like soils based on N_{60}. The correlation of Kulhawy and Mayne (1990) is employed in the workbook and is presented below as

Equation 3.1. It has also been graphed and is included in the worksheet SPT Su Correlations along with several other SPT-Su correlations. Kulhawy and Mayne (1990) state "Correlations have been attempted for estimating Su from SPT N values, even though it is known that these correlations are weak". Despite this warning, the correlations between SPT blow count and Su are often times the only way of estimating Su and must be employed in order to determine a factor of safety for the liquefaction susceptibility of clays and silts. Measured undrained shear strength data entered in the Input Data worksheet will override this correlation.

$$Su = Pa * 0.6 * N_{60} \qquad \text{Equation 3.1}$$

Stress Correction Factor (C_N) –The equation used to calculate C_N is a function of $(N_1)_{60}$ and is the second circular reference in the Calculations worksheet of Idriss and Boulanger (2008).

$\Delta(N_1)_{60}$ – This column calculates $\Delta(N_1)_{60}$, which is the change in blow count according to the percentage of fines. This is added to $(N_1)_{60}$ to determine $(N_1)_{60cs}$.

Stress Reduction Coefficient (r_d) – Similar to Youd et al. (2001) this column uses a lookup function to determine r_d from a table in the Calculation Tables worksheet, except here, the r_d table is populated by employing Equations 2.5-2.7 (refer to Section 2.3.1). The maximum recommended depth for which this r_d correlation should be used, due to the increasing uncertainty with increasing depth, is 20 m (65 ft). Idriss and Boulanger (2008) state "Liquefaction evaluations at greater depths often involve special conditions for which more detailed analyses can be justified". Despite this recommendation, this workbook employs the r_d relationship to a depth of 36 m (120 ft).

In order to remind the user of the increasing uncertainty with depth, the table titled Stress Reduction Coefficient in the Calculation Tables worksheet has been highlighted red below a depths of 20 m (65 ft).

Cσ Coefficient – This column calculates the intermediate variable Cσ, which is used in to determine Kσ. Cσ is a function of $(N_1)_{60}$, and relates the relative density of the soil to Kσ (refer to Section 2.4.2).

Overburden Correction Factor (Kσ) – Kσ is related to the relative density of the soil via Cσ. Boulanger and Idriss (2006) state "The interpretation and proper execution of in-situ and laboratory tests [for clays] requires a careful accounting of the effective consolidation stress and stress history conditions in the field. Accordingly, there is no need to introduce an overburden correction factor for the cyclic strength of clay as was done for the sand". Because of this, Clay-like and Cohesive soils are assigned a Kσ =1.0, so that CRR values remain unaffected.

Cyclic Resistance Ratio ($CRR_{M=7.5,1\ atm}$) – The unadjusted CRR is calculated differently depending on the Clay-like or Sand-like designation. The Sand-like soils CRR will be calculated according to $(N_1)_{60cs}$. For Clay-like and Cohesive soils, the CRR is calculated based on correlated Su estimates unless Su values have been measured in the lab and entered on the Input Data worksheet. For Sand-like soils, a $(N_1)_{60cs} \geq 37.5$ is interpreted as too dense too liquefy, as recommended in Appendix A of Idriss and Boulanger (2008) (refer to section 2.4). These soils are assigned a $CRR_{M=7.5,1\ atm}$ of 2.0, which is carried through the $CRR_{M,K\sigma}$, Preliminary F.S., and Final F.S. columns.

Cyclic Resistance Ratio adjusted for MSF and Kσ ($CRR_{M,K\sigma}$) – The $CRR_{M,K\sigma}$ is also adjusted differently according to the Sand-like or Clay-like designations. This is accomplished by employing different MSF and Kσ values, as discussed in this Section, and in Section 3.5.2.

Clay-like or Sand-like Behavior – This column is repeated here to remind the user of the soil type, and help determine the final factor of safety classification. If the soil is Cohesive and has not had the proper laboratory index tests performed, then this column will return the designation of Cohesive rather than Clay-like.

Final F.S. – Here, there are four possible designations, they include; (1) a numerical F.S. between 0.00 - 2.00, (2) "2.00" (assigned to any soil with a preliminary F.S. $\geq$ 2.00 based on high penetration resistance), (3) "Unsat" (assignment for soils above the water table), or (4) "Cohesive" (designates that the fine-grained soils have not had the proper laboratory tests performed and the preliminary factor of safety is less than 1.0). Soils designated as "Cohesive" require the user to apply engineering judgment to determine liquefaction susceptibility.

3.5.3 SPT Su Correlation Worksheet

This worksheet includes four different SPT-Su correlations. A plot in the worksheet is presented below as Figure 3.19. It presents four correlations between SPT blow count and Su. The uncertainty in this correlation is evident based on the large differences of the various relationships. The red line indicates the correlation used by some AHTD personnel (Personal Communication, Steven Peyton, August, 2010). It is the same correlation as Kulhawy and Mayne (1990), and is the correlation employed to

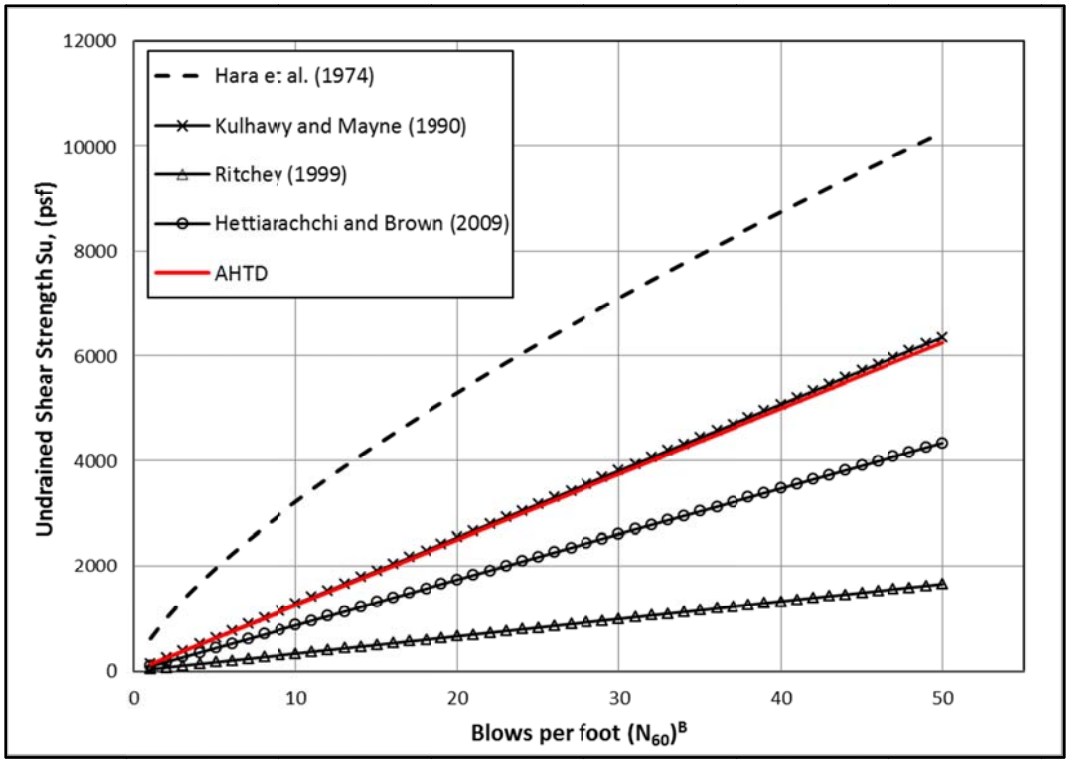

Figure 3.19. SPT blow count, Su correlations plot in the SPT Su Correlations worksheet.

estimate Su in the Calculations worksheet (refer to Section 3.5.2.1). Kulhawy and Mayne (1990) used N instead of N_{60} in their original correlation because much of the data available to them at the time did not indicate a standard energy level. However, in this study N_{60} has been used because many of the automatic hammers which are now in common use have hammer efficiencies greater than 80%. These raw N values must be adjusted to an efficiency that was more common in older hammers (i.e. approximately 60%) for use in older correlations. Therefore, for the purpose of estimating undrained shear strength, N_{60} is used herein. Other correlations are presented in the figure could be used to estimate Su, but in the author's opinion, provide no better approximation than the correlation currently employed.

3.5.4 Output and Reference Worksheets

The Output Boring El., and Output Grade El. worksheets are the same as in the Youd et al. (2001) workbook. The Output Graphs worksheet includes a F.S. plot but does not include the plot for fine grained screening criteria proposed by Bray and Sancio (2006). A plot representing the clean sand CRR curve recommended by Idriss and Boulanger (2008) is included in the Output Graphs worksheet and is included here as Figure 3.20. The red x's denote the calculated CSR values and the vertical dashed line represents the interpreted cutoff between liquefiable and non-liquefiable material (refer to Section 2.4).

3.6 CONCLUSIONS

The three most commonly used SPT-based liquefaction triggering procedures (Youd et al. 2001, Cetin et al. 2004, and Idriss and Boulanger 2008) have been programmed into Microsoft Excel workbooks. This chapter has reviewed the workbooks, and has provided direction about how to complete an SPT-based liquefaction susceptibility evaluation using the workbooks. This chapter is meant to supplement the workbooks and the comments therein.

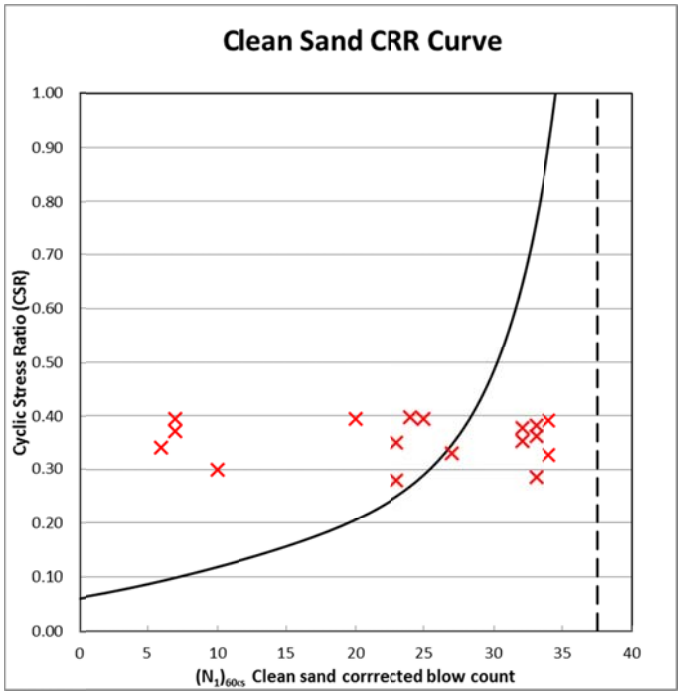

Figure 3.20. Clean sand curve recommended by Idriss and Boulanger (2008) shown with data generated in the Calculations worksheet.

Chapter 4

Site-Specific Comparisons

4.1 INTRODUCTION

Many complicated and inter-related variables are calculated for each of the three SPT-based liquefaction triggering procedures (i.e. Youd et al. [2001], Cetin et al. [2004], and Idriss and Boulanger [2008]). General differences between some of these variables have been discussed in Chapter 2 for simplified conditions. However, the interaction between many of these variables is complex, and it can be difficult to determine how fluctuations in a single variable impact the final F.S. against liquefaction triggering. In order to determine how these variables interact to yield differences in the F.S. predictions for the three SPT-based liquefaction triggering procedures, site-specific comparisons have been made for a number of SPT borings at actual bridge sites in eastern Arkansas. The boring logs from these sites were provided by AHTD (refer to Section 1.3).

4.2 SITE-SPECIFIC COMPARISONS

This section will present site-specific comparisons of the SPT-liquefaction triggering procedures for three different bridge sites in eastern Arkansas (refer to Figure 4.1). The discussion of each site will begin by comparing the F.S. for each of the three procedures as a function of depth/vertical effective stress. In order to clarify any potential confusion, the "final" F.S. discussed in Section 3.3.2.1 is the only one used for comparison in this chapter, and will simply be denoted herein as the F.S. Note that a F.S. = 2.0 is assigned based on high penetration resistance or a designation of "Not Sus".

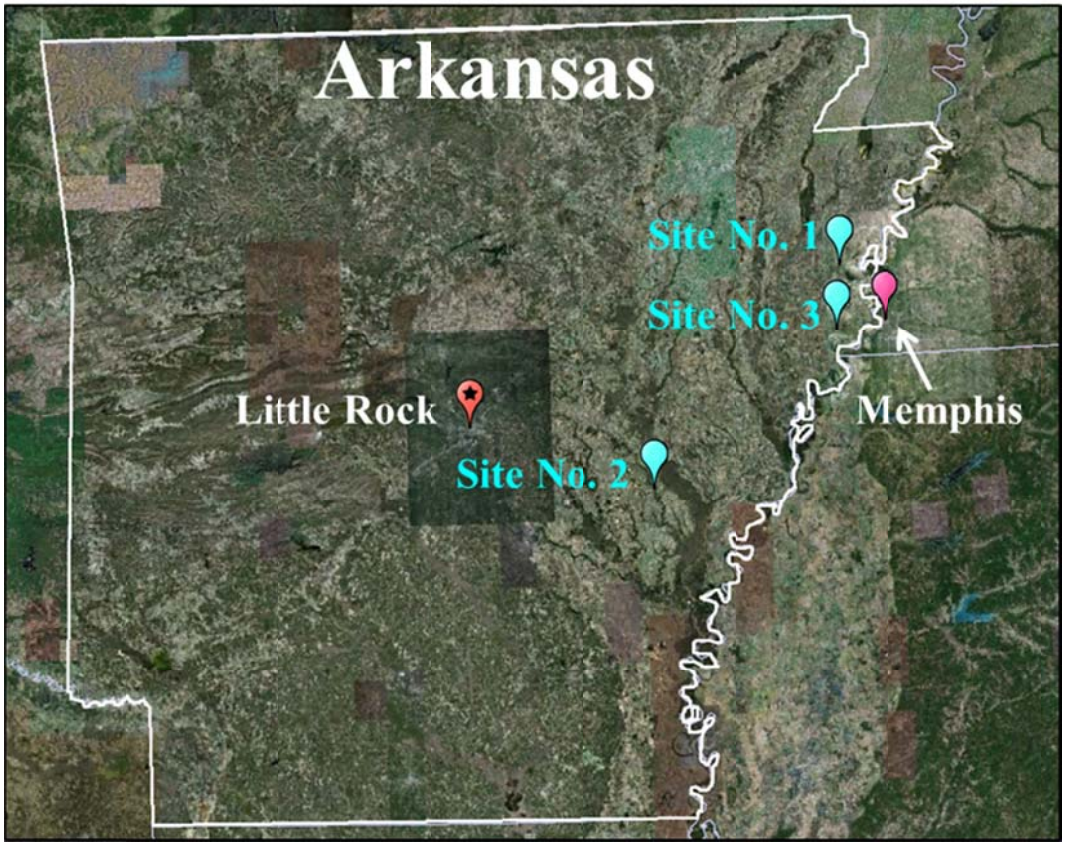

Figure 4.1. Locations of the soil borings that have been chosen for site specific comparisons (image from Google Earth, © 2010 Google).

Other designations for the final F.S. will not show up on these plots (refer to Section 3.3.3). Following the comparison of the F.S., the discussion will work its way backward through the liquefaction triggering procedures to examine what variables (r_d, C_N, $K\sigma$, etc.) are primarily responsible for variations in the F.S. estimates.

Like Chapter 2, all of the figures presented in this chapter that have dual vertical axes (depth and effective stress) assume a uniform soil profile with a unit weight of 18.8 kN per cubic meter (120 pcf) and a water table at the ground surface to compute the approximate vertical effective stress in the soil. Furthermore, in the comparison figures presented below, the Youd et al. (2001) data is always shown as black triangles, the Cetin

et al. (2004) data is shown as green squares, and the Idriss and Boulanger (2008) data is shown as red circles.

4.2.1 Site No. 1

Site No. 1 is located near Gilmore, Arkansas. The soil conditions are classified as Site Class D based on the measured SPT blow counts. The site-adjusted design peak horizontal ground acceleration (a_{max}) with a 7% probability of exceedance in 75 years for this site is 0.82 g and the estimated moment magnitude (M_W) is 7.58 (refer to Section 3.3.1.1). The soil is mostly clay from the surface to a depth of 6 m (20 ft), beneath the clay a sandy layer is present to the depth of 33 m (110 ft) followed by a stiff clay to 37 m (120 ft).

The F.S. values for each of the three procedures (refer to Figure 4.2) agree very well for all depths down to 24 m (80 ft). However, at depths greater than 24 m (80 ft) the F.S. values begin to separate from one another, with the F.S. from the Idriss and Boulanger (2008) procedure being consistently greater than the others. Despite this, the only depths where the three procedures actually yield a different prediction for liquefaction triggering are at 24 m (80 ft) and from 29-32 m(95-105 ft), where the Idriss and Boulanger (2008) procedure produces a F.S. > 1.0 and the other two procedures do not. In order to understand the driving cause for this variation in F.S. at depth, some of the depth dependent variables(r_d, C_N, $K\sigma$, ect.) are examined below.

Figure 4.3 presents the variable r_d for each of the three procedures. The relationship of Idriss and Boulanger (2008) consistently yields the highest r_d values and

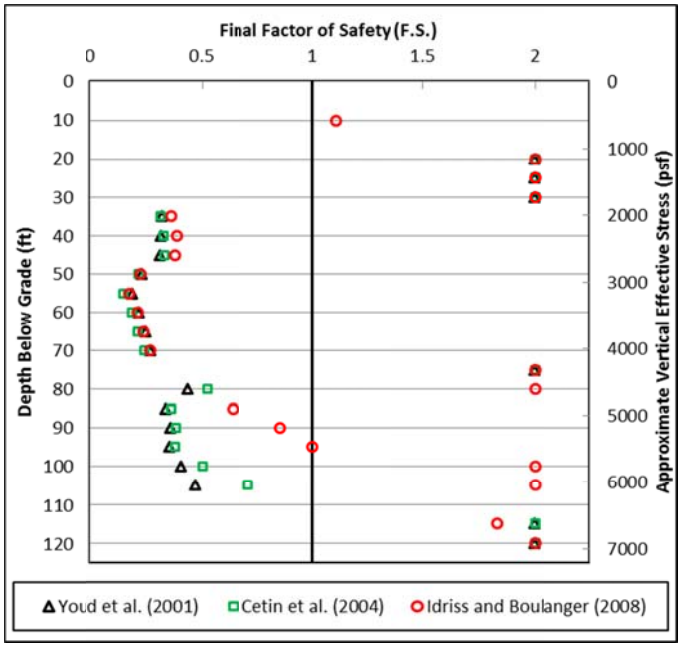

Figure 4.2.Comparison of the factor of safety against liquefaction triggering at Site No.1 for all three simplified procedures.

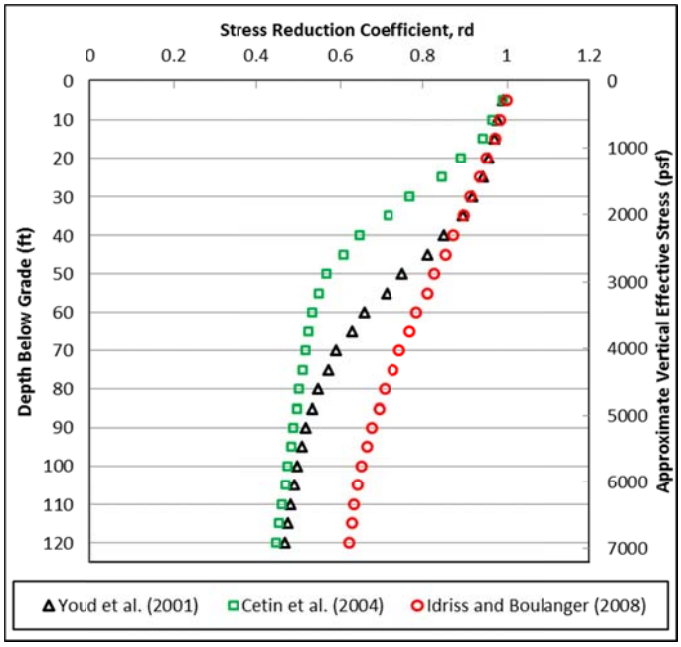

Figure 4.3.Comparison of the r_d values at Site No. 1 for all three simplified procedures.

the Cetin et al. (2004) procedure produces the lowest values. At least two interesting things are noted by examining Figure 4.3 relative to Figure 4.2: (1) despite significant differences in r_d values over virtually the entire depth range (most significantly around 15m [50 ft], where the r_d values vary by 45%), the F.S. values are nearly identical for all procedures down to a depth of 24 m (80 ft), and (2) lower r_d values directly result in lower CSR values(refer to Figure 4.4) according to Equation 2.2, thereby leading one to assume higher F.S. estimates would be obtained from those procedures with the lowest CSR values according to Equation 2.1; this trend is not observed.

Figure 4.4 presents the unadjusted CSR ($CSR_{M=7.5,\ 1\ atm}$) for each of the three procedures. Notice the extremely high $CSR_{M=7.5,\ 1\ atm}$ values, all of which exceed 0.4 and many of which exceed 0.6. This is a concern because the liquefaction case history data points used in the development of these procedures nearly all have CSR values less than 0.4 (refer to Figures 2.1, 2.5, and 2.6); the applicability of simplified procedures for CSR values greater than 0.5 is of uncertain validity. Obviously, due to the direct relationship between r_d and CSR, the same trends discussed relative to Figure 4.3 are apparent in Figure 4.4 (i.e. very significant differences between procedures ranging up to 45% at a depth of 15 m [50 ft]). However, as noted above, these differences do not necessarily result in significant variations in the F.S. estimates at equivalent depths.

Additionally, contrary to expectations, the procedure with the highest CSR values (Idriss and Boulanger 2008) also yields the highest F.S. below 24 m (80 ft). It will be noted that one reason higher r_d and CSR values do not translate directly into lower F.S. estimates (and vice-versa) is that the CRR boundary curves for each method were developed using the r_d relationships recommended in their respective procedure.

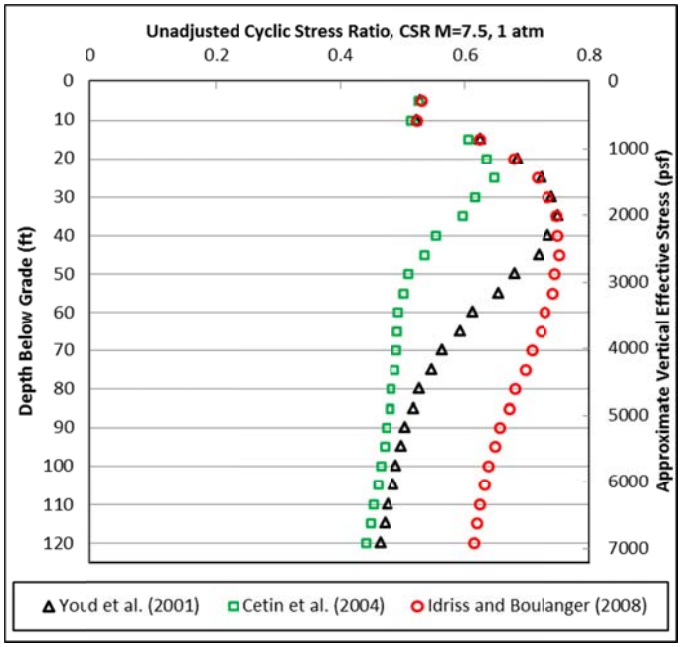

Figure 4.4. Comparison of the $CRR_{M=7.5,\ 1\ atm}$ values at Site No. 1 for all three simplified procedures.

Therefore, the CSR values and CRR curves are directly linked to one another, reminding us that r_d estimates should not be mixed across procedures (Seed 2010).

Figure 4.5 presents the variable C_N for each of the three procedures. The C_N values agree quite well over the depth range of 5-21 m (15-70 ft) (approximately 0.47-1.9 atm [1000-4000 psf]). However, at depths greater than 23 m (75 ft), the C_N values of Idriss and Boulanger (2008) range from 25-60%higher than the other procedures, interestingly mirroring the deviation in the F.S. values below this same depth (refer to Figure 4.2). One important point that will be noted is the close agreement in C_N values at a depth of 33.5 m (110 ft), which is contrary to the general trend observed at depth. In order to understand what drives these differences/similarities the SPT blow count must be inspected.

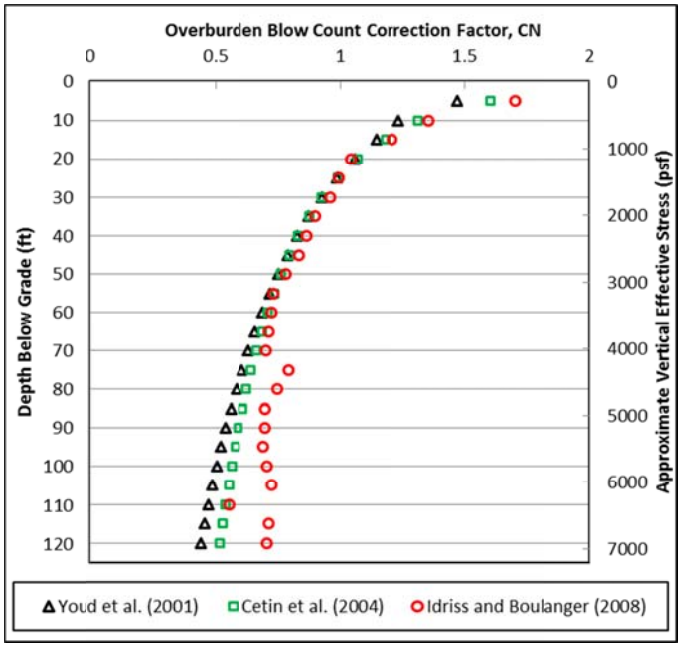

Figure 4.5.Comparison of the C_N values at Site No. 1 for all three simplified procedures.

C_N, along with the other blow count correction factors, directly influences the $(N_1)_{60cs}$ values (according to Equation 2.15) used in the deterministic SPT-procedures to obtain the unadjusted CRR ($CRR_{M=7.5,1atm}$). Figure 4.6 presents the $(N_1)_{60cs}$ values for each of the three procedures. The raw N values are also provided for reference purposes. The three dashed vertical lines represent the boundaries between liquefiable and non-liquefiable material for the each of the SPT procedures (refer to Section 2.4): $(N_1)_{60cs}$ = 30 for Youd et al. (2001), $(N_1)_{60cs}$ = 35 for Cetin et al. (2004), and $(N_1)_{60cs}$ = 37 for Idriss and Boulanger (2008). At depths less than 21 m (70 ft), the $(N_1)_{60cs}$ values for each of the procedures agree quite well, with the *largest* difference of 13% occurring at a depth of 9 m (30 ft), where the corrected blow counts are all greater than 40 and too stiff to liquefy. At depths greater than 21 m (70 ft), excluding the $(N_1)_{60cs}$value at 34 m (110 ft), the differences between $(N_1)_{60cs}$ values for each of the procedures begin to increase, with the

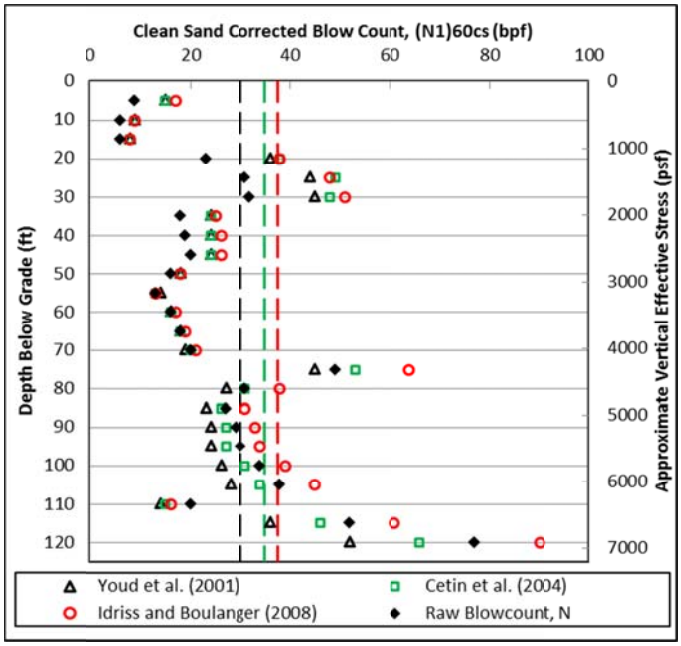

Figure 4.6.Comparison of the $(N_1)_{60cs}$ values at Site No. 1 for all three simplified procedures.

smallest difference between procedures being 34% at 26 m (85 ft). At these depths, the Youd et al. (2001) procedure always yields the lowest $(N_1)_{60cs}$ values, while the Idriss and Boulanger (2008) procedure yields the highest, directly following the C_N trends. Furthermore, at depths greater than 24 m (80 ft), the $(N_1)_{60cs}$ values for the Idriss and Boulanger (2008) procedure have been corrected above the raw N values, while they are consistently corrected below the raw N values for the other two procedures. It is particularly important to note that when the depth is significant and the N value is less than about 23,the C_N and $(N_1)_{60cs}$ values for the Idriss and Boulanger (2008) procedure are in closer agreement with the other procedures (refer to Figures 4.5 and 4.6). However, when the N value at depth is greater than about 23 their C_N and $(N_1)_{60cs}$values become significantly larger than the others, resulting in higher CRR values and, hence, higher F.S. estimates. It appears that the procedures would yield much more similar

results if the Idriss and Boulanger (2008) equation for C_N was not dependent on blow count (specifically, iterative with $(N_1)_{60}$). This comment should not be misconstrued to mean that the Idriss and Boulanger (2008) equation for C_N is not valid. It simply means that C_N appears to have a very strong influence on the agreement/disagreement of the techniques at depth.

Figure 4.7 presents the unadjusted Cyclic Resistance Ratio ($CRR_{M=7.5,1atm}$) for each of the three procedures. The $CRR_{M=7.5,1atm}$ relationship, like C_N, mirrors the deviations in the F.S. estimates, with the Idriss and Boulanger (2008) procedure yielding the highest values. It will be noted that $CRR_{M=7.5,1atm}$ still needs to be adjusted (multiplied) by the MSF and Kσ factors to obtain the adjusted CRR ($CRR_{M, K\sigma}$). Because the design magnitude from the NMSZ, in eastern Arkansas is close to 7.5, and all of the procedures have very similar MSF for $M_w > 7.0$ (refer to Section 2.4.3), the MSF are not responsible for any of the variations in F.S. However, the various Kσ relationships do have an impact.

Figure 4.8 presents the Kσ values for each of the three procedures. At depths between 11-21 m (35-70 ft), the Kσ values of Idriss and Boulanger (2008) are higher than the other procedures. For example, at a depth of 15 m (50 ft) the Kσ values differ by 10%, while the F.S. values are within 6% of one another(refer to Figure 4.2). This indicates that while noticeable differences exist in the Kσ relationships, they do not have

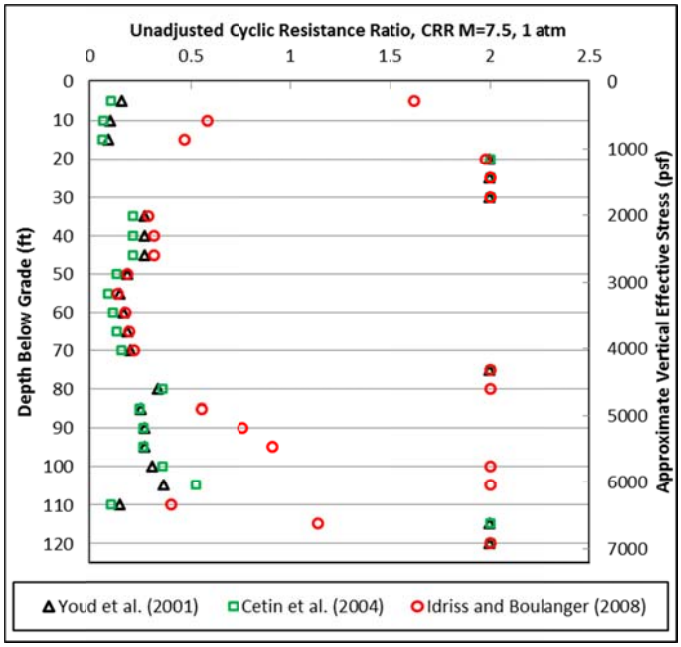

Figure 4.7.Comparison of the $CRR_{M=7.5,\ 1\ atm}$ values at Site No. 1 for all three simplified procedures.

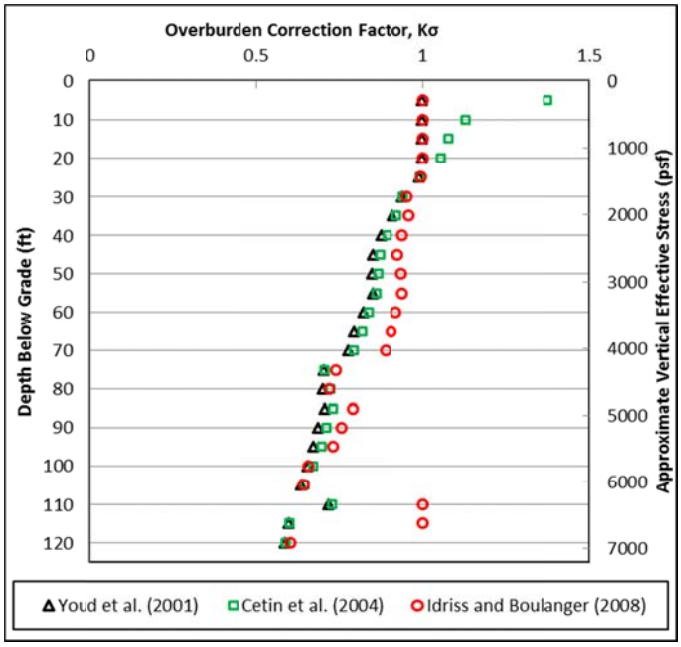

Figure 4.8.Comparison of the Kσ values at Site No. 1 for all three simplified procedures.

a very significant impact on the variations in F.S. at depth. While not a main focus of this research, it will be noted that the shallow Kσ values can vary significantly between procedures based on the choice of a limiting upper value (refer to Section 2.4.2). Additionally, it will be noted that the Idriss and Boulanger (2008) Kσ values are equal to 1.0 at depths of 33.5 and 35 m (110 and 115 ft) because these are "clay-like" soils (refer to Section 3.5.2.1).

In summary, the F.S. values for each of the three procedures at Site No. 1 (refer to Figure 4.2) agree very well for all depths down to 24 m (80 ft). However, at depths greater than 24 m (80 ft) the F.S. values begin to disperse from one another, with the F.S. from the Idriss and Boulanger (2008) procedure being consistently greater than the others. Despite this, the only depths where the three procedures actually yield a different prediction for liquefaction triggering are at 24 m (80 ft) and from 29-32 m (95-105 ft), where the Idriss and Boulanger (2008) procedure produces a F.S. > 1.0 and the other two procedures do not. It appears that variations in the overburden blow count correction factor (C_N) are primarily responsible for the differences in the F.S. estimates at these depths. At depths above 24 m (80 ft) the C_N values are generally within 7% of one another, while at greater depths the C_N values of Idriss and Boulanger are generally 25-50% greater. These differences primarily occur for N values greater than about 23 and are driven by the Idriss and Boulanger (2008) equation for C_N, which is an iterative function of $(N_1)_{60}$. Kσ also plays a role in the variation of F.S. at depth, but its impact is less significant than that of C_N. For example, Kσ values vary by as much as 14% at depths between 11-21 m (35-70 ft). However, there are very minimal differences in the F.S. at these depths. At depths greater than 24 m (80 ft), the Kσ values of Idriss and

Boulanger (2008) are generally less than 12% different, but can contribute to significant differences in F.S. when combined with the higher C_N values over this depth range. In general, when the deterministic liquefaction triggering procedures do not all agree about the potential for liquefaction triggering (i.e. F.S. < 1.0), the author recommends going with the prediction supported by two out of the three procedures.

4.2.2 Site No. 2

Site No. 2 is located near LaGrue, Arkansas. The soil conditions are classified as Site Class D based on the measured SPT blow counts. The site-adjusted design peak horizontal ground acceleration (a_{max}) with a 7% probability of exceedance in 75 years for this site is 0.34 g and the estimated M_w is 7.46 (refer to Section 3.3.1.1). The soil is mostly clayey-silt (CL-ML) from the surface to a depth of 5 m (15 ft), beneath the clayey-silt a silty-sand (SM) layer is present to the depth of 24 m (80 ft) followed by a another silty-sand layer with fewer fines (SW-SM) to 30 m (100 ft).

The F.S. values for each of the three procedures are included as Figure 4.9. Liquefaction is consistently predicted to occur in three isolated layers between the depths of 6-7.5, 23-24, and 29-30 m (20-25, 75-80, and 95-100 ft). Although numerical differences in the F.S. values are calculated for each procedure, the only depths were liquefaction triggering evaluations disagree are at 20 and 27 m (65 and 90 ft). At depths were liquefaction is predicted, the Cetin et al. (2004) procedure yields the lowest F.S., while the Youd et al. (2001) procedure yields the highest F.S., except at a depth of 29 m (95 ft). This trend is different from the F.S. values presented for Site No. 1. (refer to Figure 4.2), where the Idriss and Boulanger (2008) F.S. values were consistently the

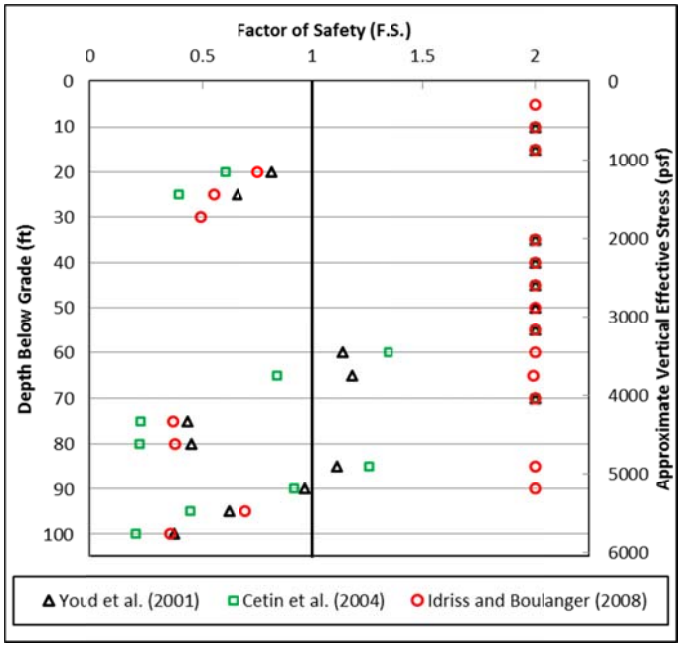

Figure 4.9.Comparison of the factor of safety against liquefaction triggering at Site No.2 for all three simplified procedures.

highest. Examination of the depth dependent variables (r_d, C_N, $K\sigma$, ect.), will help determine the cause of the variation in F.S. values.

Figure 4.10 presents the variable r_d for each of the three procedures. At depths greater than 12 m (40 ft) the relationship of Idriss and Boulanger (2008) yields the highest r_d values, while at depths between 6-18 m (20-60 ft) the relationship of Cetin et al. (2004) yields the lowest r_d values. At depths greater than 20 m (65 ft) the Youd et al. (2001) procedure yields the lowest r_d values. The maximum differences in r_d are variable with depth, but generally are in the range of 25% at depths greater than 15 m (50 ft). Even though the r_d values of Youd et al. (2001) and Idriss and Boulanger (2008) differ by 26% at a depth of 30 m (100 ft), the F.S. values at this depth are nearly identical.

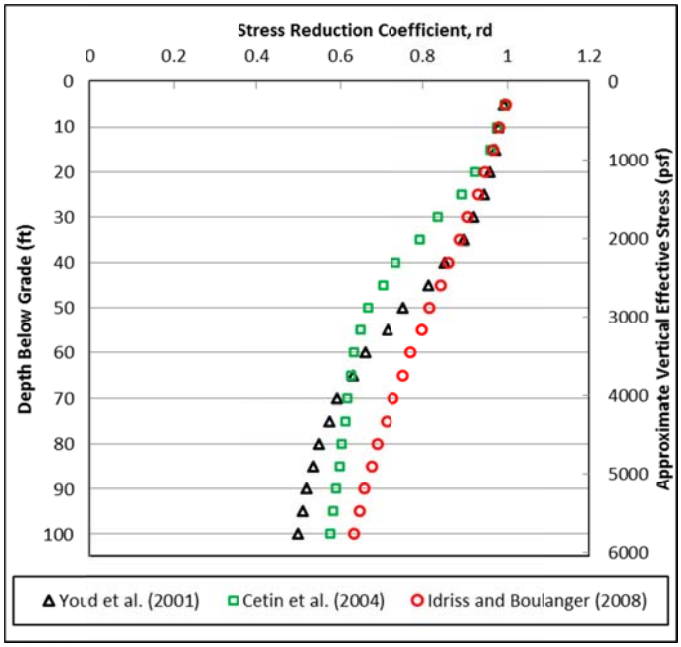

Figure 4.10.Comparison of r_d at Site No.2 for all three simplified procedures.

Figure 4.11 presents the unadjusted $CSR_{M=7.5,1atm}$ for each of the three procedures. The $CSR_{M=7.5,1atm}$ values are generally between 0.2 – 0.4, which is within the range used in the case history database employed in the development of these procedures (refer to Figures 2.1, 2.5, and 2.6). Due to the direct relationship between r_d and CSR, the same trends discussed relative to Figure 4.10 are apparent in Figure 4.11.

Figure 4.12 presents the variable C_N for each of the three procedures. The C_N values agree very well over the depth range of 6-15 m (20-50 ft) (approximately 0.47-1.4 atm [1000-3000 psf]). Despite this, the F.S. values still vary by approximately 60% at depths of 6 and 7.5 m (20 and 25 ft), indicating that C_N is not the driving difference in the F.S. values (noting that all three procedures still predict liquefaction) at these depths. At depths greater than 15 m (50 ft), the C_N values of Idriss and Boulanger (2008) generally range from 12-26% higher than the other procedures, except at discrete depths of 23, 24,

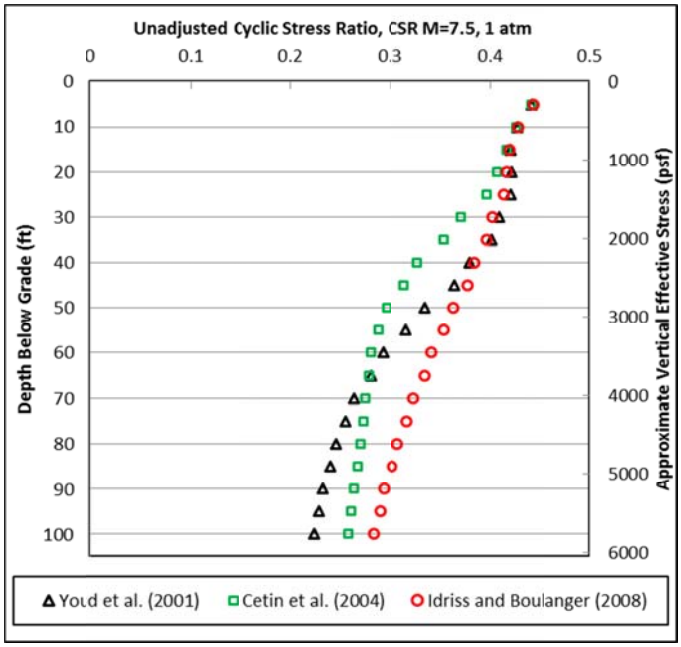

Figure 4.11. Comparison of the $CRR_{M=7.5,\ 1\ atm}$ values at Site No. 2 for all three simplified procedures.

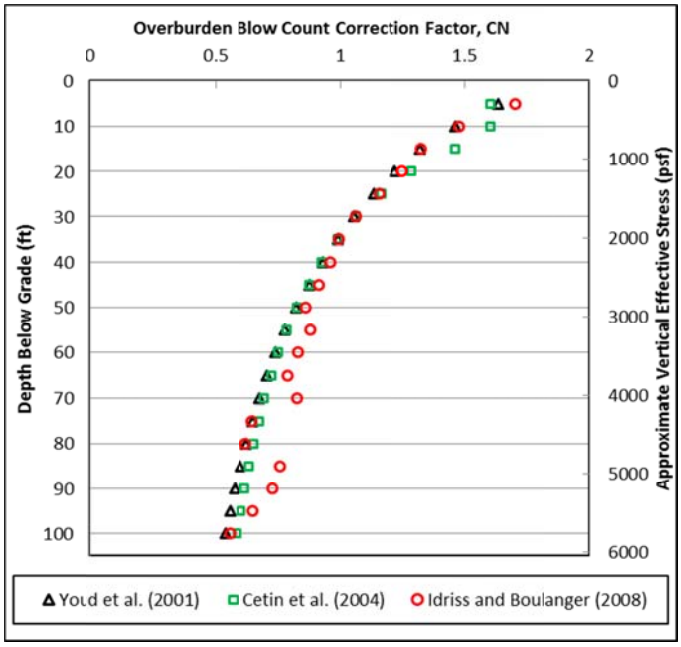

Figure 4.12. Comparison of the C_N values at Site No. 2 for all three simplified procedures.

and 30 m (75, 80, and 100 ft), where the raw N value is low (10, 10, and 12, respectively). Once again, at these depths the C_N values are also quite similar, yet the F.S. values vary by as much as 100% (although, all three procedures still predict liquefaction).

Figure 4.13 presents the raw N values and the $(N_1)_{60cs}$ values for each procedure. To understand how $(N_1)_{60cs}$ values influence differences in F.S. values, it is easiest to only consider a few depths at a time. At depths of 6 and 7.5 m (20 and 25 ft), the fines contents are 42% and 49%, respectively. As noted above, the C_N values are within 5% of one another and the F.S. values differ by as much as 60% (although, all three procedures still predict liquefaction). Obviously, C_N is not largely responsible for the differences in the F.S. values at these depths. The values for all the correction factors used to adjust N to $(N_1)_{60cs}$ at a depth of 7.5 m (25 ft) are tabulated in Table 4.1. Notice the good agreement (< 3%) between all the correction factors, except for the Clean Sand correction. The Clean Sand correction for a F.C. of 49% is virtually the only contributor to the differences between $(N_1)_{60cs}$ values. As noted above, the $(N_1)_{60cs}$ values control the CRR at each depth, which influence the F.S. values. However, in this case the Clean Sand correction is influencing differences in $(N_1)_{60cs}$ values not C_N.

Figure 4.14 presents $CRR_{M=7.5,1atm}$ for all three procedures. At depths of 26 and 27.5 m (85 and 90 ft), the $CRR_{M=7.5,1atm}$ values of Idriss and Boulanger (2008) are significantly greater than the other two procedures. These high CRR values are a direct result of the larger C_N values at these depths (refer to Figure 4.12), which push the $(N_1)_{60cs}$ values (refer to Figure 4.13) of Idriss and Boulanger (2008) close to, or just beyond, the limiting upper value for liquefaction. Therefore, C_N seems to directly

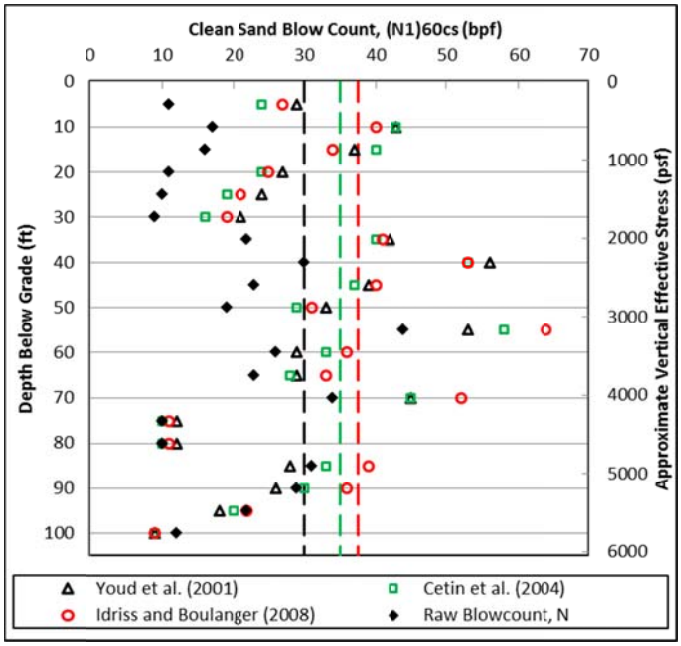

Figure 4.13.Comparison of the $(N_1)_{60cs}$ values at Site No. 2 for all three simplified procedures.

Table 4.1. Comparison of blow count correction factors for Site No. 2, at a depth of 8 m (25 ft)

	Raw N value	C_E	C_R	C_B	C_S	C_N	$(N_1)_{60}$	Clean Sand Correction[1]	$(N_1)_{60cs}$
Youd et al. (2001)	10	1.29	0.95	1.00	1.20	1.13	16	+8	24
Cetin et al. (2004)	10	1.29	0.95	1.00	1.16	1.16	16	+3	19
Idriss and Boulanger (2008)	10	1.29	0.95	1.00	1.20	1.15	16	+5	21

1. Calculated using the recommendations from each procedures, as the change from $(N_1)_{60}$ to $(N_1)_{60cs}$, based on a F.C. of 49% (refer to Section 2.4.1).

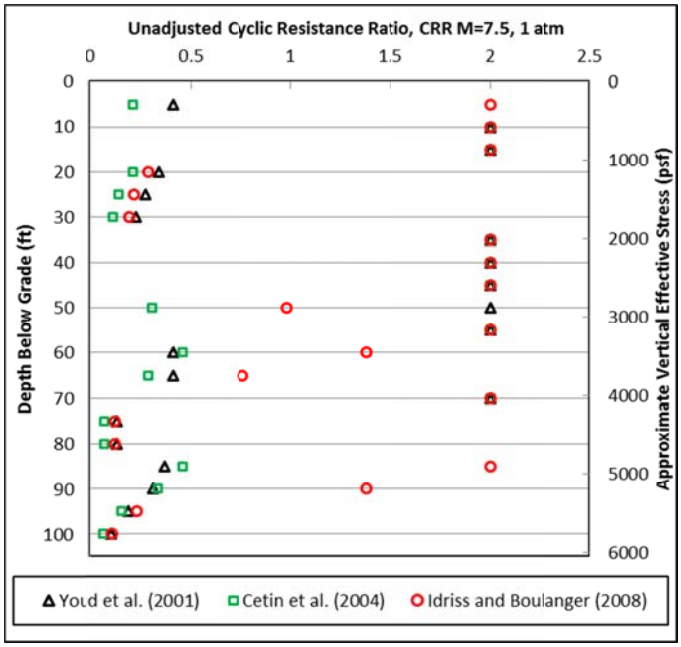

Figure 4.14. Comparison of the $CRR_{M=7.5,\ 1\ atm}$ values at Site No. 2 for all three simplified procedures.

influence the large differences in $CRR_{M=7.5,1atm}$ values at the depths of 26 and 27.5 m (85 and 90 ft). Conversely, at the depths of 23, 24, and 30 m (75, 80 and 100 ft) the $CRR_{M=7.5,1atm}$ values from each procedure are very similar, due to the very similar $(N_1)_{60cs}$ and C_N values. Despite these similarities, the F.S. estimates at these depths are not in close agreement, even though all three procedures predict liquefaction (refer to Figure 4.9).

For example, at a depth of 30 m (100 ft), the F.S. values differ by approximately 81%, with Cetin et al. (2004) yielding the lowest value and Youd et al. (2001) yielding the highest value. This difference is caused by a combination of the depth dependent variables r_d and $K\sigma$. At 30 m (100 ft), Youd et al. (2001) yields the lowest r_d and Idriss and Boulanger (2008) yield the highest r_d. According to Equations 2.1 and 2.2, higher r_d values result in higher CSR values which result in lower F.S. estimates, all other things

being equal. However, at a depth of 30 m (100 ft) the Kσ value of Idriss and Boulanger (2008) is 14% higher than either of the other procedures (refer to Figure 4.15). This difference tends to make the Idriss and Boulanger (2008) F.S. higher than the other two procedures, all other things being equal. Therefore, it is this combination of the lowest CSR and the highest Kσ that causes the Idriss and Boulanger (2008) procedure to yield intermediate F.S. estimates relative to the other two procedures at a depth of 30 m (100 ft). This same trend is responsible for both the order and percent difference of the F.S. values at depths of 23 and 24 m (75 and 80 ft).

In summary, numerical differences in the F.S. values are calculated for each procedure, the only depths were liquefaction triggering evaluations disagree, are at 20 and 27.5 m (65 and 90 ft). At depths were liquefaction is predicted, the Cetin et al. (2004) procedure yields the lowest F.S., while the Youd et al. (2001) procedure yields the highest F.S., except at a depth of 29 m (95 ft). This trend is different from the F.S. values presented for Site No. 1. (refer to Figure 4.2), where the Idriss and Boulanger (2008) F.S. values were consistently the largest.

Differences between the three procedures in predicting liquefaction triggering only occur at two discrete depths in the soil profile at Site No. 2. These differences occur at 20 and 27.5 m (65 and 90 ft), where the Idriss and Boulanger (2008) procedure produces F.S. estimates > 1.0 and the Cetin et al. (2004) procedure produces F.S. estimates < 1.0. However, even at depths where all procedures predict liquefaction triggering, absolute differences in the F.S. values often range from 60% – 80% between procedures, with the Youd et al. (2001) procedure often yielding the highest F.S. While

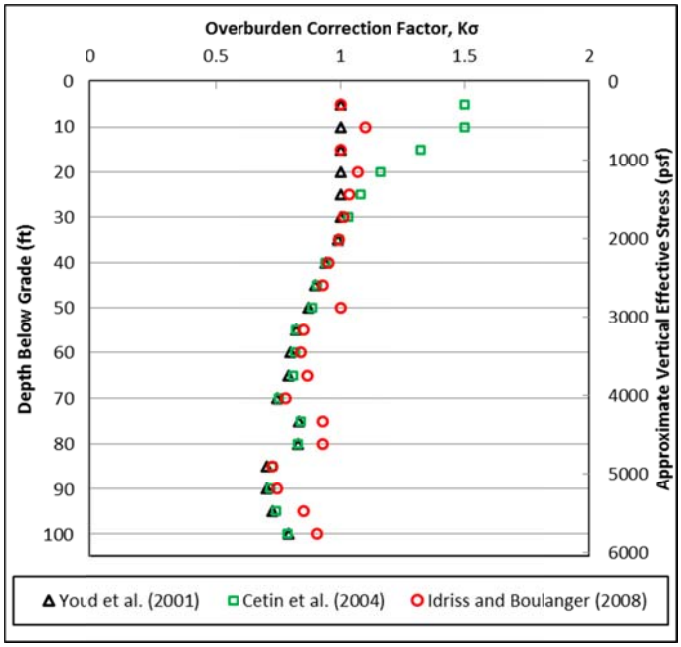

Figure 4.15. Comparison of the Kσ values at Site No. 2 for all three simplified procedures.

at Site No. 1, differences in the F.S. at depth were clearly driven by high C_N values resulting from the Idriss and Boulanger (2008) procedure, it was impossible to pin down a single controlling factor at Site No. 2. Rather, differences in the F.S. estimates were controlled by various factors at different depths, including r_d, C_N, fines content, and Kσ, which interact in a complex manner. It will be noted that the extremely high CSR values at Site No. 1 (caused by a_{max} = 0.82 g) may have masked some of the more subtle influences of that were apparent at Site No. 2.

4.2.3 Site No. 3

Site No. 3 is located near Edmundson, Arkansas. The soil conditions are classified as Site Class E based on the measured SPT blow counts. The site-adjusted design peak horizontal ground acceleration (a_{max}) with a 7% probability of exceedance in

75 years for this site is 0.44 g and the estimated M_w is 7.42 (refer to Section 3.3.1.1). The soil profile consist of clay from the surface to a depth of 9 m (30 ft), followed by a thick sandy layer down to a depth of 33 m (110 ft).

Figure 4.16 presents the F.S. values at Site No. 3 for each of the three procedures. The depths where the three procedures yield a different prediction for liquefaction triggering include 17-24 m and 32 m (55-80 ft and 105 ft). At these depths, the F.S. from the Idriss and Boulanger (2008) procedure are consistently greater than the others. Furthermore, the Idriss and Boulanger (2008) procedure also predicts cyclic softening in the clay between 6-7.5 m (20-25 ft), whereas these soils are not directly considered in the procedures of Youd et al. (2001) and Cetin et al. (2004). Like previous sections, the variables (r_d, C_N, $K\sigma$, ect.) are presented below.

Figure 4.17 presents the variable r_d for each of the three procedures. The relationship of Idriss and Boulanger (2008) consistently yields the highest r_d values and the Cetin et al. (2004) procedure produces the lowest values. The maximum difference is approximately 60% between the depths of 12-15 m (40-50 ft), yet the F.S. estimates at this depth are almost identical. Although large differences in r_d are *usually* not a significant source of difference in the F.S. estimates between procedures (due to the use of r_d in the development of the CRR curves), in some circumstances r_d can influence F.S. results between procedures, as was noted at Site No. 2.

Figure 4.18 presents the $CSR_{M=7.5,1atm}$ at Site No. 3 for all three procedures. The CSR values are all mostly less than 0.4 and directly mirror the similarities and differences in r_d.

Figure 4.16.Comparison of the factor of safety against liquefaction triggering at Site No.3 for all three simplified procedures.

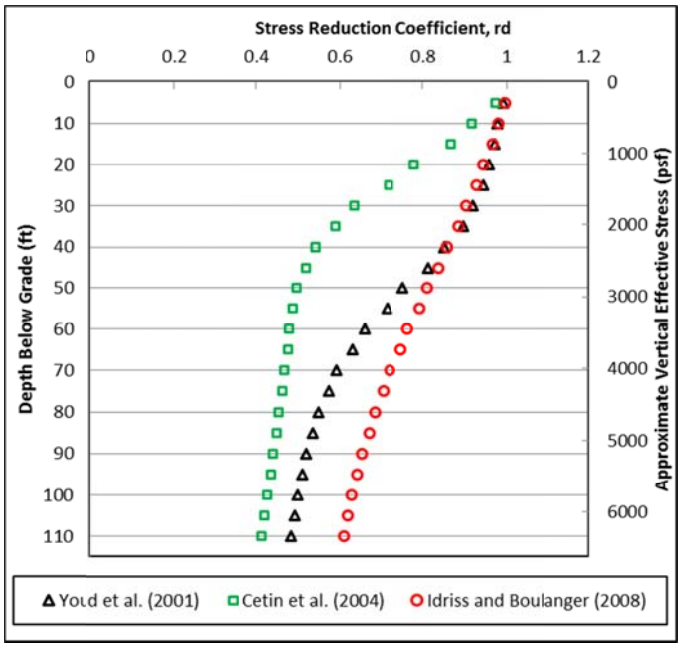

Figure 4.17.Comparison of the r_d values at Site No. 3 for all three simplified procedures.

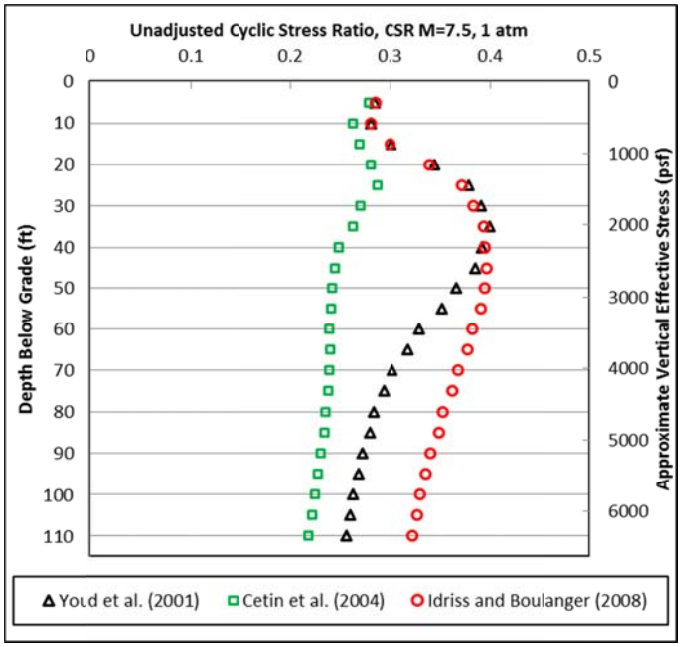

Figure 4.18. Comparison of the $CSR_{M=7.5,\ 1\ atm}$ values at Site No. 3 for all three simplified procedures.

Figure 4.19 presents the variable C_N for each of the three procedures. The C_N values agree quite well over the depth range of 6-15 m (20-50 ft) (approximately 0.47-1.4atm [1000-3000 psf]). However, at depths greater than 17 m (55 ft) the C_N values of Idriss and Boulanger (2008) range from 10-30% higher than the other procedures, interestingly mirroring the deviation in the F.S. values below this same depth (refer to Figure 4.16).

In general, C_N is typically responsible for most of the difference in the $(N_1)_{60cs}$ values between procedures, but C_S also contributes in some cases. In order to observe which of these variables is most influential for Site No. 3, Table 4.2 presents all of the blow count correction factors at a depth of 20 m (65 ft). In this table, the C_R, C_B, C_E, and Clean Sand correction are identical for each of the three procedures. The C_S values are

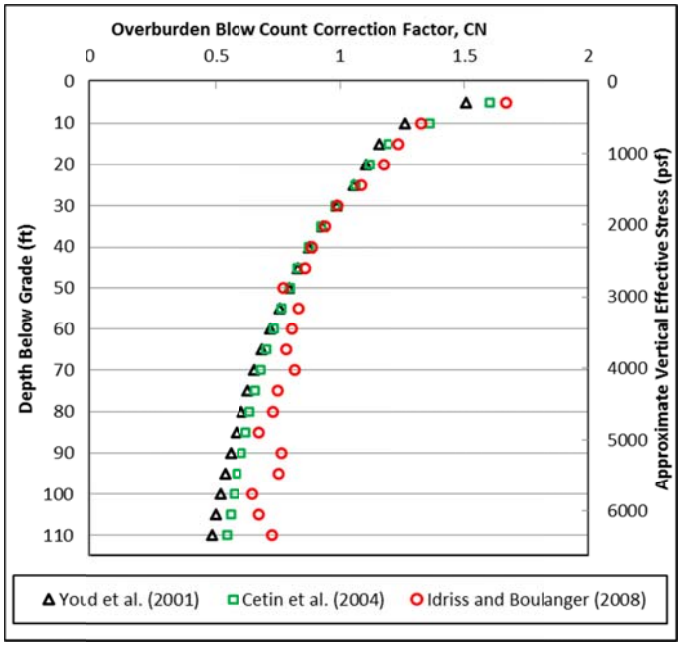

Figure 4.19.Comparison of the C_N values at Site No. 3 for all three simplified procedures.

Table 4.2. Comparison of blow count correction factors for Site No. 3 at a depth of 20 m (65 ft)

	Raw N value	C_E	C_R	C_B	C_S	C_N	$(N_1)_{60}$	Clean Sand Correction[1]	$(N_1)_{60cs}$
Youd et al. (2001)	25	1.28	1.00	1.00	1.20	0.69	26	0	26
Cetin et al. (2004)	25	1.28	1.00	1.00	1.28	0.71	28	0	28
Idriss and Boulanger (2008)	25	1.28	1.00	1.00	1.30	0.78	32	0	32

1. No F.C. data available for this sample depth.

the lowest for the Youd et al. (2001) procedure and the highest for the Idriss and Boulanger (2008) procedure, exhibiting a difference of 8%. The C_N values follow this same trend, but produce differences of 13%. Combining the effects of C_S and C_N results in a difference of 23% in $(N_1)_{60cs}$ values (refer to Figure 4.20), making it apparent that the

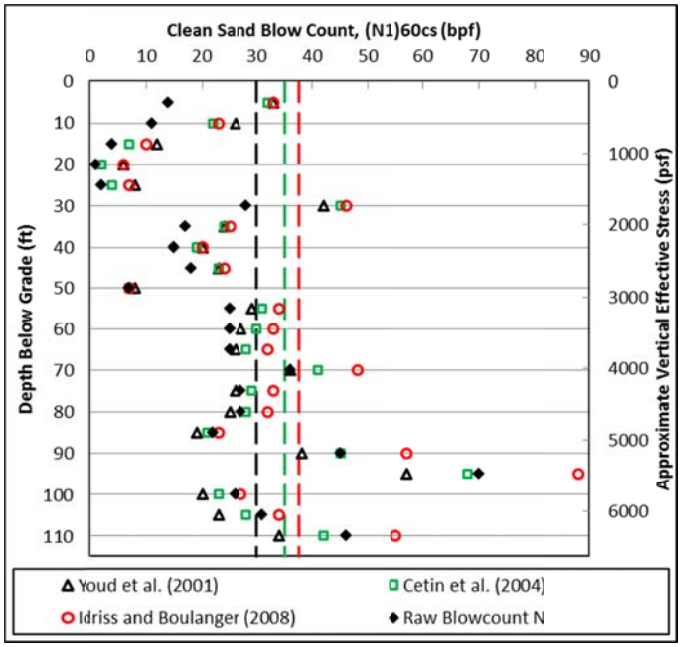

Figure 4.20.Comparison of the $(N_1)_{60cs}$ values at Site No. 3 for all three simplified procedures.

differences in $(N_1)_{60cs}$ values at a depth of 20 m (65 ft) are a direct result of the combined differences of C_S and C_N. Although Table 4.2 only presents data for the depth of 20 m (65 ft), similar trends for depths greater than 17 m (55 ft) are observed in Figure 4.20. Notice that at a depth of 26 m (85 ft) the raw N value is 22, resulting in minimal differences in $(N_1)_{60cs}$ values because differences in C_N values are minimal at this depth (refer to Figure 4.19).

Figure 4.21 presents the $CRR_{M=7.5,1atm}$ values for each of the procedures. There are significant differences between the Idriss and Boulanger (2008) CRR values and the other two procedures between the depths of 17 and 24 m (55 and 85 ft), despite relatively minor differences in the $(N_1)_{60cs}$ values at these same depths. This is due to the proximity of the corrected blow counts to the steep part (i.e. the limiting upper-bound) of the CRR

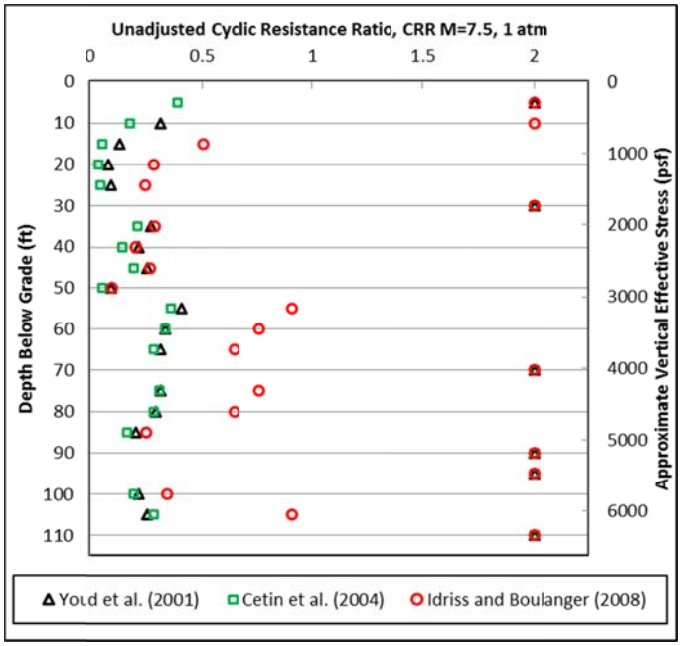

Figure 4.21.Comparison of the $CRR_{M=7.5,\ 1\ atm}$ values at Site No. 3 for all three simplified procedures.

triggering curve. Surprisingly, below a depth of 17 m (55 ft) the differences that were observed in the $(N_1)_{60cs}$ values between Youd et al. (2001) and Cetin et al. (2004) are not apparent in the $CRR_{M=7.5,1atm}$ values. This is because the Cetin et al. (2004) triggering curve lies beneath the Youd et al. (2001) curve (refer to Figure 2.7). While the CRR values for these two procedures are nearly identical below this depth, the CSR values are not (refer to Figure 4.18), resulting in variations in the F.S. (refer to Figure 4.16). Also, it is noted that at depths between 5-7.5 m (15-25 ft), the Idriss and Boulanger (2008) procedure yields $CRR_{M=7.5,1atm}$ values that are substantially greater than the Youd et al. (2001) procedure, despite both procedures having very similar $(N_1)_{60cs}$ values. Based on the clean sand triggering curves presented in Figure 2.7, one would expect the CRR to be very similar for both procedures given a similar $(N_1)_{60cs}$ value. However, the soil between these depths is clay, and the Idriss and Boulanger (2008) procedure analyzes it

based on the cylic softening potential of the soil (i.e. clay-like criteria), not the standard liquefaction potential (i.e. sand-like criteria). This is also why the Idriss and Boulanger (2008) procedure yields a F.S. at these depths (refer to Figure 4.16), while the other two procedures do not.

Figure 4.22 presents the Kσ values for each of the procedures. As discussed above, the differences in Kσ at shallow depths (i.e. the significantly larger Kσ values for the Cetin et al. (2004) procedure) are generally not a concern for these studies because most of the liquefaction potential occurs at depths greater than 6 m (20 ft). At all other depths the Kσ values generally agree within about 5%, except at the discrete depths of 26 and 30 m (85 and 100 ft), where the Kσ values of Idriss and Boulanger (2008) are 15% higher than the other procedures, which directly increases the F.S. by this same percentage. This deviation in Kσ is typically evident when the raw N values are low, because the Kσ values for each of the procedures are dependent on the relative density of the soil (refer to Section 2.4.2) via the "f" factor. As relative densities (and N values) decrease, the Kσ values at effective stresses higher than 1 atm (2116 psf) tend to increase. However, the Kσ values of Idriss and Boulanger (2008) increase by larger amounts than other two procedures, especially at low N values and high effective stresses. This effect is often masked by the opposite trend in C_N, which increases with increased relative densities (and N values).

In summary, the F.S. values for each of the three procedures at Site No. 3 (refer to Figure 4.16) disagree the most at depths between 17-24 m (55-80 ft). Over this same depth range there is often disagreement between procedures about the potential for liquefaction triggering, with the Idriss and Boulanger (2008) procedure predicting no

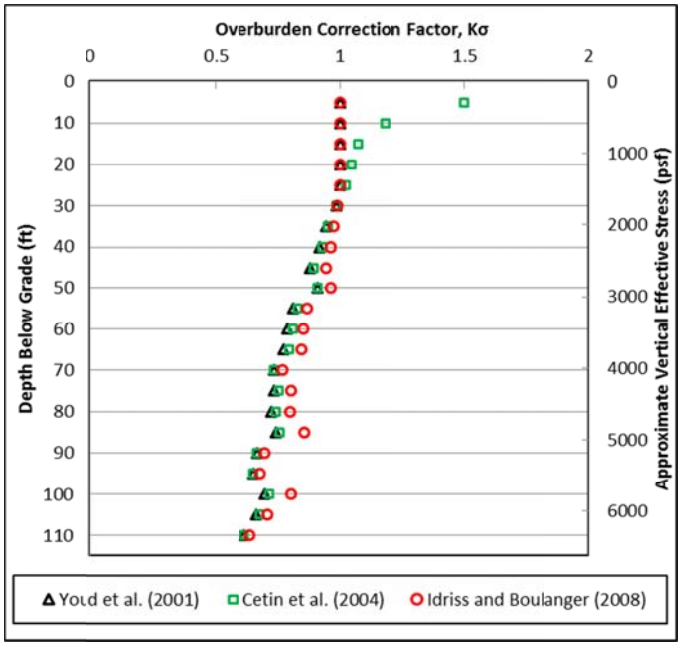

Figure 4.22.Comparison of the Kσ values at Site No. 3 for all three simplified procedures.

liquefaction (F.S. >1.0) and the other two procedures yielding F.S. estimates that are closer to, but generally below, unity. It appears that these differences in liquefaction triggering are primarily driven by variations in the blow count correction factor C_N. Specifically, the iterative, blow count dependent C_N relationship of Idriss and Boulanger (2008) tends to yield significantly greater C_N values when the raw blow count of the material is greater than about 23. These larger values of C_N directly result in larger $(N_1)_{60cs}$ values, which result in higher $CRR_{M=7.5,1atm}$ values and a higher F.S. Differences in F.S. estimates between procedures can become more pronounced as corrected blow counts from a given procedure approach the limiting upper-bound threshold for triggering liquefaction. Other factors like r_d, C_S and Kσ play a role in the variation of liquefaction triggering (i.e. F.S.), however, it seems like differences in C_N dominate. When liquefaction triggering predictions vary between procedures, such as the depth range of

17-24 m (55-80 ft) at Site No. 3, the author recommends predicting liquefaction based on agreement between two out of the three procedures. For example, at a depth of 17 m (55 ft) one would predict no liquefaction because both the Idriss and Boulanger (2008) and Cetin et al. (2004) procedures predict a F.S. >1.0. However, at a depth of 24 m (80 ft) one would predict liquefaction because both the Youd et al. (2001) and Cetin et al. (2004) procedures predict a F.S. < 1.0.

4.3 CONCLUSIONS

This chapter has compared SPT liquefaction triggering evaluations for three different sites in eastern Arkansas. In particular, the comparisons generally focused on evaluating differences in the F.S. estimates at depth (i.e. depths greater than approximately 15 m [50 ft]). These comparisons have revealed situations (specific depths at specific sites) where the three liquefaction triggering procedures yield nearly identical F.S. estimates, and situations where they yield significantly different F.S. estimates. Examinations of depth/stress dependent variables such as r_d, C_N, $(N_1)_{60cs}$, and $K\sigma$ have revealed that no single depth-dependent variable is exclusively responsible for the differences between the liquefaction triggering procedures when F.S. estimates disagree. Surprisingly, in some situations the variable r_d was found to vary by as much as 45% - 60% between procedures for the exact same depth, yet the F.S. estimates for all procedures were nearly identical at these same depths. In other situations, the impact of smaller variations in r_d was evident. In general, it was found that variations in r_d really did not seem to impact the F.S. estimates as much as anticipated. This is likely because each procedure used its respective r_d relationship to define the CRR boundary curve in

the back analyses of the case history database; thereby influencing both the CSR and CRR in forward analyses.

In general, it can be stated that the Idriss and Boulanger (2008) procedure typically yields the highest F.S. estimates at depth. While this is somewhat driven by higher $K\sigma$ values at depth (generally ranging from 5% - 15% greater than the other two procedures), it seems to primarily be a result of significantly higher C_N values at depth (generally ranging from 15% - 60% greater than the other two procedures for higher blow count material). Specifically, the iterative, blow count dependent C_N relationship of Idriss and Boulanger (2008) tends to yield significantly greater C_N values when the raw blow count of the material is greater than about 23. These larger values of C_N directly result in larger $(N_1)_{60cs}$ values, which result in higher $CRR_{M=7.5,1atm}$ values and higher F.S. estimates. Furthermore, as this difference is most pronounced at higher blow counts, and the CRR relationship is very steep and nonlinear, somewhat subtle differences in $(N_1)_{60cs}$ values can result in very significant differences in $CRR_{M=7.5,1atm}$ values.

Overall, for the sites analyzed herein, which have fairly high to very high peak ground accelerations, the three procedures agreed in predicting or not predicting liquefaction at many depths. This lends confidence to these types of deterministic triggering analyses where a "yes" or "no" answer is required. For situations where the three procedures do not agree on liquefaction triggering, the author recommends using the prediction agreed upon by two out of the three procedures. This seems logical given the debate that is ongoing regarding which procedure is "best". The liquefaction triggering workbooks that have been developed in this work enable easy data transfer

between workbooks and facilitate quick and simple comparisons between all three procedures.

Chapter 5

Residual Strength of Liquefied Soils

5.1 Introduction

In order to better assess the post-liquefaction performance of piles, AHTD has expressed interest in developing guidelines for assessing residual shear strengths (Sr) for liquefied soils. Although many correlations for Sr have been proposed over the past 20 - 25 years, some are used more frequently than others. Furthermore, even given a single correlation, the assessment of Sr often falls back to engineering judgment as the design engineer must choose between an upper-bound, lower-bound, or intermediate value. The correlations to estimate Sr that are presented in this chapter have been developed primarily for slope stability applications, not for post-liquefaction performance of piles. But, since no guidance is available for assigning Sr for post-liquefaction pile capacity, these correlations offer the only available alternative. In order to understand the available Sr correlations and their development, a brief review is provided below.

5.2 Review of Past Sr Correlations

Many researchers have used laboratory and/or field data to determine the residual shear strength of liquefied soils (Poulos et al. 1985, Seed 1987, Seed and Harder 1990, Stark and Mesri 1992, Olsen and Stark 2002, Idriss and Boulanger 2008). Poulos et al. (1985) developed a procedure using laboratory tests and steady state soil mechanics theory to determine Sr. This procedure assumed that the void ratio remained constant during the earthquake and flow slide. However, due to water/void redistribution during liquefaction (refer to Section 5.2.3), this assumption was argued to be invalid (Seed 1987,

Pilecki 1988). Furthermore, various sample preparation methods were found to influence the slope of the steady state line (Dennis 1988), causing the validity of results obtained from reconstituted specimens to be questioned relative to their true in-situ behavior. As a result of these findings, researchers began to focus on developing empirical Sr estimates based on back analyses of slope failure case histories from previous earthquakes.

5.2.1 Seed and Harder (1990)

Seed (1987) analyzed 12 liquefaction-induced slope failure case histories to back-calculate a relationship between SPT blow count and Sr. These results were later adjusted by Seed and Harder (1990) to account for kinetic movement of the failure mass. The Seed and Harder (1990) relationship, presented in Figure 5.1, has been used extensively to determine Sr (Seed 2010). This Sr correlation includes an upper- and lower-bound and allows the engineer to use some judgment when determining Sr. However, Seed and Harder (1990) recommend using the lower bound relationship to remain conservative. The raw data in this correlation also includes error bars, which represent the difficulty in back-calculating shear strength and assigning a representative SPT blow-count (Olsen and Stark 2002).

In Figure 5.1, $(N_1)_{60\text{-}cs}$ is used to denote the corrected clean sand SPT blow count along the horizontal axis. This is an unfortunate designation because it is not the same as the corrected clean sand blow count used within liquefaction triggering evaluations (i.e. $(N_1)_{60cs}$, as discussed in Chapter 2). The fines content correction factor used to determine $(N_1)_{60\text{-}cs}$ for obtaining Sr is different than the fines content correction used to determine

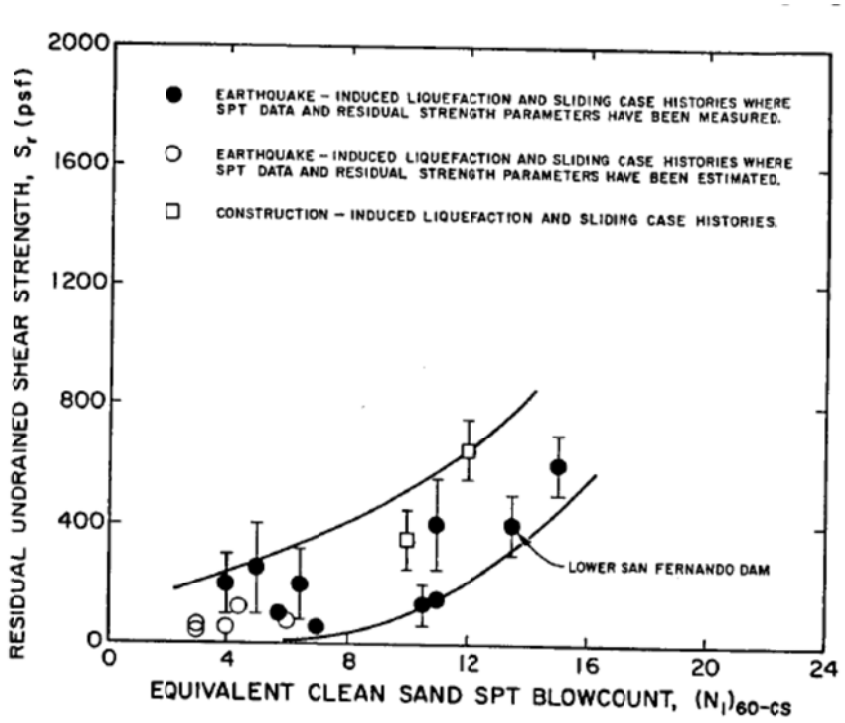

Figure 5.1. Relationship between Sr and $(N_1)_{60cs\text{-}Sr}$ proposed by Seed and Harder (1990).

$(N_1)_{60cs}$ within the liquefaction triggering relationships. In order to more clearly distinguish between these two corrected blow counts, the nomenclature used by Idriss and Boulanger (2008) has been adopted within this report: $(N_1)_{60cs\text{-}Sr}$ will designate the corrected blow count adjusted for fines content and used for evaluation of Sr, while $(N_1)_{60cs}$ designates the corrected blow count that is to be employed for the liquefaction triggering evaluation.

Table 5.1 presents the Sr fines content correction factors $[\Delta(N_1)_{60\text{-}Sr}]$. These are the original factors proposed by Seed (1987), and have been adopted by Seed and Harder (1990) and Idriss and Boulanger (2008). These factors should be used according to Equation 5.1.

Table 5.1. Values of $\Delta(N_1)_{60\text{-}Sr}$ recommended by Seed (1987)

Fines Content % passing No. 200 sieve	$\Delta(N_1)_{60\text{-}Sr}$
10	1
25	2
50	4
75	5

$$(N_1)_{60cs-Sr} = (N_1)_{60} + \Delta(N_1)_{60-Sr} \qquad \text{Equation 5.1}$$

5.2.2 Olsen and Stark (2002)

Due to an increase in soil shear strength at high confining pressures, Stark and Mesri (1992) proposed that a relationship between Sr and blow count should be based on the residual shear strength ratio (or liquefied shear strength ratio). The residual shear strength ratio is calculated by normalizing Sr by the pre-failure in-situ vertical effective stress (σ'_v). Accordingly, Stark and Mesri (1992) developed a correlation based on the ratio of Sr/σ'_v by analyzing the case histories from Seed and Harder (1990) plus three additional case histories. Later, a coalition of workshop participants (Stark et al. 1998) determined that liquefaction induced lateral spreading did not correspond to the same shear strength mobilized within the slope stability-type failures and should be analyzed separately (Olsen and Stark 2002). So, a few of the case history data points were removed from the original Stark and Mesri (1992) correlation.

Olsen and Stark (2002) incorporated new case histories, along with kinetics, to update the earlier recommendations of Stark and Mesri (1992) and Stark et al. (1998). Their correlation is labeled "proposed relationship" within Figure 5.2. This figure also

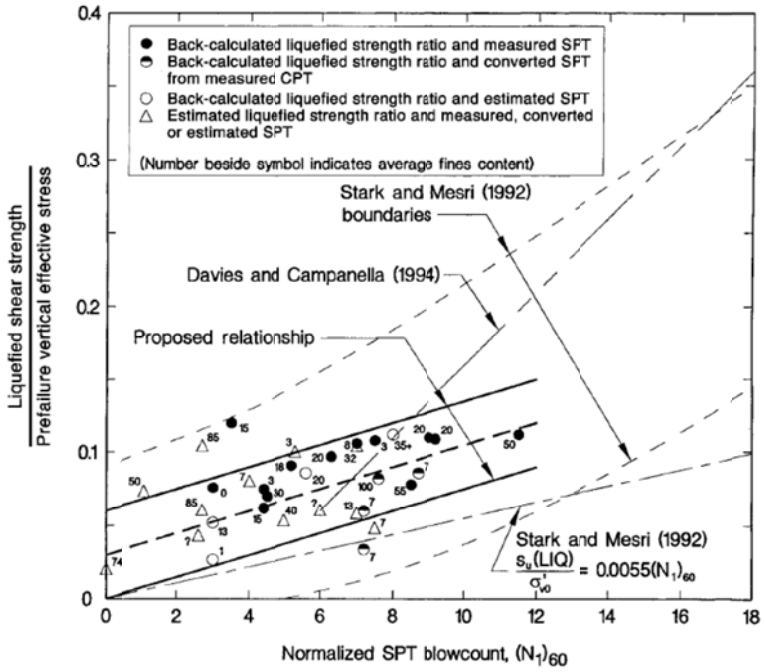

Figure 5.2. Residual shear strength ratio (Sr/σ'_v) correlation proposed by Olsen and Stark (2002).

includes other correlations, including the one proposed by Stark and Mesri (1992). Notice the bottom axis of the graph is the corrected blow count without any fines correction [i.e. $(N_1)_{60}$]. In order to use this correlation properly, the authors do not recommend any correction for fines content because as Olsen and Stark (2002) state: "The data reveal no trend in liquefied strength ratio with respect to fines content." The proposed relationship includes a band of possible values, which demonstrate a clear trend, albeit with considerable scatter. The relationship recommended by Olson and Stark (2002) is the average between the lower- and upper-bound, although the lower-bound should be employed if conservatism is desired.

5.2.3 Idriss and Boulanger (2008)

Because the debate between using direct Sr correlations or correlations using Sr/σ'_v is ongoing (Seed 2010), Idriss and Boulanger (2008) report two separate correlations, as presented below in Figures 5.3 and 5.4. Eighteen case histories previously published in Seed (1987), Seed and Harder (1990), and Olsen and Stark (2002) were re-analyzed to develop these correlations. Each correlation has been extrapolated to SPT blow counts beyond what was available in the case history data base, as indicated by the dashed lines within the figures. Idriss and Boulanger (2008) have determined that the extrapolation of this data is necessary based on current needs of the engineering community. The data presented in Figure 5.3 has been grouped into three bins based on the geometry and SPT information available for each case history data point. Group one includes both adequate geometric and SPT data, group two has good SPT data but lacks good geometric details, and group three has complete geometric details with limited SPT data.

Two possible relationships based on the residual shear strength ratio (Sr/σ'_v) are presented in Figure 5.4. The upper curve should be used in cases were void redistribution is expected to be minimal and the lower curve should be employed when void redistribution effects could be significant. Void redistribution occurs within a liquefied zone when dissipation of excess pore water pressures are impeded by a relatively impervious boundary. This impedance allows a water film to develop within a localized area at the boundary between the soil layers. While this small area may exhibit shear strengths near zero, the average shear strength over a larger area is unlikely to be zero (Idriss and Boulanger 2008). The effects of void redistribution can significantly lower

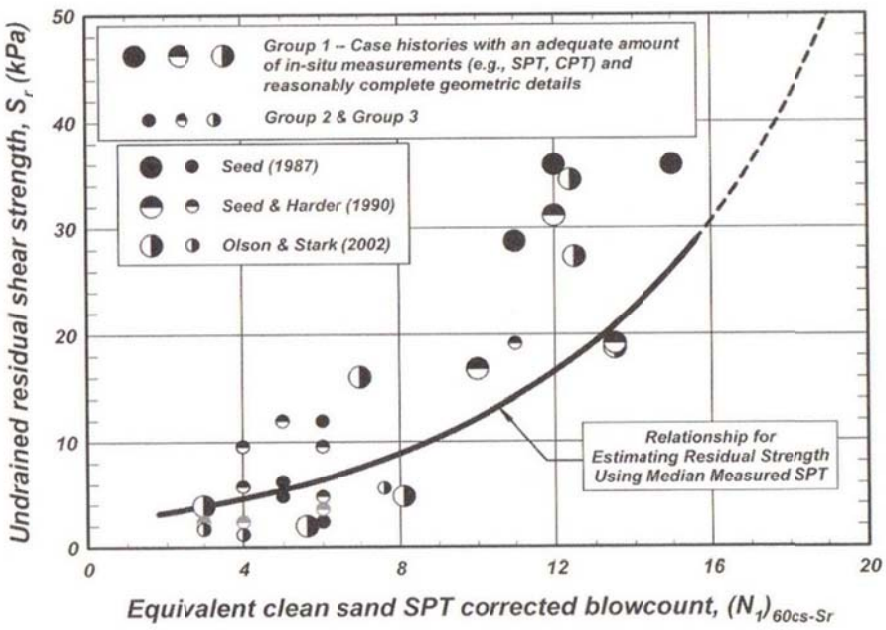

Figure 5.3. Relationship between Sr and $(N_1)_{60cs-Sr}$ proposed by Idriss and Boulanger (2008).

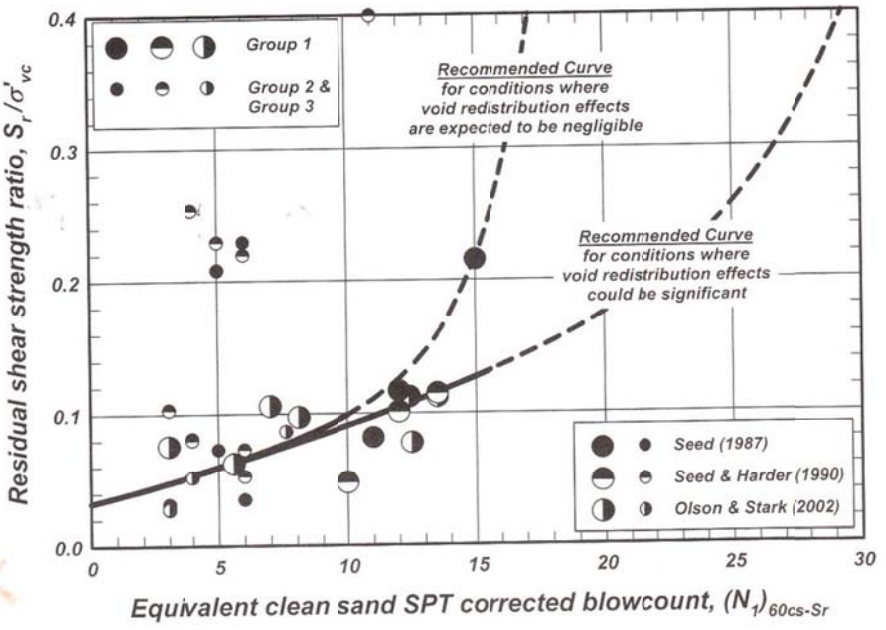

Figure 5.4. Residual shear strength ratio (Sr/σ'_v) correlation proposed by Idriss and Boulanger (2008).

the residual shear strength in localized areas, and using this relationship will result in a more conservative assessment of Sr/σ'_v. In eastern Arkansas, most of the liquefiable sandy soil deposits are overlain by a thick clay layer, which will most likely impede the flow of excess pore water pressure and result in significant void redistribution near the layer interface. However, the potentially liquefiable soil layer is often quite thick, and one would not expect significant void redistribution within the liquefiable layer.

5.3 Comparison of Direct Strength and Strength Ratio Relationships

In order to more easily compare direct Sr correlations, the relationships proposed by Seed and Harder (1990) and Idriss and Boulanger (2008) have been digitized and are presented together in Figure 5.5. The correlation of Idriss and Boulanger (2008) is near the middle of the range proposed by Seed and Harder (1990), except at blow counts larger than 15, were Idriss and Boulanger (2008) have extrapolated their correlation to account for a lack of case history data. Not surprisingly, these correlations yield similar results because the same case history data were used in their development.

In a similar manner, the Sr/σ'_v correlations of Stark and Mesri (1992), Olsen and Stark (2002), and Idriss and Boulanger (2008) are compared in Figure 5.6. The Idriss and Boulanger (2008) relationships are very near the average Sr/σ'_v relationship proposed by Olsen and Stark (2002), except at blow counts above 12, where the relationships have been extrapolated.

The direct Sr and Sr/σ'_v relationships have been compared graphically in Figures 5.5 and 5.6. However, it is impossible to compare these two approaches outright without applying the relationships using specific blow counts and effective confining stresses. A

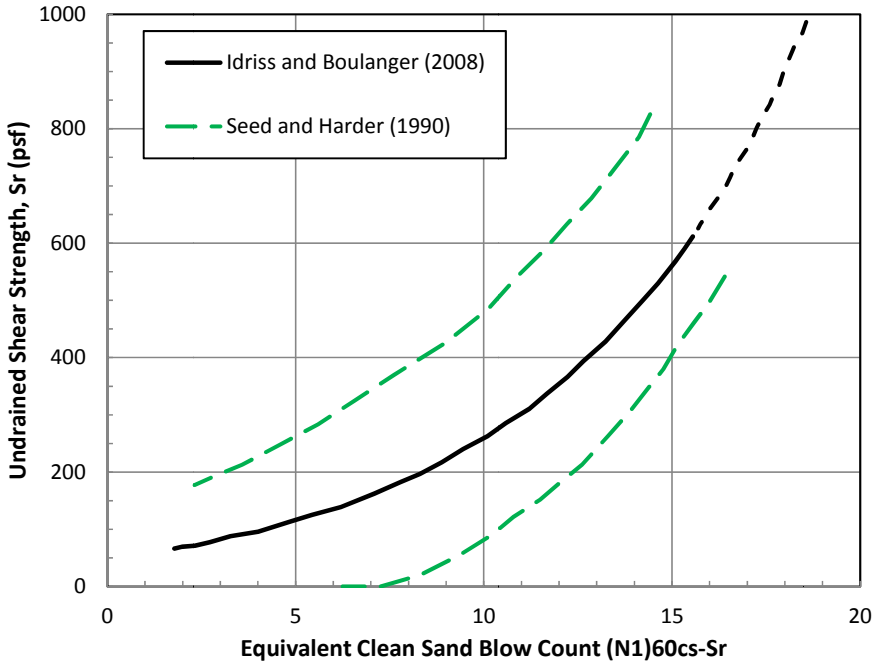

Figure 5.5. Comparison of Sr as a function of $(N_1)_{60cs\text{-}Sr}$.

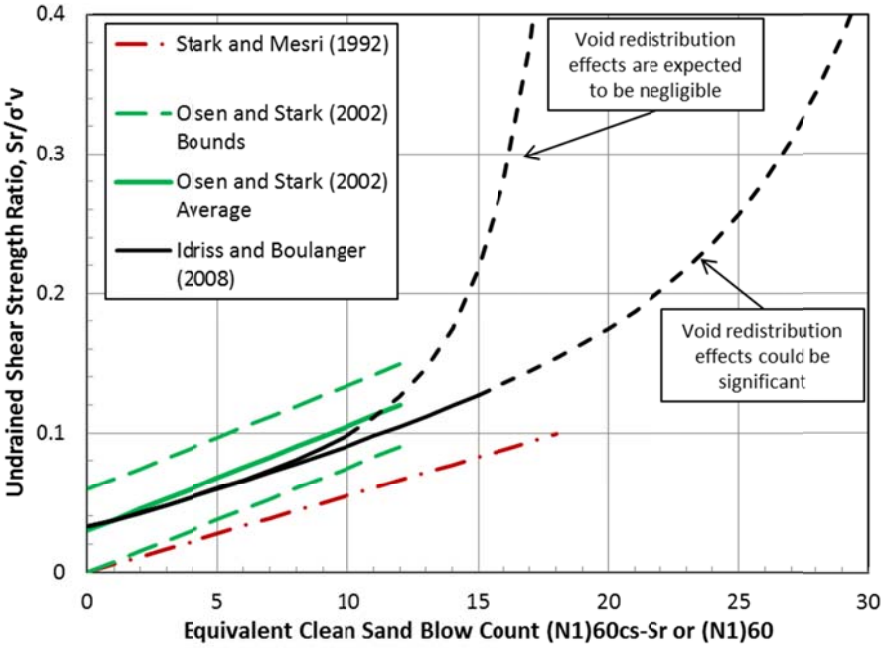

Figure 5.6. Sr/σ'_v correlations as a function of $(N_1)_{60cs\text{-}Sr}$ or $(N_1)_{60}$.

simple table (refer to Table 5.2) has been prepared to hypothetically compare the various Sr estimates one would obtain from typical values of blow count and effective stress using the direct Sr and Sr/σ'_v relationships presented above. Corrected blow counts ranging from 5-15 and effective stresses ranging from 0.54-2.72 atm (1152-5760 psf) were used. Therefore, the Sr estimates provided in Table 5.2 are representative of values one might obtain from the various relationships when applied to soft soils approximately 6-30 m (20-100 ft) below the surface.

At a depth of 6 m (20 ft) and a corrected blow count of 5, the relationships yield Sr estimates ranging from 0-5.3 kPa (0-112 psf), with the direct Sr relationship of Idriss and Boulanger (2008) yielding the highest estimate. At a depth of 12 m (40 ft) and a corrected blow count of 10, the relationships yield Sr estimates ranging from 2.6-11.5 kPa (55-241 psf). Interestingly, for these parameters, all of the Sr estimates are within 15% of one another, except for the estimate obtained from the relationship of Seed and Harder (1990), which is a lower-bound prediction. At a depth of 21 m (70 ft) and a corrected blow count of 10, the relationships yield Sr estimates ranging from 2.6-20.2 kPa (55-423 psf), with the Sr/σ'_v relationship of Olsen and Stark (2002) yielding the highest estimate. The blow count was purposely fixed at 10 for both of these depths (i.e. 12 and 21 m [20 and 70 ft]) to demonstrate the difference between the direct Sr and Sr/σ'_v relationships. The reader will notice that the Sr estimates increase with increasing depth/effective confining pressure when using the Sr/σ'_v relationships even if the blow count remains constant. Therefore, at significant depths/confining stresses the Sr/σ'_v relationships will always yield higher Sr estimates for a given blow count.

Table 5.2. Sr estimates obtained from direct Sr and Sr/σ'_v relationships using hypothetical blow counts and effective confining stresses.

			Sr Relationships		Sr/σ'_v Relationships		
Depth (m / ft)	Approximate Effective Stress[1] σ'_v (atm / psf)	Corrected Blow Count, (blows/ft)	Seed and Harder[2] (1990), (kPa / psf)	Idriss and Boulanger (2008), (kPa / psf)	Olsen and Stark[3] (2002), (kPa / psf)	Idriss and Boulanger (2008) Significant Redistribution, (kPa / psf)	Idriss and Boulanger (2008) Insignificant Redistribution, (kPa / psf)
6 / 20	0.54 / 1152	5	0 / 0	5.3 / 112	3.7 / 77	3.2 / 68	3.2 / 68
12 / 40	1.09 / 2304	10	2.6 / 55	11.4 / 240	11.5 / 241	10 / 209	10.9 / 227
21 / 70	1.91 / 4032	10	2.6 / 55	11.4 / 240	20.2 / 423	17.5 / 366	19 / 398
30 / 100	2.72 / 5760	15	18.1 / 379	25.3 / 529	NA	35 / 732	59.7 / 1248

1. Stresses calculated assuming a uniform soil profile (refer to section 2.3.1)
2. Lower-bound relationship
3. Average relationship

At a depth of 30 m (100 ft) and a corrected blow count of 15, the relationships yield Sr estimates ranging from 18.1-59.7 kPa (379-1248 psf). The Sr/σ'_v relationships of Idriss and Boulanger (2008) yield significantly higher estimates of Sr than either of the direct Sr relationships. However, the "significant redistribution" Sr estimate is much smaller than the "insignificant redistribution" estimate, demonstrating the importance of predicting if void redistribution is likely for soils with corrected blow counts greater than approximately 12 (refer to Figures 5.4 and 5.6).

5.4 Site-Specific Comparison of Direct Strength and Strength Ratio Relationships

Unlike previous comparisons in this chapter, this section presents estimated Sr values using actual data from a soil boring completed in Northeast Arkansas. Table 5.3 is a compilation of information needed to estimate Sr, while Table 5.4 provides the estimated Sr values. At a depth of 9 m (30 ft) and raw blow count of 11 (corrected to 14 and 15), the relationships yield estimates between 17.2-31.4 kPa (379-665 psf). Although this is a fairly large spread (75%), the three lowest Sr values differ by less than 10%.

Table 5.3. Site-specific information used to estimate Sr.

Depth (m / ft)	F.S.[1]	Raw blow count N (blows/ft)	Fines Content (%)	Effective Stress σ'_v (atm / psf)	$(N_1)_{60}$, [1] (blows/ft)	$(N_1)_{60cs\text{-}Sr}$, [2] (blows/ft)
9 / 30	0.2	11	9	1.45 / 3070	14	15
18 / 60	0.17	13	5	2.29 / 4848	12	13
27 / 90	0.29	27	4	3.2 / 6776	20	21

1. Determined using workbook of Youd et al. (2001) accompanying this report.
2. Determined using the recommendations of Seed (1987) (refer to Section 5.2.1).

Table 5.4. Sr estimates obtained from direct Sr and Sr/σ'v relationships using site-specific information.

	Sr Relationships		Sr/σ'_v Relationships		
Depth (m / ft)	Seed and Harder[1] (1990), (kPa / psf)	Idriss and Boulanger (2008), (kPa / psf)	Olsen and Stark[2] (2002), (kPa / psf)	Idriss and Boulanger (2008) Significant Redistribution, (kPa / psf)	Idriss and Boulanger (2008) Insignificant Redistribution, (kPa / psf)
9 / 30	17.2 / 379	24.3 / 529	19.2 / 414[3]	18.2 / 390	31.4 / 665
18 / 60	10.1 / 212	18.2 / 393	27.3 / 581	25.3 / 542	33.4 / 708
27 / 90	NA	NA	NA	59.7 / 1269	194.5 / 4065

1. Lower-bound relationship.
2. Average relationship.
3. Extrapolated beyond maximum SPT of 12 (refer to Figure 5.2).

At a depth of 18 m (60 ft) and a raw blow count of 13 (corrected to 12 and 13), the relationships yield Sr values ranging from 10.1 to 33.4 kPa (212 to 708 psf), a difference of 230%. At this overburden pressure (2.29 atm [4848 psf]) all of the Sr/σ'_v relationships yield larger estimates of Sr than the direct Sr relationships. This is a trend that becomes more distinguishable as σ'_v increases. At 27 m (90 ft) and a raw blow count of 27 (corrected to 21), the extrapolated Sr/σ'_v relationships of Idriss and Boulanger (2008) offer the only available estimates of Sr. The "insignificant redistribution"

relationship must be limited to a maximum Sr/σ'_v value, which Idriss and Boulanger (2008) recommend as the tangent of the soils internal angle of friction (assumed to be 0.6 in this table). Even with the maximum permissible Sr/σ'_v employed, the "insignificant redistribution" relationship yields a Sr of 194.5 kPa (4065 psf), which is 220% higher than the "significant redistribution" Sr of 59.7 kPa (1269 psf). This large spread in Sr demonstrates again, the importance of predicting if void redistribution is likely for soils with corrected blow counts greater than approximately 12.

Site-specific information such as; corrected blow count, fines content, and depth of the sample (effective stress), influence the Sr estimates these relationships provide. This makes it challenging to determine which relationship will provide the most, or least, conservative estimate for a given set of data. However, as effective stresses increase the Sr estimates from Sr/σ'_v relationships are usually higher than the direct Sr relationships. At very shallow depths (low effective stresses), the blow count governs the estimated Sr values, and any of the correlations could provide the lowest, or highest estimate of Sr. The author recommends comparing results from at **least** three relationships in order to assign an estimated Sr with some level of confidence.

5.5 CONCLUSIONS AND RECOMMENDATIONS

The available correlations for estimating Sr are based on back-analyses of liquefaction-induced slope failure case histories. The use of these correlations in post-liquefaction performance of piles, while not entirely accurate, provides the only available alternative for calculating the residual shear strength of liquefied soils using SPT data. Other correlations based on soil sampling and laboratory testing, have been shown to be

invalid (refer to Section 5.2). Although this chapter did not present all of the available correlations, the most widely used correlations have been discussed.

When obtaining Sr directly from corrected blow count, without considering σ'_v, the lower-bound relationship proposed by Seed and Harder (1990) may be used if the lowest value of Sr is desired. However, the relationship proposed by Idriss and Boulanger (2008) falls within the upper- and lower-bound of the Seed and Harder (1990) relationship and it seems reasonable to use if less conservatism is desired (i.e. higher Sr estimates). The Idriss and Boulanger (2008) relationship is the only option for blow counts greater than 15.

When obtaining Sr using the residual shear strength ratio (Sr/σ'_v) approach, all three of the procedures produce similar results for blow counts less than 12. At blow counts higher than 12, only the relationships proposed by Idriss and Boulanger (2008) provide an estimate of Sr. The engineer will have to determine whether or not to include the effects of void redistribution (refer to Section 5.2.3). The author recommends employing at least three correlations and comparing the results. This should enable the engineer to have some confidence in the assignment of the estimated Sr.

Chapter 6

Potential Liquefaction Mitigation Techniques

6.1 Introduction

There are many ground improvement techniques that can be used to mitigate soil liquefaction. These varied techniques have been utilized in many soil conditions and have been developed by both the construction industry and research institutions. Often, new techniques are developed when difficult circumstances are encountered in the field and necessity facilitates invention. These new ground improvement techniques are then refined and become part of the expanding set of available mitigation measures. Which of these techniques to employ depends on many variables, including; soil type, cost of improvement, and local site conditions (i.e. low overhead clearance, large or small area of improvement, etc…), just to name a few. Discussing the intricate details associated with each of the mitigation techniques is beyond the scope of this report, however, a brief description of each of the ground improvement techniques, applicable treatment soil types, and the likelihood of effectiveness are discussed herein.

6.2 Soil Liquefaction Mitigation Techniques

Many ground improvement techniques are available to mitigate soil liquefaction. The mechanisms these techniques employ include; densification, drainage, reinforcement and confinement. Table 6.1 lists possible liquefaction mitigation techniques along with the mechanism of improvement. Because typical depths of improvement for past applications have been less than or equal to 15 m (50 ft), much of the experience and

Table 6.1. Liquefaction mitigation techniques discussed in this report

Method of Improvement	Mechanism of Improvement
Vibratory Compaction (Sand piles)	Densification/Drainage
Stone Columns	Densification/Drainage/Reinforcement
Vibro Concrete Columns	Densification/Reinforcement
Dynamic Compaction	Densification
Compaction Grouting	Densification
Permeation/Chemical Grouting	Compensation
Jet Grouting	Reinforcment/Replacement
Deep Soil Mixing	Confinement
Deep Blasting	Densification
Earthquake Drains	Drainage
Dewatering	Drainage
Removal and Replacement	Replacement

design guidance are limited to these depths. Also, the large depths of improvement needed in certain areas of the New Madrid Seismic Zone (NMSZ) (>15 m, [50 ft]) should be kept in mind while reading this chapter and any available literature. Each of the mitigation techniques included in this table will be discussed in more detail in subsequent sections.

6.2.1 Vibratory Methods

Vibratory methods have been used to successfully densify soil in the U.S. since 1948 (Schaefer 1997). The three types of vibratory methods discussed in this chapter include; Sand Compaction Piles, Stone Columns and Vibro-Concrete Columns. Each of these methods employs somewhat similar equipment and construction techniques. A probe is vibrated to the maximum depth of improvement. Then, material (sand, gravel or concrete) is introduced into the soil either through a tube in the probe or the annulus between the probe and the soil. As the probe is raised and lowered the material is forced laterally into the soil, thus densifying it.

6.2.1.1 Sand Compaction Piles

Sand Compaction Piles, or Vibro-Compaction, is common between depths of 3 to 15 m (10 to 50 ft), although soil depths up to 36 m (120 ft) have been successfully densified (Schaefer 1997). This soil improvement technique uses clean sand as a backfill material or, the site may be lowered an amount equal to the densification of the in-situ soil. Figure 6.1 illustrates the Sand Compaction Pile construction process and finished product. Sand Compaction Piles can be completed with or without water jets (i.e. wet or dry method). The use of water jets aid penetration and reduce inter-granular forces, thereby encouraging compaction (Dobson and Slocombe 1982). Wet or dry, this type of treatment is best suited for clean granular soils. One drawback is that improvement must be continued throughout the entire depth of insertion, even if only a deep isolated layer is susceptible to liquefaction, which could result in a large cost increase. The degree of densification that Sand Compaction Piles are capable of is highly dependent on; vibrator type and size, penetration spacing, soil type, and compaction procedures (Hayden and Baez 1994).

6.2.1.2 Stone Columns

Stone Columns are similar to Sand Compaction Piles, but use crushed gravel for the backfill material. Figure 6.2 illustrates the stone column construction process and finished product, which is a stone column that is tightly interlocked with the surrounding soil (Munfakh et al. 1987). The gravel densifies the soil adjacent to the stone column and provides a path to relieve the potential buildup of excess pore water pressures. This technique is especially effective in clean sands, but can be used in soils with high fines content if drainage is provided (Mitchell et al. 1998). Like Sand Compaction Piles,

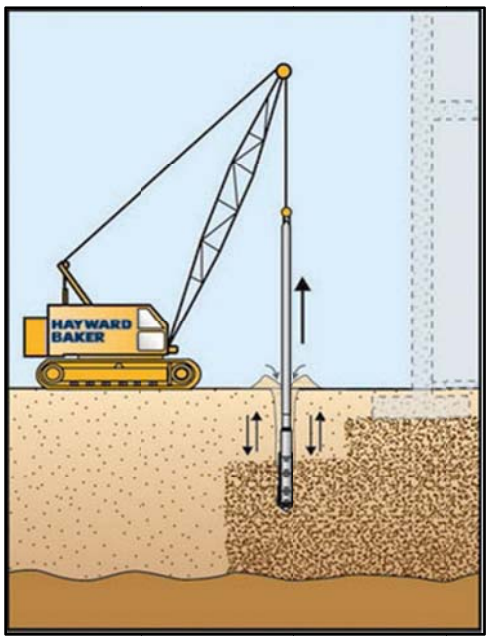

Figure 6.1. Illustration of the Sand Compaction Pile construction process (Hayward Baker Inc. 2010b).

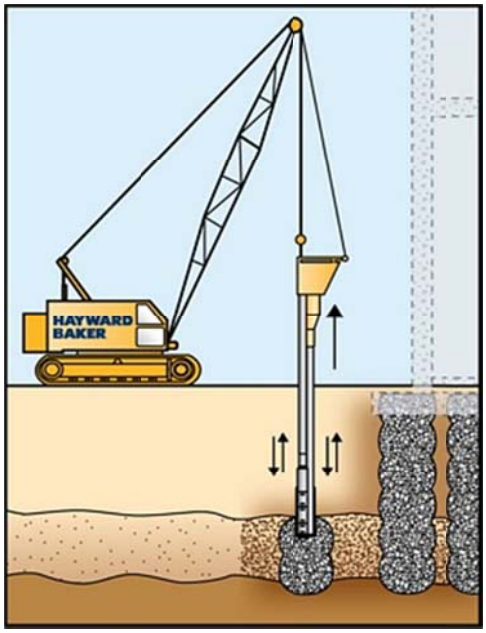

Figure 6.2. Illustration of the Stone Column construction process (Hayward Baker Inc. 2010b).

improvement must be continued throughout the entire depth of insertion, even if only a deep isolated layer is susceptible to liquefaction. The cost and effectiveness of stone columns depend on the availability of clean gravel and the spacing and diameter of the columns.

6.2.1.3 Vibro-Concrete Columns

Vibro-Concrete Columns were developed by the Keller Company and have been used substantially in Europe since 1976 (Hayden and Baez 1994). Figure 6.3 illustrates the Vibro-Concrete Column construction process and final product. Instead of sand or gravel, concrete is pumped to the vibrator tip. Initially, at depth, the vibrator moves up and down forcing the concrete into the surrounding soil to form a mushroom. After the initial mushroom is formed, the vibrator is withdrawn as concrete is pumped into the void space producing a concrete column. Vibro-Concrete Columns transfers loads from the surface to deeper more competent strata and densify looser layers.

6.2.2 Deep Dynamic Compaction

Dynamic Compaction is a method of densifying the soil by repeatedly dropping a heavy weight (9,000-27,000 kg [20,000-60,000 lbs]) from heights of 15-40 m (50-120 ft). The energy imparted into the soil rearranges and densifies the particles, as portrayed in Figure 6.4. This method has been shown to improve cohesionless soils to a maximum depth of 10 m (30 ft) under ideal conditions when using a 1 m (3 ft) thick "working mat" of dry granular soil on the surface (Hayden and Baez 1994). Notice that this method is unlikely to improve the density of the soil at the depths greater than 10 m (30 ft). Furthermore, typical soil conditions in northeast Arkansas include a thick clay layer at the

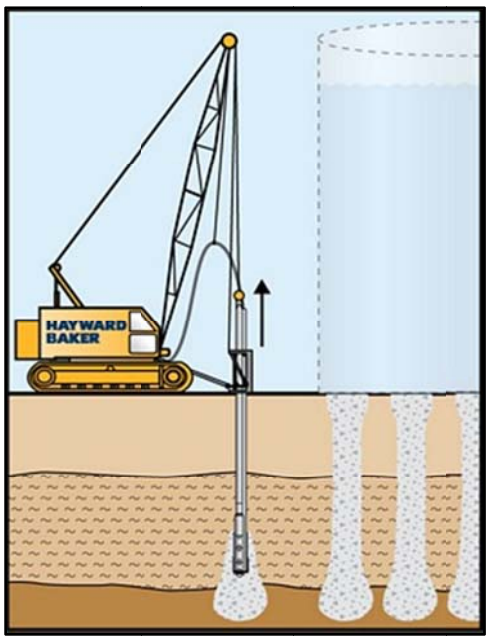

Figure 6.3. Illustration of Vibro-Concrete Column construction process. (Hayward Baker Inc. 2010b).

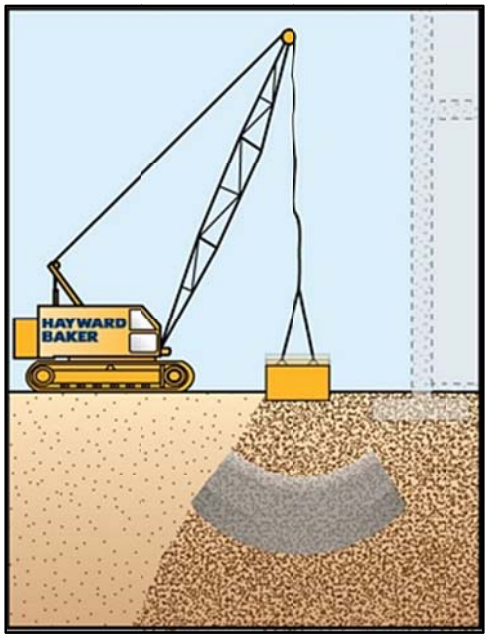

Figure 6.4. Illustration of Deep Dynamic Compaction (Hayward Baker Inc. 2010b).

surface. This clay layer is likely to heave and absorb/attenuate any of the energy that would normally be transmitted to deeper layers. The use of dynamic compaction is not recommended by the author for liquefaction mitigation of these deep sandy soils overlain by clay.

6.2.3 Compaction Grouting

Compaction Grouting began in the 1950's as a remedial technique to fix differential settlement in existing buildings. During the 1980's, the method began to be used as a densification technique for loose soils (Moseley and Kirsch 2004). Figure 6.5 illustrates the bottom-up Compaction Grouting construction sequence. A grout rod is drilled to the maximum depth of improvement, then a low slump grout is injected under pressure, and a grout bulb forces the particles together to densify the sand. The grout rod is incrementally moved up and the process is repeated until the entire target layer has been treated. Compaction grouting is difficult at depths less than 6 m (20 ft), due to a lack of confining pressure. Improvement is especially cost effective in soils containing deep isolated layers of liquefiable material because grout can be injected at the target layers without having to treat the entire soil column (Idriss and Boulanger 2008). The cost of this technique is dependent on the depth and spacing needed to achieve the required densification.

6.2.4 Permeation Grouting

Permeation Grouting, sometimes referred to as Chemical Grouting, is a process of injecting materials into the pore spaces of a loose soil, thereby cementing the particles together and filling the void spaces (Idriss and Boulanger 2008). Grouting materials can

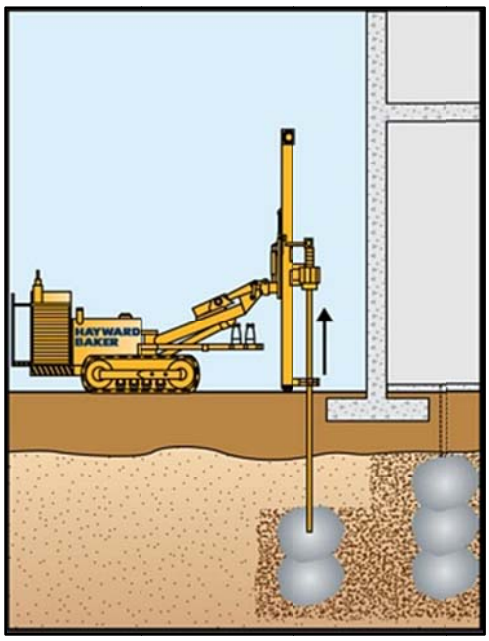

Figure 6.5. Illustration of compaction grouting technique (Hayward Baker Inc. 2010b).

consist of a wide range of substances from chemical grouts to microfine cement with admixtures. The grouting material is forced into the soil under pressure and permeates out radially into the pore spaces of the soil. The choice of material depends on, the pore space of the soil being treated, setting time, required strengths, environmental constraints and cost. The injection process, although conceptually simple, requires control of injection volumes, rates, pressures and intervals, making the construction and injection process complex (Idriss and Boulanger 2008).

Figure 6.6 illustrates some common uses associated with permeation grouting. This method is especially advantages when disturbance of the in-situ soil is undesirable (Thevanayagam and Jia 2003). The depth to which this technique can be feasibly applied has not been found in current literature. This relatively new technique can be

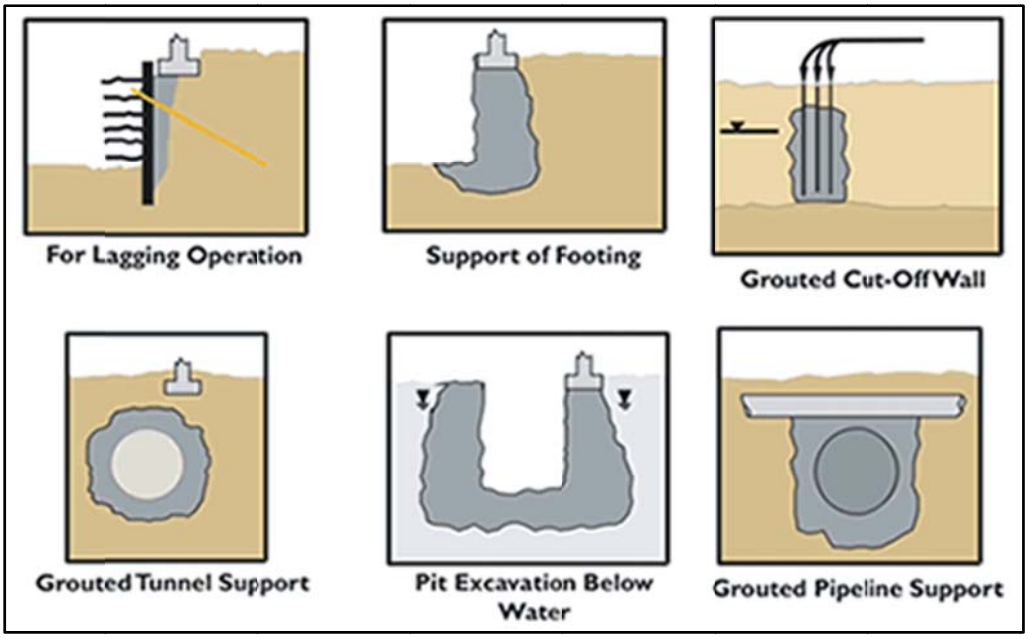

Figure 6.6.Common Permeation Grouting applications (Hayward Baker Inc. 2003).

more expensive than other ground improvement methods, hence its use is generally limited to special situations (Idriss and Boulanger 2008).

6.2.5 Jet Grouting

Jet Grouting uses the mechanism of replacement and/or confinement to mitigate liquefaction. Figure 6.7 illustrates the Jet Grouting construction procedure. A drill rod, with a high pressure port/ports, is advanced to the maximum depth of improvement. Then, high velocity jets of air, water, and grout erode and mix the soil as the drill rod is rotated and lifted. The result is a soil-crete column throughout the entire target layer. Jet Grouting can be used to make in-ground shear walls by overlapping columns, or as an underpinning technique. For liquefaction mitigation, this technique could employ overlapping shear walls in a pattern to confine the soil or to improve entire blocks of liquefiable material within a target layer. Many different jet grouting systems are

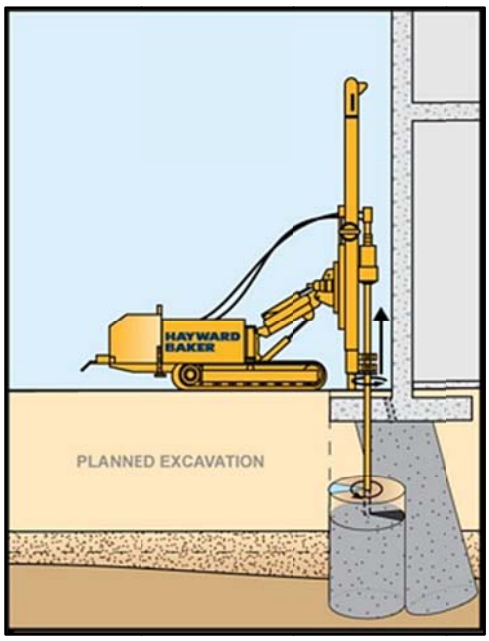

Figure 6.7. Illustration of Jet Grouting construction process using triple fluid system (Hayward Baker Inc. 2010b).

available for site-specific soil and project requirements, these include; single, double and triple fluid systems, as well as SuperJet and X-Jet grouting arrangements (Burke 2004). Although each of these arrangements is different, the final product is very similar. Like Compaction Grouting, Jet Grouting is particularly advantages for a finite layer of liquefiable material located at depth.

6.2.6 Deep Soil Mixing

Deep soil mixing consists of an auger, or row of overlapping augers, being rotated to the target depth, followed by cement being pumped near the tip of the augers while the augers are being rotated and lifted. This causes the cement and the soil to mix, producing a soil-crete column or row of columns (Idriss and Boulanger 2008), as illustrated in figure 6.8. The columns can be arranged into many different patterns, as illustrated in

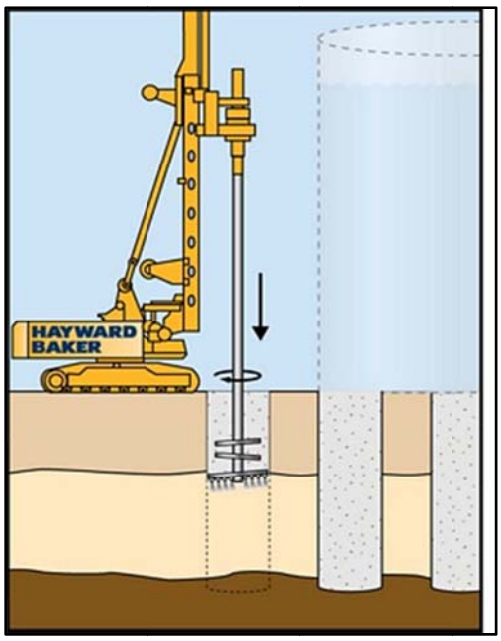

Figure 6.8. Illustration of Deep Soil Mixing construction process (Hayward Baker, Inc. 2010b).

figure 6.9. Often, the patterns are interlocked geometric (i.e. square or hexagonal) configurations called lattice (Porbaha et al. 1999). The lattice configuration mitigates soil liquefaction in three ways; (1) it reduces the earthquake induces shear stains, thereby reducing excess pore water pressure buildup, (2) it restrains the soil from deformation if it does liquefy, and (3) it restricts the migration of excess pore water pressure from unimproved ground (Idriss and Boulanger 2008). Deep soil mixing is applicable for depths of over 30 m (100 ft) and can be used with fine grained material. The drill rig does require large overhead clearance, and the entire column of soil down to the target depth must be treated.

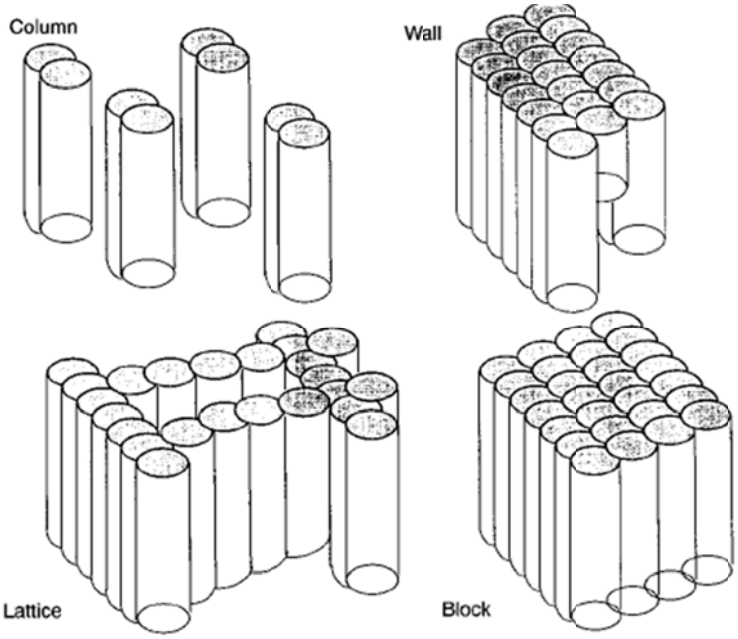

Figure 6.9. Patterns for Deep Soil Mixing (Porbaha et al. 1999).

6.2.7 Deep Blasting

Deep blasting is a method of densification that uses explosive charges to destroy the existing soil structure and rearrange particles in a more compact state (Narin van Court and Mitchell 1995). The use of blasting was used to densify soils to depths of 40 m (130 ft) as documented by Solymar (1983). Usually, small scale drilling equipment can be used to place charges in a pre-arranged grid pattern, which, along with proper timing of the charges, can increase cyclic loading while decreasing offsite vibrations (Narin van Court and Mitchell 1995). Successful densification must be confirmed with post-blasting in-situ testing and surveys to confirm settlements. The effectiveness of blasting could be an issue at shallow depths or for sands with fines contents greater than 15-20 % (Idriss and Boulanger 2008). Usually blasting is most effective over large areas

and can often be coupled with a testing program to ensure proper spacing, depth, and weight of charges. Obtaining permits for blasting, off-site vibration requirements and quantifying the area of improvement are some of the considerations when determining if this is the best technique for liquefaction mitigation.

6.2.8 Earthquake Drains

Earthquake Drains have been used to provide drainage of excess pore water pressures and reduce total settlements in liquefied soil layers (Chang et al. 2004). Earthquake Drains consist of, 75-150 mm (3-6 inch) diameter corrugated pipe with open slots, covered with filter fabric. The open slots allow excess pore water to flow into the pipe while the filter fabric keeps fines from entering and clogging the slots. The drains can be installed using casing and conventional drilling techniques, or a modified vibrating mandrel (Chang et al. 2004). Figure 6.10 illustrates the mandrel type installation technique. Earthquake Drains can be installed to depths of 25 m (85 ft) (Hayward Baker Inc. 2010a), and are best suited for free-draining soils.

6.2.9 Dewatering Techniques

Dewatering is a possible liquefaction mitigation technique because the absence of water makes the buildup of excess pore water pressure impossible. The use of this technique is typically limited to short-term applications because of the high cost and maintenance associated with continual pumping and the deterioration of pumping efficiency over time. Dewatering, along with a cut-off wall, was used as an interim soil liquefaction mitigation technique by the Bureau of Reclamation on the downstream slope of Bradbury Dam. The wells pumped for 18 months while permanent solutions could be

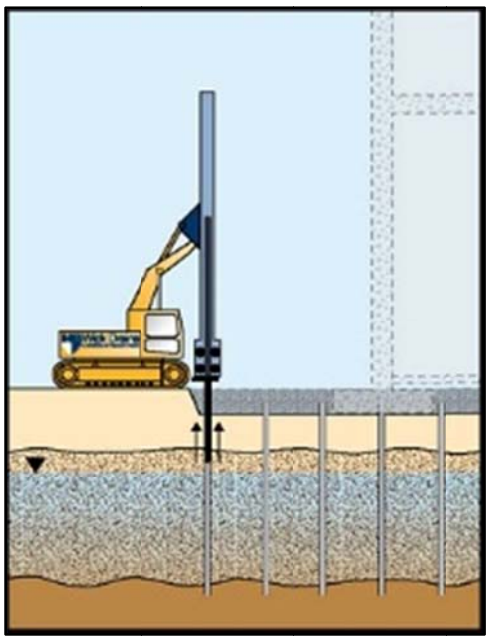

Figure 6.10. Illustration of Earthquake Drain installation using a vibrating mandrel (HB Wick Drains 2009).

designed and built. Gillette and Bliss (1997) concluded that this alternative was unsuitable for a permanent solution because the high cost of operation and the possibility of perched water above the target drawdown elevation. This method is unlikely to mitigate the liquefaction susceptibility in the NMSZ due to a virtually unlimited recharge area and the depth of estimated improvement. The author does not recommend this technique as a long term (design life) option for liquefaction mitigation.

6.2.10 Removal and Replacement

The most direct method for liquefaction mitigation is to remove the liquefiable soil and replace it as compacted fill. This method gives the engineer a high level of confidence in the final product. Unfortunately, this alternative is often too expensive, except at shallow depths (Idriss and Boulanger 2008). In the NMSZ the liquefiable

layers are often below 10 m (30 ft). This fact, combined with the relatively high ground water level (3-6 m, 10-20 ft below the surface), make the removal and replacement method an unlikely option.

6.3 COST COMPARISON

Tables 6.2 is included to compare costs of some liquefaction mitigation techniques discussed in the previous section. The data has been copied from a publication provided by Hayward Baker Inc. (2003), in which a few assumptions were made to come up with relative cost estimates. The assumptions include; (1) the data is applicable to medium-size projects, and (2) the cost data for each technique is applicable to specific soil types (not included in this table). Because of these assumptions, and the fact that the depth of the liquefiable soils encountered in the NMSZ is significant, the costs in Table 6.2 are not appropriate for current design. Still, this table can be used to provide initial "back of the napkin" calculations to determine if further investigation concerning cost information is justified. If further investigation is justified, the engineer can devote more time and effort to determine more accurate cost information.

The cost of mobilization in Table 6.2 reveals that Jet Grouting and Deep Soil Mixing are much more expensive initially then any of the other techniques. The treatment costs of Compaction and Jet Grouting are also higher than the others, but may be offset, depending on site specifics, because only layers susceptible to liquefaction need to be treated. Many seemingly viable options (i.e. Earthquake Drains, Deep Blasting, etc.) are difficult to find cost information for, and this table will have to be supplemented

Table 6.2. Cost estimates of liquefaction mitigation techniques (after Hayward Baker Inc. 2003)

Method of Improvement	Estimated Costs	
	Mobilization	Treatment
Vibratory Compaction (Sand piles)	$5,000-$15,000	$2.00 per 6 yd^3 of treated soil, plus cost of backfill (5-15% of treated soil volume)
Stone Column	$5,000-$35,000	$2.00 per 6 yd^3 of treated soil, plus cost of backfill (5-15% of treated soil volume)
Vibro Concrete Columns	NA	NA
Dynamic Compaction	$25,000-$50,000	$0.75-$2.00 per ft^2, plus cost of fill to maintain site elevation
Compaction Grouting	$10,000-$15,000	$100-$300 per yd^3 of grout $10-$20 per linear ft of drilling
Permeation/Chemical Grouting	$10,000-$15,000	$4.00-$12.00 per ft^3 of soil grouted $15-$50 per linear ft of sleeveport pipe
Jet Grouting	$30,000-$50,000	$100-$300 per yd^3 of grout could be more for small projects
Deep Soil Mixing	$50,000-$100,000	$50-$100 per yd^3 of grout could be more for small projects, highly dependant on binder requirements
Deep Blasting	NA	NA
Earthquake Drains	NA	NA
Dewatering	NA	NA
Removal and Replacement	NA	NA

with current or past cost data provided from another source to determine site-specific cost information.

6.4 Summary and Conclusions

This chapter has presented many current soil improvement techniques used to mitigate soil liquefaction. A few methods such as Deep Dynamic Compaction, Dewatering, and Removal and Replacement have been ruled out as applicable for most soil profiles in northeast Arkansas due to the significant depth and thickness of the liquefiable soil layer. Because site-specific conditions change from one project to another, a range of other possible techniques have been presented as viable options. These will need to be evaluated on a site-by-site basis using up to date cost information. The engineer should also recognize the possibility of combining several techniques in order to achieve the desired level of service.

Site-specific soil conditions and cost considerations prohibit the recommendation of any one liquefaction mitigation technique. Initially, all reasonable possibilities should be considered. Then, as soil properties and cost data are considered some of the techniques will be disqualified, leaving only a few possible alternatives that can produce the desired outcome.

Chapter 7

Conclusions and Recommendations

7.1 Conclusions

Northeastern Arkansas has some of the largest design earthquake ground motions in the continental U.S. (e.g., PGA values ranging up to 1.0 g and greater) due to its location within the New Madrid Seismic Zone (NMSZ). These large earthquake ground motions are particularly problematic when coupled with the unknown seismic response of the deep, soft soils of the Mississippi Embayment. Based on empirical standard penetration test (SPT) liquefaction triggering analyses, many soils in this area exhibit apparent liquefaction susceptibility at depths up to 30-plus m (100-plus ft). However, there is very little guidance in the literature on what to do in these situations, because soils soft enough to liquefy at great depths (i.e. greater than approximately 20 m [65 ft]) have not been documented in the case history databases from previous earthquakes.

The primary task of this research was to help AHTD, and other interested entities involved with design and construction of deep foundations in the NMSZ, update procedures used to evaluate earthquake-induced soil liquefaction triggering, particularly with respect to liquefaction of soils at great depths. Specific subtasks of this research project included providing recommendations and insights concerning: (1) appropriate use of SPT-based liquefaction triggering procedures, (2) residual shear strength of liquefied soils, and (3) potential liquefaction mitigation measures (i.e. possible ground improvement techniques). The conclusions regarding each of these subtasks are presented below.

7.1.1 SPT-based Liquefaction Triggering Procedures

To help evaluate potential liquefaction susceptibility of deep soil deposits in the Mississippi Embayment, the three most commonly used SPT-based liquefaction triggering procedures (Youd et al. 2001, Cetin et al. 2004, and Idriss and Boulanger 2008) have been examined, systematically compared, and programmed into user-friendly Excel workbooks. This is not a trivial topic, as the most appropriate method to use for liquefaction triggering is currently debated at the highest levels of the geotechnical earthquake engineering community (Seed 2010, Finn et al. 2010). These workbooks allow the liquefaction triggering results (i.e., factors of safety and other depth dependent variables) from all three procedures to be readily compared at a given site. The development of these workbooks (including making sure they were user-friendly and technically accurate) occupied a significant portion of the time dedicated to this project. These workbooks will be provided free of charge to anyone interested in using them.

Overall, for the sites analyzed herein, which have fairly high to very high peak ground accelerations, the three procedures agreed in predicting or not predicting liquefaction at many depths. This should not be misconstrued to mean that the numerical values of the F.S. estimates were similar at many depths, but rather that in many circumstances the F.S. estimates were similarly either greater than or less than 1.0, yielding a similar prediction about liquefaction susceptibility. The agreement between all three procedures at a given depth lends confidence to these types of deterministic triggering analyses where a "yes" or "no" answer is required. For situations where the three procedures do not agree on liquefaction triggering, the author recommends using the prediction (i.e., "yes" or "no" liquefaction) agreed upon by two out of the three

procedures. This seems logical given the debate that is ongoing regarding which procedure is "best" (Finn et al. 2010).

Site-specific comparisons of the three liquefaction triggering procedures for boring logs in eastern Arkansas have revealed situations (specific depths at specific sites) where the three procedures yield nearly identical F.S. estimates, and situations where they yield significantly different F.S. estimates. Examinations of depth/stress dependent variables such as r_d, C_N, $(N_1)_{60cs}$, and $K\sigma$ have revealed that no single depth-dependent variable is exclusively responsible for the differences between the liquefaction triggering procedures when F.S. estimates disagree. Surprisingly, in some situations the variable r_d was found to vary by as much as 45% - 60% between procedures for the exact same depth, yet the F.S. estimates for all procedures were nearly identical at these same depths. In other situations, the impact of smaller variations in r_d was evident. In general, it was found that variations in r_d really did not seem to impact the F.S. estimates as much as anticipated. This is likely because each procedure used its respective r_d relationship to define the CRR boundary curve in the back analyses of the case history database; thereby influencing both the CSR and CRR in a similar manner for forward analyses.

In general, it can be stated that the Idriss and Boulanger (2008) procedure typically yields the highest F.S. estimates at depth. While this is somewhat driven by higher $K\sigma$ values at depth (generally ranging from 5% - 15% greater than the other two procedures), it seems to primarily be a result of significantly higher C_N values at depth (generally ranging from 15% - 60% greater than the other two procedures for higher blow count material). Specifically, the iterative, blow count defendant C_N relationship of Idriss and Boulanger (2008) tends to yield significantly greater C_N values when the raw blow

count of the material is greater than about 23. These larger values of C_N directly result in larger $(N_1)_{60cs}$ values, which result in higher $CRR_{M=7.5,1atm}$ values and higher F.S. estimates. Furthermore, as this difference is most pronounced at higher blow counts, where the CRR relationship is very steep and nonlinear, somewhat subtle differences in $(N_1)_{60cs}$ values can result in very significant differences in $CRR_{M=7.5,1atm}$ values. In-depth comparisons of the F.S. estimates and depth-dependant variables may be found in Chapter 4.

7.1.2 Residual Shear Strength

Chapter 5 presented available correlations for estimating the residual shear strength (Sr) of liquefied soil based on back-analyses of liquefaction-induced slope failure case histories. The use of these correlations in post-liquefaction performance of piles, while not entirely accurate, provides the only available alternative for calculating the residual shear strength of liquefied soils using SPT data. The correlations presented in Chapter 5 can be categorized into one of two groups; (1) direct estimation of Sr based on $(N_1)_{60cs-Sr}$ values or, (2) estimation of Sr based on the residual shear strength ratio $(Sr/\sigma'v)$, which incorporates the influence of the vertical effective stress $(\sigma'v)$.

When obtaining Sr directly from corrected blow count, without considering $\sigma'v$, the lower-bound relationship proposed by Seed and Harder (1990) may be used if the most conservative value of Sr is desired. However, the relationship proposed by Idriss and Boulanger (2008) falls within the upper- and lower-bound of the Seed and Harder (1990) relationship and it seems reasonable to use if less conservatism is desired (i.e.,

higher Sr estimates). Furthermore, the Idriss and Boulanger (2008) relationship is the only option for estimating Sr directly for soil with blow counts greater than 15.

When obtaining Sr using the residual shear strength ratio (Sr/σ'v) approach, the available procedures yield similar results for blow counts less than 12. At blow counts greater than 12, only the relationships proposed by Idriss and Boulanger (2008) provide an estimate of Sr. In order to estimate Sr using the relationships proposed by Idriss and Boulanger (2008), the engineer will have to determine whether or not to include the effects of void redistribution (refer to Section 5.2.3), which can significantly influence the results (differences in Sr > 200%).

Site-specific information such as corrected blow count, fines content, and depth of the sample (effective stress) influence the Sr estimates provided by all of these relationships. This makes it challenging to determine which relationship will provide the most, or least, conservative estimate of Sr for a given set of conditions without making the calculations. However, at depth the Sr estimates from Sr/σ'v relationships can be significantly higher than the direct Sr relationships because a benefit is derived from the high effective confining pressures. Because site specific data influences the Sr estimates, the author recommends comparing results from at least three different relationships in order to assign an estimated Sr with some level of confidence. Examples of how to make these comparisons on a site-specific basis are provided in Chapter 5.

7.1.3 Ground Improvement Techniques

Chapter 6 presented many current soil improvement techniques used to mitigate soil liquefaction. A few methods such as Deep Dynamic Compaction, Dewatering, and

Removal and Replacement were ruled out as applicable for most soil profiles in northeast Arkansas due to the significant depth and thickness of the liquefiable soil layer. Because site-specific conditions change from one project to another, a range of other possible techniques have been presented as viable options. These will need to be evaluated on a site-by-site basis using up to date cost information. The engineer should also recognize the possibility of combining several techniques in order to achieve the desired level of service.

Site-specific soil conditions and cost considerations prohibit the recommendation of any one liquefaction mitigation technique. Initially, all reasonable possibilities should be considered. Then, as soil properties and cost data become available some of the techniques will be disqualified, leaving only a few possible alternatives that can produce the desired outcome.

7.2 FUTURE WORK

While the validity of predicting liquefaction susceptibility at significant depths (i.e. greater than 20 m [65 ft]) using simplified SPT procedures is uncertain given the shallow depth range of liquefaction case history data points, one thing is certain: often times all three available procedures predict liquefaction susceptibility at depths of 30-plus m (100-plus ft) for the soil conditions and design PGA values encountered in eastern Arkansas. In the short term, it is recommended that design engineers evaluate liquefaction triggering using all three SPT-based procedures and then use the prediction (i.e., "yes" or "no" liquefaction) agreed upon by two out of the three procedures. However, in the long term additional research is needed to understand not only the

potential for triggering liquefaction in these deep soil deposits but also the consequences of liquefaction given it is triggered.

The ambiguity of predicting deep soil liquefaction is currently an ongoing debate at the highest levels of geotechnical earthquake engineering (Seed 2010, Finn et al. 2010). This argument has particular implications for design and retrofit of dams, and is now receiving much attention. If it were an easy problem, it would have been solved already. However, in lieu of knowing which, if any, of the current liquefaction triggering procedures is "best", it may be appropriate to take a closer look at the PGA values that are driving the liquefaction hazard in the New Madrid Seismic Zone (NMSZ). The AASHTO Guide Specifications for LRFD Seismic Bridge Design (2009) allow seismic design forces obtained from general, code-based procedures to be reduced up to 33% (i.e. 2/3 of the code-based ground motions) if site-specific ground motion response analyses are performed. This potential benefit would allow structural seismic loads and peak ground accelerations used in soil liquefaction analyses and retaining wall designs to be decreased substantially should the site response analyses indicate it is possible. It is very likely that this would be the case, especially for short-period ground motions like PGA, due to soil nonlinearity at significant strains induced by large input rock motions. The AASHTO Guide Specifications (2009) directly mention deep, soft soil deposits (like those found within the NMSZ) as locations where site-specific ground motion response analyses should be performed. Otherwise, "longer-period [i.e. long-span, relatively flexible] bridges may be under-designed and shorter-period [i.e. short-span, relatively stiff] bridges may be over-designed". It is recommended that AHTD perform site-specific ground motion response analyses to investigate the possibility of reducing PGA

values to 2/3 of the code-based procedures. This could have a significant impact on the liquefaction triggering predictions at some sites.

In terms of evaluating the consequences of liquefaction in these deep, thick soil deposits, much is unknown about the post-liquefaction axial and lateral capacity of pile foundations. It is possible that blast-induced liquefaction studies could be used to provide important insights for evaluating axial down-drag (negative skin friction) and revised p-y curves for predicting lateral load response in liquefiable soils. Conducting full-scale axial and lateral pile load tests before and after initiating liquefaction via blasting would be invaluable for confidently evaluating post-liquefaction axial and lateral capacity of piles in the unique soil conditions of northeast Arkansas. Due to the significant thickness of the overlying clay layer at typical sites (6 – 9 m [20 – 30 ft]), it is possible that very significant increases in axial forces caused by down-drag may be induced as the 15-plus m (50-plus ft) layer of underlying clean sand liquefies and consolidates. This potential problem needs additional study. While the effects of lateral spreading also need to be considered, it is possible that lateral spreading may not be as significant a problem as in many areas because the top of the liquefiable layer may be below the bottom of the river channel.

References

American Association of State Highway and Transportation Officials (2009). "Guide Specifications for LRFD Seismic Bridge Design." 1st Edition, Washington, DC.

Andrew, D.C.A., and G.R. Martin. (2000), "Criteria for liquefaction of silty soils." 12th World Conference on Earthquake Engineering, January, 29-February 5, Auckland, New Zealand.

Andrus, R.D., Stokoe, K.H., II, (2000). "Liquefaction Resistance of Soils from Shear - Wave Velocity." Journal of Geotechnical and Geoenvironmental Engineering, ASCE, Vol. 126, No. 11, Nov. pgs, 1015-1025

Bray, J.D., and Sancio, R.B. (2006). "Assesment of Liquefaction Susceptibility of Fine-Grained Soils." Journal of Geotechnical and Geoenvironmental Engineering, ASCE, Vol. 132, No. 9, Sep. pp. 1165-1177.

Bray, J.D., Sancio, R.B., Durgunolu, H.T., Onalp, A., Seed, R.B., Stewart, J.P., Youd, T.L., Baturay, M.L., Cetin, K.O., Christensen, C., Karadayilar, T., and Emrem, C. (2001). "Ground Failure in Adapazari, Turkey." Proc. of Earthquake Geotechnical Engineering Satellite Conference of the XVth International Conference on Soil Mechanics and Geotechnical Engineering, Istanbul, Turkey, August 24-25.

Boulanger, R.W. (2003). "High Overburden Stress Effects on Liquefaction Analyses." Journal of Geotechnical and Geoenvironmental Engineering, ASCE, Vol. 129, No. 12, Dec. pp. 1071-1082.

Boulanger, R.W., and Idriss, I.M. (2004). "State Normalization of Penetration Resistance and the Effect of Overburden Stress on Liquefaction Resistance." Proc. of 11th International Conf. on Soil Dynamics and Earthquake Engineering, and 3rd International Conf. on Earthquake Geotechnical Engineering, Berkeley, CA. Vol. 2, pp. 484-491.

Burke, G.K. (2004). "Jet Grouting Systems: Advantages and Disadvantages." GSP 124, Proc. Geosupport Conference, Orlando, FL. pp. 1-12.

Cetin, K.O., Seed, R.B., Kiureghain, A.D., Tokimatsu, K., Harder, L.F., Kayen, R.E., Moss, R.E.S. (2004). "Standard Penetration Test-Based Probabilistic and Deterministic Assesment of Seismic Soil Liquefaction Potential." Journal of Geotechnical and Geoenvironmental Engineering, ASCE, Vol. 130, No. 12, Dec. pp. 1314-1340.

Chang, W-J., Rathje, E.M., Stokoe, K.H. II, Cox, B.R. (2004). "Direct Evaluation of Effectiveness of Prefabricated Vertical Drains in Liquefiable Sand". Soil Dynamics and Earthquake Engineering, Vol. 24, pp. 723-731.

Cox, B.R. (2001). "Shear Wave Velocity Profiles at Sites Liquefied by the 1999 Kocaeli, Turkey Earthquake." M.S. Thesis, Utah State University, Logan, Utah, p. 274.

Dennis, N.D. (1988). Discussion on "Liquefaction Evaluation Procedure" Journal of Geotechnical Engineering Division, ASCE, Vol. 114, No. 2, pp. 241-243.

Dobson, T. and Slocombe, B. (1982). "Deep Densification of Granular Fills." 2nd Geotechnical , Conference and Exhibit on Design and Construction, April 26-28, Las Vegas, NV.

Finn, W.D.L., Kramer, S. L., O'Rourke, T.D., and Youd, T.L. (2010). "Final Report: Technical Issues in Dispute with EERI MNO-12, Soil Liquefaction During Earthquakes." Ad Hoc Committee on Soil Liquefaction During Earthquakes, Earthquake Engineering Research Institute, pp, 1-8.

Finn, W. D. L. and Wightman, A. (2010). "Evaluation of Liquefaction Potential by Simplified Method with Probabilistic Ground Accelerations." Proc., 9th U.S. National and 10th Canadian Conference on Earthquake Engineering, July 25-29, Toronto, Canada, paper no. 1660.

Florin, V.A., and Ivanov, P.L. (1961). "Liquefaction of Saturated Sandy Soils". Proc., 5th International Conf. on Soil Mechanics and Foundation Engrg., Paris, France, 1961.

Fuller, M. L. (1912). "The New Madrid Earthquake." United States Geological Survey, Bulletin 494, Government Printing Office.

Gibbs, H.J., and Holtz, W.G. (1957). "Research on Determining the Density of Sands by Spoon Penetration Testing." Proc., 4th International Conf. on Soil Mechanics and Foundation Engrg., London, England, 12-14 August 1957. Vol. 1, pp. 35-39.

Gillette, D.R., and Bliss, R.M. (1997). "Dewatering for Interim Mitigation of Liquefaction Hazard at Bradbury Dam." Ground Improvement, Ground Reinforcement, Ground Treatment developments 1987-1997, Shaefer, V.R. (ed) GSP No. 69, ASCE, pp. 525-542.

Golesorkhi, R. (1989). "Factors Influencing the Computational Determination of Earthquake-Induced Shear Stresses in Sandy Soils, Ph.D. thesis, University of California at Berkeley, 395 pp.

Gonzalez, L., Abdoun, T., and Sharp, M.K. (2002). "Modelling of Seismically Induced Liquefaction Under High Confining Stress." Proc., International Journal of Physical Modeling in Geotechnics. Vol. 2 No. 3, pp. 1-15

Google (2010). "Google Earth © 2010." <http://www.google.com/earth/index.html>, Jan. 29, 2011.

Harder, L.F. (1988). "Use of Penetration Tests to Determine the Cyclic Loading Resistance of Gravelly Soils During Earthquake Shaking." Ph.D. Thesis, Dept. of Civil Engrg., Univ. of California, Berkeley.

Hayden, R.F., and Baez, J.I. (1994). "State of the Practice for Liquefaction Mitigation in North America." Proc., 4th U.S.-Japan Workshop on Soil Liquefaction; Remedial Treatment of Potentially Liquefiable Soils, July 4-6, Tsukuba, Japan, pp. 27-47.

Hayward Baker Inc. (2003). "Services." <http://www.haywardbaker.com/> (Sep. 13, 2010).

Hayward Baker Inc. (2010a) “Earthquake Drains” Informational Brochure, Publication No. HBWDEQ-A.

Hayward Baker Inc. (2010b). “Techniques” http://www.haywardbaker.com/WhatWeDo/Techniques/default.aspx (Jan. 18, 2011).

HB Wick Drains (2009). “Earthquake Drains” <http://www.hbwickdrains.com/WhatWeDo/EarthquakeDrains/default.aspx> (Jan. 18, 2011).

Hynes, M.E., and Olsen, R.S. (1999). “Influence of Confining Stress on Liquefaction Resistance.” Proc., International Workshop on Phys. And Mech. of Soil Liquefaction, Balkema, Rotterdam, The Netherlands, pp. 145-152.

International Code Council, Inc. (ICC). (2009). “International Building Code.” Washington D.C.

Idriss, I.M. (1999). “An Update of the Seed-Idriss Simplified Proceedure for Evaluating Liquefaction Potential.” Proc., TRB Workshop on New Approaches to Liquefaction, Publication No. FHWA-RD-99-165, Federal Highway Administration, January.

Idriss, I.M., and Boulanger, R.W. (2004). “Semi-empirical Procedures for Evaluating Liquefaction Potential During Earthquakes.” Proc. 11th International Conference on Soil Dynamics and Earthquake Engineering, and 3rd International Conference on Earthquake Engineering, D. Doolin et al., eds., Stallion Press, Vol 1, pp. 32-56.

Idriss, I. M., and Boulanger, R. W. (2008) "Soil Liquefaction during Earthquakes." MNO-12, Earthquake Engineering Research Institute, Oakland, CA.

Imai, T., Tonouchi, K. and Kanemori, T. (1981). “The Simple Evaluation Method of Shear Stress Generated by Earthquakes in Soil Ground.” Bureau of Practical Geologic Investigation, Report No. 3, pp. 39-58.

Ishihara, K. (1977). “Simple Method of Analysis for Liquefaction of Sand Deposits During Earthquakes.” Soil and Foundations, Vol. 17, No. 3, pp. 1-17.

Iwasaki, T., Tatsuoka, F.,Tokida, K., and Yasuda, S. (1978). “A Practical Method for Assessing Soil Liquefaction Potential Based on Case Studies as Various Sites in Japan.” Proc. International Conference on Microzonation for Safer Construction - Research and Application. Vol. 2, pp. 885-896.

Kayen, R.E., Mitchell, J.K., Seed, R.B., Lodge, A., Nishio, S., and Coutinho, R. (1992). “Evaluation of SPT-, CPT-, and shear wave-based methods for liquefaction potential assessment using Loma Prieta data.” Proc., 4th Japan-U.S. Workshop on Earthquake-Resistant Des. Of Life-line Fac. And Countermeasures of Soil Liquefaction, Vol. 1, pp. 177-204.

Kulhawy, F. H. and Mayne, P.W. (1990). "Manual on Estimating Soil Properties for Foundation Design." Electric Power Research Institute, Palo Alto, Calif.

Liao, S.S.C., and Whitman, R.V. (1986). "Overburden Correction Factors for SPT in Sand." Journal of Geotechnical Engineering Division, ASCE, Vol. 112, No. 3, pp. 373-377.

Marcuson, W.F., and Bieganousky, W.A. (1977a). "Laboratory Standard Penetration Tests on Fine Sands." Journal of Geotechnical Engineering Division, ASCE, Vol. 103, No. GT6, pp. 565-587.

Marcuson, W.F., and Bieganousky, W.A. (1977b). "SPT and Relative Density in Course Sands." Journal of Geotechnical Engineering Division, ASCE, Vol. 103, No. GT11, pp. 1295-1309.

Maslov, N.N. (1957). "Questions of Seismic Stability of Submerged Sandy Foundations and Structures." Proc., 4th International Conf. on Soil Mechanics and Foundation Engrg., London, England, 1957.

Mitchell, J.K., Cooke, H.G., and Schaeffer, J.A. (1998). "Design Considerations if Ground Improvement for Seismic Risk Mitigation." Proc. Geotechnical Engineering and Soil Dynamics III, ASCE Geotechnical Special Publication No. 75, Reston, VA, pp. 580-613.

Moseley, M.P., and Kirsch, K. (2004). Ground Improvement. 2nd Edition. Compaction Grouting pp.197-219, Spon Press, New York, NY.

Munfakh, G.A., Abramson, L.W., Barksdale, R.D. and Juran, I. (1987). "Insitu Ground Reinforcement." Soil Improvement - A Ten Year Update, ASCE Geotechnical Special Publication No. 12, pp. 1-17.

Narin van Court, W.A., and Mitchell, J.K. (1995). "New Insights into Explosive Compaction of Loose, Saturated, Cohesionless Soils." Geotechnical Special Publication no. 49, Conf. Soil Improvement for Earthquake Hazard Mitigation, ASCE, pp. 51-65.

Olsen, S.M. and Stark, T.D. (2002). "Liquefied strength ratio from liquefaction flow failure case histories." Canadian Geotechnical Journal, Vol. 39, pp. 629-647.

Peck, R.B., Hansen, W.E., and Thornburn, T.H. (1974). "Foundation Engineering, 2nd ed." John Wiley and Sons, Inc., New York, NY.

Pileki, T.J. (1988). Discussion on "Liquefaction Evaluation Procedure" Journal of Geotechnical Engineering, ASCE, Vol. 114, No. 2, pp. 246-247.

Pillai, V.S., and Byrne, P.M. (1994) "Effect of Overburden Pressure on Liquefaction Resistance of Sand." Canadian Geotechnical Journal, Vol. 31, pp. 53-60.

Poulos, S.J., Castro, G., and France, W. (1985). "Liquefaction evaluation procedure." Journal of Geotechnical Engineering Division, ASCE, Vol. 111, No. 6, pp. 772-792

Porbaha, A., Zen, K., and Kobayashi, M. (1999). "Deep Mixing Technology of Liquefaction Mitigation." Journal of Infrastructure Systems, Vol. 5, No. 1.

Schaefer, V.R., Editor (1997) "Ground Improvement, Ground Reinforcement, Ground Treatment Developments 1987-1997." Proc. of Geo-Logan, ASCE Geotechnical Special Publication No. 69.

Seed, H.B. (1987). "Design Problems in Soil Liquefaction." Journal of Geotechnical Engrg. Vol. 113, No. 8, pp. 827-845.

Seed, H.B. (1983). "Earthquake-Resistant Design of Earth Dams." Proc., Symposium on Seismic Design of Embankments and Caverns, ASCE, Philadelphia, May 6-10.

Seed, H.B. (1979). "Soil Liquefaction and Cyclic Mobility Evaluation for Level Ground During Earthquakes." Journal of Geotechnical Engineering Division, ASCE, Vol. 105, No. 2, pp. 201-255.

Seed, H.B., and Idriss, I.M. (1971). "Simplified Procedure for Evaluating Soil Liquefaction Potential." Journal of the Soil Mechanics and Foundation Division, Proc., of ASCE. Vol. 97, No. SM9.

Seed, H.B. and Idriss, I.M. (1982). "Ground Motions and Soil Liquefaction During Earthquakes." Earthquake Engineering Research Institute Monograph No. 5, Oakland, California.

Seed, H.B., Idriss, I.M., Makdisi, F., and Banerjee, N. (1975). "Representation of Irregular Stress Time Histories by Equivalent Uniform Stress Series in Liquefaction Analyses." Report No. EERC 75-29, Earthquake Engineering Research Center, University of California at Berkeley, CA, October.

Seed, H.B., and Lee, K.L. (1966). "Liquefaction of Saturated Sands During Cyclic Loading." Journal of the Soil Mechanics and Foundation Division. Proc. of the ASCE, Vol. 92, No. SM6.

Seed, H.B., Tokimatsu, K., Harder, L.F., and Chung, R.M. (1985). "The Influence of SPT procedures in soil liquefaction resistance evaluations." Journal of Geotechnical and Geoenvironmental Engineering, ASCE, Vol. 111, No. 12, pp. 1425-1445.

Seed. R.B. (2010). "Technical Review and Comments: 2008 EERI Monograph Soil Liquefaction During Earthquakes." Geotechnical Report No. UCB/GT – 2010/01, University of California at Berkeley.

Seed, R.B., Cetin, K.O., Moss, R.E.S., Kammerer, A.M., Wu, J., Pestana, J.M., and Riemer, M.F. (2001), "Recent Advances in Soil Liquefaction Engineering and Seismic Site Response Evaluation." Proc. 4th International Conf. on Recent Advances in Geotech. Earthquake Engrg. and Soil Dynamics and Symposium in Honor of Professor W.D. Liam Finn. San Diego, CA, March 26-31, Paper No. SPL-2, pp. 1-45.

Seed, R.B., and Harder, L.F. (1990). "SPT- Bases Analysis of Cyclic Pore Pressure Generation and Undrained Residual Strength." Proc., of the H.B. Seed Memorial Symposium, Vol. 2, pp. 351-376.

Sharp, M.K., and Steedman, R.S. (2000). "Cyclically-Induced Pore Pressure at High Confining Stress." Report: U.S. Army Corps of Engineers, Engineering Research and Development Center.

Stark, T.D., and Mesri, G. (1992). "Undrained shear strength of liquefied sands for stability analysis." Journal of Geotechnical Engineering Division, ASCE, Vol. 118, No. 11, pp. 1727-1747

Stark, T.D., Olsen, S.M., Kramer, S.L., and Youd, T.L. (1998). "Shear strength of liquefied soils." Proc. of the Workshop on Post-Liquefaction Shear Strength of Granular Soils, University of Illinois at Urbana-Champaign, Urbana, Illinois, pp. 288.

Steedman, R.S., Ledbetter, R.H., and Hynes, M.E. (2000). "The influence of high confining stress on the cyclic behavior of saturated sand." Proc., of Sessions of Geo Denver, Soil Dynamics and Liquefaction, Geotechnical Special Publication 107.

Teng, W.C. (1962). "Foundation Design." Civil engineering and engineering mechanics series. Prentice-Hall, Inc. Englewood Cliffs, N.J.

Thevanayagam, S., and Jia, W. (2003). "Electric-Osmotic Grouting for Liquefaction Mitigation in Silty Soils." Grouting and Ground Treatment (GSP 120). Proc. 3rd International Specialty Conference on Grouting and Ground Treatment.

Tuttle, M.P., Schweig, E.S., Sims, J.D., Lafferty, R.H., Wolf, L.W., and Haynes, M.L. (2002). "The Earthquake Potential of the New Madrid Seismic Zone." Bulletin of the Seismology Society of America, Vol. 92, No. 6, pp. 2080-2089.

United States Geological Survey (2008). "Seismic Design Parameters Version 2.10" (CD-ROM) Publication code USGSEIS-1-CD.

U.S. National Research Council, (1985). “Liquefaction of Soils During Earthquakes.” National Academy Press, Washington, D.C.

Vaid, Y.P., Chern, J.C. and Tumi. H. (1985). “Confineing Pressure, Grain Angularity, and Liquefaction.” Journal of Geotechnical Engineering Division, ASCE, Vol. 111, No. 10, pp. 1229-1235

Youd, T. L., Idriss, I.M., et al. (2001). "Liquefaction resistance of soils: Summary report from the 1996 NCEER and 1998 NCEER/NSF workshops of evaluation of liquefaction resistance of soils." Journal of Geotechnical and Geoenvironmental Engineering, ASCE, Vol. 127, No. 4, pp. 297-313.